

1 **Timing of formation of neoglacial landforms in the South Shetland Islands (Antarctic**  
2 **Peninsula): regional and global implications**

3 David Palacios<sup>1</sup>, Jesus Ruiz-Fernández<sup>2</sup>, Marc Oliva<sup>3</sup>, Nuria Andrés<sup>1</sup>, José M.  
4 Fernández-Fernández<sup>1</sup>, Irene Schimmelpfennig<sup>4</sup>,  
5 Laëtitia Leanni<sup>4</sup>, Benjamín González-Díaz<sup>2</sup>, ASTER Team<sup>4,5</sup>

6  
7 1 Department of Geography, Complutense University of Madrid, Spain

8 2 Department of Geography, University of Oviedo, Spain

9 3 Department of Geography, Universitat de Barcelona, Spain

10 4 Aix-Marseille Université, CNRS, IRD, Coll. France, UM 34 CEREGE, Aix-en-  
11 Provence, France

12 5 Consortium: Georges Aumaître, Didier Bourlès, Karim Keddadouche

13  
14 **Key words:** Antarctic Peninsula, Byers Peninsula, Neoglaciation, surface exposure  
15 dating.

16 **Abstract**

17 The timing of neoglacial advances in the Antarctic Peninsula (AP) is not yet well  
18 constrained. Accurate temporal reconstruction of Neoglaciation in the AP is needed to  
19 better understand past glacial responses and regional and global teleconnections during  
20 the Holocene. Here, we examine all available information about neoglacial advances in  
21 the South Shetland Islands (SSI) as well as in the broader geographical context of the AP  
22 region and Antarctic continent. In order to shed light on the contrasting chronologies  
23 existing for neoglacial advances in these regions, we focused on a case study where a  
24 detailed picture of the Holocene deglaciation was already available. Lake sediments  
25 revealed that Byers Peninsula, west of Livingston Island (SSI), was fully deglaciated  
26 during the Holocene Thermal Maximum. To complement this approach, we identified  
27 glacially polished bedrock surfaces, erratic boulders and a moraine ridge near the present  
28 front of the glacier in the SE corner. We applied cosmogenic ray exposure (CRE) dating  
29 using in situ <sup>36</sup>Cl for basalt rocks and <sup>10</sup>Be for granitic rocks in: (i) 8 samples from glacial  
30 erratic and ice-rafted boulders, (ii) 2 samples from moraine boulders, (iii) 2 samples from  
31 polished bedrock surfaces, and (iv) 1 sample from an erratic boulder deposited on one of

32 these surfaces. The CRE dates indicate that the onset of deglaciation started around  $9.9 \pm$   
33  $1.2$  ka, with two phases of glacier expansion during the Mid-Late Holocene forming  
34 moraines at  $\sim 4.1 \pm 0.5$  and  $\sim 1.0 \pm 0.2$  ka, respectively. The main neoglacial advances in  
35 the AP and the SSI were mostly synchronous and coincided with cold periods, as shown  
36 by other records (e.g. glacio-isostatic marine terraces, marine and lake sediments). In  
37 addition, these periods of glacial expansion show a similar timing to those recorded in the  
38 Arctic. These results suggest that Neoglaciation was driven by global climate forcing in  
39 both polar areas despite temporal variations at regional and local scale.

40

## 41 **1. Introduction**

42 The Antarctic Peninsula (AP; Fig. 1) is affected by intense warming, which is recorded  
43 through reliable meteorological measurements since approximately 1950. This most  
44 recent period has been called Recent Rapid Warming (RRW), and is characterized by an  
45 accelerated temperature increase being four times greater in the AP region than the  
46 Earth's average (Vaughan et al., 2003; Turner et al., 2005). This dramatic temperature  
47 rise caused fast melting of glaciers and a generalized retreat of glacier fronts (Vaughan  
48 and Doake, 1996; Cook et al., 2005; Kunz et al., 2012; Pritchard et al., 2012). However,  
49 since 1998 a tendency towards cooling in the AP and a return to positive mass glacial  
50 balances has been detected (Navarro et al. 2013; Engel et al., 2018). This shift is  
51 associated with an increase in the frequency of low pressure systems that has led higher  
52 precipitation and lower summer temperatures in the region, particularly in the N and NE  
53 AP region, including the South Shetland Islands (SSI) (Turner et al., 2016; Sancho et al.,  
54 2017; Oliva et al., 2017a) (Fig. 2). Therefore, the question arises whether RRW is the  
55 beginning of a trend towards deglaciation in the AP, or a brief warming within the long-  
56 term cooling trend affecting this region over the last millennia, continuation of the long-  
57 term cooling started since the Neoglaciation (Vaughan et al., 2003; Bentley et al., 2009).  
58 However, the timing, distribution, evolution and origin of the neoglacial advances in the  
59 AP region is still poorly understood because of: (i) the lack of historical information on  
60 this continent, (ii) the limited number of terrestrial natural archives as sources of  
61 palaeoenvironmental information, and (iii) the difficulties of dating these glacial  
62 advances in Antarctica (Davies et al., 2012).

63 Porter and Denton (1967) proposed the generalization of the term Neoglaciation to refer  
64 to the glacial advances that occurred after the Holocene Thermal Maximum (HTM: 11-5

65 ka, [Renssen et al., 2009](#)) until the end of the Little Ice Age (LIA). Evidence of Late  
66 Holocene glacial advances has been found in a great variety of latitudes and continents  
67 ([Solomina et al., 2015](#)), widespread also in mountains of the Southern Hemisphere  
68 ([Clapperton and Sugden, 1988](#); [Porter, 2000](#)) and Antarctica ([Clapperton and Sugden,](#)  
69 [1988](#); [Clapperton et al., 1989](#); [Ingólfsson et al., 1998](#)). However, delimiting the end of the  
70 HTM and the onset of the neoglacial chronology in the Polar Regions is a matter of great  
71 complexity ([Kaufman et al., 2004](#); [Renssen et al., 2009, 2012](#)). Similarly, the concept of  
72 Neoglaciation in the Arctic has been proposed as a tendency to climate cooling ([McKay](#)  
73 [et al., 2018](#)). However, phases of glacial advances in the Arctic during Neoglaciation  
74 alternated with warm periods and glacial retreat, occurring asynchronously across the  
75 region without a clear regional pattern ([McKay et al., 2018](#)).

76 As in the Arctic, the chronology of Neoglaciation varied significantly within the AP and  
77 throughout the Antarctic continent ([Bentley and Hodgson, 2009](#)). According to the  
78 available glacio-marine sedimentary records, cold phases during Neoglaciation in the AP  
79 region were short, not exceeding 0.5 ka ([Yoon et al., 2010](#)), and alternated with longer  
80 warm periods ([Davies et al., 2012](#)). The first synthesis on climatic and glacial evolution  
81 in the AP during the Holocene was carried out by [Ingólfsson et al. \(1998\)](#) who suggested  
82 the first neoglacial advances after 5 ka. [Ingólfsson et al. \(2003\)](#) proposed several other  
83 neoglacial advances between 3 and 1 cal ka BP. [Bentley et al. \(2009, 2014\)](#) reported a  
84 generalized warm period in the AP between 4.5 and 2.8 cal ka BP followed by a relatively  
85 widespread cold period between 2.5 and 1.2 cal ka BP. [Bentley and Hodgson \(2009\)](#)  
86 highlighted that Late Holocene cold phases in different sites across the AP were not  
87 synchronous, even in close regions. [Hall \(2009\)](#) provided a synthesis of Holocene glacial  
88 evolution for the entire Antarctic continent, including the AP, with many references to  
89 neoglacial landforms. Subsequent studies provided new glacial evidence of neoglacial  
90 landforms in other regions, thus confirming the occurrence of the Neoglaciation as a  
91 widespread pattern of glacial advance in the AP ([Davies et al., 2012, 2013](#); [Carrivick et](#)  
92 [al., 2012](#); [Cofaigh et al., 2014](#)). However, these new data also introduce new uncertainties  
93 about the time range of neoglacial phases in different areas across this region ([Allen et](#)  
94 [al., 2010](#); [Davies et al., 2012](#); [Barnard et al., 2014](#); [Cofaigh et al., 2014](#)). The spatio-  
95 temporal variations of glacial oscillations over the last centuries are also a consequence  
96 of climate variability in the region ([Mosley-Thompson et al., 1990](#); [Guglielmin et al.,](#)  
97 [2016](#); [Brightley, 2017](#)). Recently, [Čejka et al. \(2019\)](#) examined the neoglacial onset in

98 the AP region through the revision of 22 studies focused on ice cores and marine and lake  
99 sediments. They concluded that the beginning of neoglacial cooling occurred, in average,  
100 at  $2.6 \pm 0.8$  cal ka BP, with large spatio-temporal differences within the AP region ranging  
101 between 4.8 ka and 1.2 cal ka BP. However, a review on glacier oscillations during  
102 Neoglaciatioin is still missing. [Kaplan et al. \(2020\)](#) provided new information about the  
103 Neoglaciatioin chronology in the AP and compared it with the neoglacial advances in  
104 Patagonia.

105 The Byers Peninsula, on the western end of Livingston Island, is the largest deglaciated  
106 terrestrial area in the SSI (Fig. 2). In this area, lake records suggest that the retreat of the  
107 Rotch Dome Glacier occurred throughout the Holocene ([Toro et al., 2013](#); [Oliva et al.,  
108 2016](#); [Ruiz-Fernández and Oliva, 2016](#)), although the existence of neoglacial landforms,  
109 such as moraines, is not yet evidenced. The application of cosmogenic radiation exposure  
110 (CRE) methods – that have not been applied yet to neoglacial landforms in the SSI –  
111 offers new possibilities to obtain a detailed chronology for the development of these  
112 neoglacial landforms. The knowledge of the age of moraines formed in neoglacial  
113 advances in the Byers Peninsula can provide important information on the possible  
114 synchrony of these advances within the context of the AP.

115 The aim of this paper is to map and date neoglacial landforms in the SSI as well as explore  
116 their paleoclimatic implications in the context of the Antarctic continent. Firstly, we  
117 review the current state of knowledge of Neoglaciatioin in Antarctica, focusing mainly in  
118 the AP. In order to provide the most detailed picture on the paleoclimatic evolution in this  
119 region, we examined all available records from ice cores, deep marine sediment cores,  
120 lake sediments and glacial landforms. Subsequently, we focused on an area of the AP  
121 region where information about Holocene glacial advances is still absent: the Byers  
122 Peninsula. In this peninsula, we have mapped the spatial distribution of possible  
123 neoglacial moraines, analyzed the geomorphological setting, and applied CRE dating to  
124 these landforms.

125

## 126 **2. The Neoglaciatioin in the Antarctic Peninsula and South Shetland Islands**

127 A recent synthesis of the evolution of the West and East Antarctic Ice Sheets shows that  
128 glacial mass loss was intense from 9 until 7-6 ka in both areas ([Mackintosh et al., 2011,  
129 2014](#)), mainly due to ocean warming, although the long-term glacial shrinking had

130 already begun before 10 ka (Larter et al., 2014). (Fig. 1, Table 1). A wide range of climatic  
131 proxies provides data on the occurrence of various cold periods in the AP for the last  
132 millennia.

133 In order to constrain the magnitude and the chronology of neoglacial advances and  
134 retreats in the SSI, we first review the climatic evolution over the Mid- and Late Holocene  
135 in the AP region based on different environmental sources:

136 (i) *Neoglaciation from ice cores in the AP.* Polar ice cores preserve and provide  
137 information on climatic changes and their causes, mainly from comparison of the  $\delta^{18}\text{O}$ ,  
138 deuterium and  $\text{CO}_2$  concentration variations in different layers, as well as on the climate  
139 and chronology from the impurities of the ice (Lorius et al., 1990). The most accurate  
140 reconstruction from ice core records in the AP comes from James Ross Island, NE AP,  
141 which revealed a cold phase between 2.5 and 0.6 cal ka BP, and a peak of cold climate  
142 that occurred roughly at 1.4 cal ka BP (Mulvaney et al., 2012; Abram et al., 2013). The  
143 last phase of intense cooling was recorded during the LIA at around AD ~1410-1460  
144 (Abram et al., 2013), as also detected in ice cores from other areas in Antarctica, e.g. Ross  
145 Sea, with a temperature ca. 2° C colder than present (Bertler et al., 2011), or in Princess  
146 Elizabeth Land, East Antarctica, with a significant cooling at AD 1450–1850 (Li et al.,  
147 2009) (Fig. 1 and Table 1).

148 (ii) *Neoglaciation from marine sediments in the AP.* Deep marine sediment cores can  
149 reveal climatic changes based on the proportion of foraminifera and microfossils that are  
150 highly sensitive to sea surface temperatures. The ratio of the oxygen isotopes from the  
151 calcium carbonate shells of foraminifera and coccoliths, and from the silicon dioxide  
152 shells of radiolarians and diatoms, is indicative of the temperature of the ocean during the  
153 build-up of every shell layer (Rothwell and Rack, 2006). Several sedimentary records  
154 were collected from areas adjacent to the AP region. As in ice core records, most records  
155 show changes in sedimentation patterns during neoglacial cold periods, with notable  
156 chronological differences. Records obtained in the Bransfield Strait reported abrupt cold  
157 conditions at 4.5 and 2.5 cal ka BP (Shevenell et al., 2011), at 3.5 and 1.2 cal ka BP (Khim  
158 et al., 2002; Heroy et al., 2008; Barnard et al., 2014) and during the LIA (Khim et al.,  
159 2002; Barnard et al., 2014). In other records from the western side of the AP, similar  
160 patterns were observed, including long-term cooling trends from 3.3 to 0.1 cal ka BP in  
161 Palmer Deep (Domack et al., 2001), from 2.8 to 0.2 cal ka BP in Marguerite Bay (Allen  
162 et al., 2010), and during the LIA in Müller Ice Shelf (Domack et al., 1995) and in Barilari

163 Bay, Graham Land (Christ et al., 2015; Reilly et al., 2016). Neoglacial cooling was also  
164 reported in the NE of the AP, as in the Firth of Tay, where marine sediment cores revealed  
165 a minor glacial advance between 6.0 and 4.5 cal ka BP, retreat between 4.5 and 3.5 cal ka  
166 BP, and glacial readvance from 3.5 cal ka BP to recent times (Michalchuk et al., 2009)  
167 (Fig. 1 and Table 1).

168 (iii) *Neoglaciation from lake sediments in the AP.* Paleolimnological studies can reveal  
169 climatic changes from a wide range of proxies including the analysis of magnetic  
170 susceptibility, grain-size distribution, geochemistry, diatoms studies, and geochronology  
171 (Zale and Karlén, 1989; Čejka et al., 2019). Čejka et al. (2019) examined the onset of  
172 Neoglaciation in the AP region from lacustrine sediments suggesting that it occurred at 2  
173 cal ka BP, with significant regional variations. Conversely, in our study, we analyzed  
174 periods during the Neoglaciation that led to glacial advances. Evidences of neoglacial  
175 advances in the AP from lacustrine sediments suggest a phase of glacial expansion at 1.2  
176 cal ka BP in James Ross Island, (Björck et al., 1996a), at around 5 ka and during the LIA  
177 in Hope Bay (Zale and Karlén, 1989) and from 2.6 until 1.1 cal ka BP in Marguerite Bay  
178 (Hodgson et al., 2013) (Fig. 1 and Table 1).

179 (iv) *Neoglaciation from raised beaches in the AP.* Rates of glacio-isostatic uplift inferred  
180 from the elevation of raised beaches are indicative of the intensity of the deglaciation  
181 (Simkins et al., 2013). Hall and Denton (1999) determined that these rates were especially  
182 high between 8 and 5 cal ka BP in the Ross Sea, suggesting that glacial shrinking  
183 decreased during the Mid Holocene. However, decreasing uplift rates can be also  
184 indicative of glacial advances (Simkins et al., 2013). In Beak Island, NE AP, the relative  
185 sea level fell from a maximum uplift rate of 3.91 mm yr<sup>-1</sup> at around 8 cal ka BP to 2.11  
186 mm yr<sup>-1</sup> between 6.9 and 2.9 cal ka BP, 1.63 mm yr<sup>-1</sup> between 2.9 and 1.8 cal ka BP, and  
187 finally to 0.29 mm yr<sup>-1</sup> during the last 1.8 ka BP. This reveals a trend towards more glacial  
188 stability and/or glacial readvances during the neoglacial period (Roberts et al., 2011) (Fig.  
189 1 and Table 1).

190 (v) *Neoglaciation from glacial landforms in the AP.* Together with these proxies, some  
191 studies have focused on the direct dating of neoglacial landforms in the AP. Radiocarbon  
192 dating of unconsolidated glacial sediments demonstrated the occurrence of six neoglacial  
193 advances at 6.5, 4.6, 3.9 cal ka BP, two around 2.6 cal ka BP, as well as glacial expansion  
194 during the LIA in James Ross Island (Strelin et al., 2006). This LIA glacial advance has  
195 been also detected in the western AP, namely in Rothera Point, Marguerite Bay



196 (Guglielmin et al., 2016) as well as in Anvers Island, where the glacier front was at or  
197 behind its present position at 0.7-0.9 cal ka BP (Hall et al., 2010) (Fig. 1 and Table 1).  
198 Outside the AP, in the Scott Coast, in Ross Sea, Late Holocene moraines are distributed  
199 on dated raised beaches indicating a neoglacial advance that occurred between 3.5 ka and  
200 the LIA (Hall and Denton, 2002).

201 However, the most reliable approach to date Neoglaciation in the AP is based on the  
202 dating of glacial landforms using CRE methods. In James Ross Island, one of the areas  
203 with most CRE dates available, deglaciation was intense until 6 ka (Hodgson et al., 2011;  
204 Glasser et al., 2014) and neoglacial advances occurred at ~4.8 ka and from 1.5 to 0.3 ka  
205 ( $^{10}\text{Be}$  ages) (Davies et al., 2014). Close to James Ross Island, in Solari Bay, the Sjögren,  
206 Boydell and Drygalski glaciers advanced at 1.4 ka ( $^{10}\text{Be}$  ages) (Balco et al., 2013).  
207 Recently, a work focusing on James Ross Island area reported 49  $^{10}\text{Be}$  ages of Holocene  
208 glacial landforms (Kaplan et al., 2020). These results suggest that the major glacial  
209 advance following the HTM occurred at ~7-4 ka, with subsequent phases of glacier  
210 expansion between 3.9 and 3.6 ka, just after 3 ka, between ~2.4 and ~1 ka, and from  
211 ~0.3 to ~0.1 ka (Kaplan et al., 2020).

212 Using CRE dating, neoglacial advances were also detected in the western AP region, as  
213 in Alexander Island, Marguerite Bay, where a period of glacial expansion took place at  
214  $4.4 \pm 0.7$  and 1 ka ( $^{10}\text{Be}$  ages) (Davies et al., 2017). Neoglacial advances have been  
215 reported in other areas in Antarctica, such as in the Darwin Mountains between 3 and 0.5  
216 ka ( $^{10}\text{Be}$  ages) (Storey et al., 2010) (Fig. 1 and Table 1).

217 *(vi) Neoglaciation in the South Shetland Islands.* The SSI archipelago, located NW of  
218 the AP, lies at 120 km from the AP. The existence of neoglacial landforms in the SSI is  
219 known since the last third of the 20th century (Fig. 2 and Table 2). In the first  
220 geomorphological studies, at the end of the 1960s and early 1970s, researchers focused  
221 on the existence of moraines distributed a few hundred meters away from the present-day  
222 glacier fronts, which transgressed and overlapped recent raised beaches (Araya and  
223 Hervé, 1966; Everett, 1971; John and Sugden, 1971; John, 1972; Sugden and John, 1973).

224 This geomorphological pattern was first described in several deglaciated areas of the SSI,  
225 such as Byers and Hurd peninsulas (Livingston Island) and Fildes peninsula (King George  
226 Island). Since then, attention has been paid to inferring the age of deglaciation of these  
227 raised beaches and their relationship with moraines which transgressed them. Previous

228 works considered that the raised beaches formed as a result of glacio-isostatic rebound  
229 due to the partial deglaciation of these islands. The existence of moraines distributed on  
230 some of these raised beaches suggest that the moraines are chronologically younger than  
231 the raised beaches. Radiocarbon dating of organic fragments interbedded in the raised  
232 beach provide a minimum age for the formation of the moraine resting on this beach. In  
233 Hurd Peninsula, [Everett \(1971\)](#) inferred a phase of glacial expansion that advanced on a  
234 raised beach at 10-12 m a.s.l. and a subsequent glacier advance that left a moraine on a  
235 raised beach at 4-6 m a.s.l., which was known as the "False Bay event" ([Everett, 1971](#)).  
236 The application of radiocarbon dating to raised beaches at 4-6 m a.s.l. in Fildes Peninsula  
237 yielded an age of 0.4-0.7 cal ka BP. As this level of the raised beach (4-6 m a.s.l.) is  
238 frequently occupied by the youngest moraines existing in the SSI, geomorphologists  
239 deduced that these moraines were of LIA age ([John and Sugden, 1971](#); [John, 1972](#);  
240 [Sugden and John, 1973](#)). Subsequently, further radiocarbon dates differentiate between  
241 two levels of raised beaches in the SSI that were covered by the last neoglacial advances:  
242 (i) the first one at 6 m a.s.l., (varying locally between 5 and 7.5 m a.s.l.) associated with  
243 a 2-3 km glacier readvance dated at the 13th to early 16th centuries A.D., and (ii) another  
244 one at 2-3 m a.s.l. associated with a 0.25-1 km glacier readvance at approximately the 15-  
245 17th centuries A.D, that in some areas overlapped the previous ([Curl, 1980](#); [Sugden and](#)  
246 [Clapperton, 1986](#); [Clapperton, and Sugden, 1988](#)). Further radiocarbon dates of raised  
247 beaches also suggest, at least, two neoglacial advances between 3 and 1 cal ka BP ([Barsch](#)  
248 [and Mäusbacher, 1986](#)). The application of lichenometric dating to the moraines  
249 distributed on the lowest raised beaches in the SSI confirmed that these landforms  
250 developed during LIA glacial advances ([Birkenmajer, 1981, 1995; 1998](#)) (Fig. 2 and  
251 Table 2).

252 To better understand the relationship between glacial advances and raised beaches  
253 transgressed by moraines, a more accurate geomorphological mapping was conducted to  
254 determine the altitude and extent of raised beaches in the Byers Peninsula ([Arche et al.,](#)  
255 [1996](#)) and their correlation with those existing in other ice-free areas in this archipelago  
256 ([Fretwell et al., 2010](#)). The abundance of ice rafted debris of allochthonous lithology on  
257 raised beaches dated between 0.25 and 1.7 cal ka BP suggest that these beaches were  
258 related to cold periods of increased glacial extent and greater iceberg delivery ([Hall and](#)  
259 [Perry, 2004](#)). In addition, the dating of the highest raised beaches (located at about 16-20  
260 m a.s.l.) indicates that the most massive deglaciation phase in this peninsula occurred



261 between 9 and 6 cal ka BP, with glaciers close to their current position by 5.5 cal ka BP  
262 (Barsch and Mäusbacher, 1986; Mäusbacher, 1991; Del Valle et al., 2002; Hall, 2003;  
263 Bentley et al., 2005; Hall, 2010; Watcham et al., 2011).

264 New records obtained during the early 21st century have improved our knowledge on the  
265 age of moraines in the SSI (Fig. 2 and Table 2). The oldest moraines in Livingston Island  
266 identified by Everett (1971) were dated at >7.3 ka, predating the formation of the oldest  
267 raised beaches (Sugden and John, 1973; Curl, 1980; López-Martínez et al., 1992; Hall  
268 and Perry, 2004; Bentley et al., 2005; Hall, 2009; Fretwell et al., 2010). Hall (2007) dated  
269 by radiocarbon the youngest moraines previously studied in Fildes and Hurd Peninsulas  
270 (Everett, 1971, John and Sugden, 1971; John, 1972; Sugden and John, 1973). However,  
271 Hall (2007) considers the possibility that there could have been previous advances as old  
272 as 2.8 cal ka BP. Radiocarbon ages from a 4-6 m raised beach related to these moraines  
273 support glacial advance and transgression during the LIA. The application of Optically  
274 Stimulated Luminescence (OSL) dating methods to these younger beaches at 4-6 m in the  
275 Fildes Peninsula confirmed an age of the 16-18th centuries AD, which coincided with the  
276 LIA (Simms et al., 2011a, 2012).

277 On the one hand, at the end of the 80s and beginning of the 90s, sediment cores collected  
278 from several lakes in Livingston and King George Islands reported radiocarbon minimum  
279 ages of 4-5 cal ka BP for deglaciation (Mäusbacher et al., 1989; Björck et al., 1991, 1993,  
280 1996b). The analysis of lake sediments from a number of lakes in the western part of the  
281 Byers Peninsula suggested the occurrence of a warm period occurring between 3.2 and  
282 2.7 cal ka BP (Björck et al., 1993) and a remarkable cooling between 1.5 and 0.5 cal ka  
283 BP (Björck et al., 1991). More recent studies suggest that the onset of the deglaciation of  
284 the Byers Peninsula occurred at 8.3 cal ka BP (Toro et al., 2013), with the deglaciation of  
285 the central plateau taking place between 8.3 and 5.9 cal ka BP and ice-free exposure of  
286 the easternmost fringe, close to the present-day glacier front, around 1.8 cal ka BP (Oliva  
287 et al., 2016).

288 CRE dating methods were applied to polished bedrock surfaces in the Barton Peninsula  
289 (King George Island) along a transect from the highest peaks to the coast. These data  
290 showed that deglaciation of this small peninsula had begun earlier than inferred from lake  
291 sediments and raised beaches, between 17 and 14 ka, and had finished 1 ka ago (Seong et  
292 al., 2009). Hall (2009) CRE dated moraines from Hurd Peninsula and Marion Cove (King  
293 George Island) at 1.5-1.0 ka (Hall and Stone, personal communication).

294 Finally, the analysis of marine sediments in Maxwell Bay (King George Island)  
295 determined that there was rapid glacial retreat from 10.1 to 8.2 cal ka BP and a period of  
296 gradual cooling and more extensive sea-ice cover in the bay from 5.9 cal ka BP onwards,  
297 with no evidence of LIA glacial advance (Milliken et al., 2009). However, a more recent  
298 study of marine sediments in Maxwell Bay confirmed that the deglaciation began as soon  
299 as 14 cal ka BP – as was proposed by CRE dating in the nearby Barton Peninsula (Seong  
300 et al., 2009) – and that deglaciation was completed by 5.9 cal ka BP, with a neoglacial  
301 advance into the bay ending at approximately 1.7 ka (Simms et al., 2011a). Recent coastal  
302 sediment analysis in Fildes Peninsula showed a cold period from 5.8 to 4.8 cal ka BP, a  
303 mid-Holocene climatic optimum between 4.4 and 2.7 cal ka BP, and the onset of  
304 Neoglaciation at 2.7 cal ka BP (Chu et al., 2017). Sediment cores obtained from the  
305 continental shelf of the northern SSI pointed to the existence of a cold period around 0.33  
306 cal ka BP, which must have corresponded to the LIA (Yoo et al., 2009).

307 To sum up, despite varied results, a common pattern can be deduced in studies of  
308 neoglacial phases in the SSI in the context of AP region. The glaciers were similar to or  
309 smaller than present-day in the AP, as in the SSI, around 6 ka.

310 Before the warmer period detected in the AP between 4.5 and 2.8 cal ka BP (Bentley et  
311 al., 2009), a cold period with the first neoglacial advances occurred around 5 ka in many  
312 places of the AP and the rest of the continent (Zale and Karlén, 1989; Mosley-Thompson,  
313 1996; Khim et al., 2002; Strelin et al., 2006; Heroy et al., 2008; Bentley et al., 2009;  
314 Michalchuk et al., 2009; Davies et al., 2012; Shevenell et al., 2011; Carrivick et al., 2012;  
315 Cofaigh et al., 2014; Barnard et al., 2014; Davies et al., 2017; Kaplan et al., 2020). So far,  
316 there is no evidence of this neoglacial advance in the SSI, except perhaps for the  
317 references made by Everett (1971) in the Hurd Peninsula about moraines in relation to  
318 the raised beaches at 10-12 m a.s.l.

319 Another period of widespread neoglacial advance took place in the AP between 2.8 and  
320 1.4 ka, with cooling intensifying between 1.8 and 1.4 cal ka BP. (Mosley-Thompson,  
321 1996; Björck et al., 1996; Khim et al., 2002; Heroy et al., 2008; Bentley et al., 2009; Yoon  
322 et al., 2010; Domack et al., 2001; Strelin et al., 2006; Michalchuk et al., 2009; Allen et  
323 al., 2010; Davies et al., 2012; Mulvaney et al., 2012; Shevenell et al., 2011; Mulvaney et  
324 al., 2012; Abram et al., 2013; Hodgson et al., 2013; Barnard et al., 2014; Davies et al.,  
325 2014; Čejka et al., 2019; Kaplan et al., 2020). To date, this glacial advance is also poorly  
326 represented in the SSI, with the only reference by Hall (2007, 2009). However, there is

327 some evidence of a cold period around 1.8 ka in the SSI from other paleoclimatic proxies,  
328 such as ice rafted debris on raised beaches (Hall and Perry, 2004), lake sediments (Björck  
329 et al., 1991, 1993; Oliva et al., 2016), and marine records (Chu et al., 2017).

330 The information available on glacial advances during the LIA is varied across the AP, as  
331 in the SSI. Similarly, there is clear evidence of advances in some areas (Strelin et al.,  
332 2006), but it is absent in archives such as lake and marine sediments (Shevenell et al.,  
333 2011; Hodgson et al., 2013) as well as in ice core records (Mulvaney et al., 2012;  
334 Brightley, 2017). In any case, it is important to note that in many areas a cooling period  
335 was observed from 1.5 ka to the first cooling events associated with the LIA (Zale and  
336 Karlén, 1989; Domack et al., 2001; Hall and Denton, 2002; Allen et al., 2010; Storey et  
337 al., 2010; Michalchuk et al., 2009; Balco et al., 2013; Davies et al., 2014; Davies et al.,  
338 2017). On the other hand, most of the studies carried out on the youngest moraines of the  
339 SSI, transgressing the 4-6 m raised beach, confirmed that they were formed during the  
340 LIA, between the 16th and 18th centuries AD, with minor age differences depending on  
341 dating methods.

342

### 343 **3. Geographical setting of the case study: the Byers Peninsula**

344 With the aim of resolving the discrepancies observed between the SSI and the rest of the  
345 AP on the timing of development of neoglacial landforms, this work explores the age of  
346 formation of several landforms in an area that is already known to have been deglaciated  
347 during the Mid-Late Holocene (Oliva et al., 2016), the Byers Peninsula, the largest ice-  
348 free area in the SSI (Fig. 2 and Table 3). The Byers Peninsula (62°34'35"–62°40'35"S,  
349 60°54'14"–61°13'07"W) is located on the western end of Livingston Island, the second  
350 largest island in the SSI, with an area of approximately 60 km<sup>2</sup>, and a maximum altitude  
351 of 265 m a.s.l.. The peninsula is part of a Jurassic-Quaternary magmatic forearc generated  
352 by Mesozoic and Cenozoic subduction processes along the South Shetland Trench  
353 (Smellie et al., 1980; Alfaro et al., 2010). This peninsula is composed of Upper Jurassic-  
354 Lower Cretaceous sedimentary deposits (mainly sandstones, mudstones and  
355 conglomerates) and volcanic and volcanoclastic rocks, with abundant intrusive igneous  
356 rocks of basalt-basaltic andesite composition (Smellie et al., 1980; Hathway and Lomas,  
357 1998; Parica et al., 2007; Alfaro et al., 2010). The geomorphology of the Byers Peninsula  
358 (Araya and Hervé, 1966; John and Sugden, 1971; López-Martínez et al., 1996) is formed  
359 by a high plateau (80-110 m), considered a marine platform, onto which protruded a series

360 of volcanic plugs such as Start Hill (265 m a.s.l.), Chester Cone (188 m), Cerro Negro  
361 (143 m), Tsamblak Hill (113 m) and Clark Nunatak (147 m). Many lakes are distributed  
362 on this plateau, such as the Limnopolar, Chester, Escondido, Cerro Negro and Domo lakes  
363 (Fig. 2, Table 3). This central plateau is encircled by an intermediate marine platform (50-  
364 80 m) that is surrounded by a lower platform above which Holocene raised beaches from  
365 2 to 15-16 m a.s.l have developed. The sequence of raised beaches is particularly well-  
366 preserved in the South beaches (S), the Robbery beaches (N), and the President beaches  
367 (W). The ice-free area of the Byers Peninsula is delimited in its eastern flank by the Dome  
368 Rotch Glacier, which covers the rest of the western part of Livingston Island reaching a  
369 maximum altitude of 360 m. Although there is no information about the recent evolution  
370 of Dome Rotch Glacier in the side of the Byers Peninsula, significant retreat has been  
371 observed in other neighbouring coastal fringes since the 1950s (Birkenmajer 2002) that  
372 seems to have decelerated in the last decade (Navarro et al., 2013; Oliva et al., 2017).

373 The mean annual temperature is around  $-2.8$  °C at 80 m and annual precipitation (rain  
374 and snowfall) reaches ca. 650 mm at this altitude (Bañón et al., 2013; De Pablo et al.,  
375 2014). Discontinuous permafrost patches have been detected in raised beaches (Correia  
376 et al., 2017) whereas permafrost is continuous at the central plateau (de Pablo et al., 2014).  
377 Abundant periglacial landforms distributed across the peninsula show evidence of active  
378 periglacial dynamics in the area, strongly conditioned by local topography and snow  
379 distribution (Serrano et al., 1996; López-Martínez et al., 2012; Hrbáček et al., 2016; Ruiz-  
380 Fernández et al., 2016; Oliva et al., 2017b). Most of the area is covered by bryophytes  
381 and lichens, including the two native Antarctic phanerogams on the raised beaches  
382 (Lindsay, 1971; Vera, 2013), which makes the Byers Peninsula a unique environment in  
383 terms of terrestrial biodiversity within Antarctica (Benayas et al., 2013; Almela et al.,  
384 2019). To protect this hotspot of biodiversity, the Byers Peninsula was designated an  
385 Antarctic Specially Protected Area (ASPA N° 126).

386 The Byers Peninsula was covered by an ice sheet distributed across the SSI during the  
387 last glacial cycle (Araya and Hervé, 1966; John and Sugden, 1971; López Martínez et al.,  
388 1996). This ice sheet was connected with the AP ice sheet during the maximum ice extent,  
389 though it became isolated as ice started thinning during the deglaciation (Cofaigh et al.,  
390 2014). Previous studies on lake sediments have determined that the deglaciation of the  
391 Byers Peninsula occurred from W to E, with a timing of 7.5 to 1.8 cal ka BP (Toro et al.,  
392 2013; Oliva et al., 2016; Ruiz-Fernández and Oliva, 2016). Domo Lake, located only at

393 350 m from the present glacier front, was deglaciated around 1.8 ka (Oliva et al., 2016).  
394 Several geomorphological landforms and deposits of glacial origin are distributed  
395 between the contemporary glacial front and the sea. This is the case of the large  
396 longitudinal ice-cored moraines located in front of the Rotch Dome Glacier (Martinez de  
397 Pisón et al., 1996; Ruiz-Fernández et al., 2016). John and Sugden (1971) observed how  
398 these moraines override all marine levels incorporating littoral deposits; they suggested  
399 that the most recent moraines were directly related to the 4-6 m beach and were  
400 contemporary in age, representing thus a recent glacial readvance. Hansom (1979)  
401 radiocarbon dated a 10 m a.s.l. raised beach at 1.8 cal ka BP, whereas Curl (1980) reported  
402 that the 6 m a.s.l. raised beach formed during the 15-17th centuries AD. Hall and Perry  
403 (2004) suggested that this beach and the 10 m a.s.l. unit formed during cold periods over  
404 the last 1.7 cal ka BP, as they are rich in ice rafted debris. Hall (2003, 2010) contributed  
405 numerous dates for all the sequences of raised beaches in the main complexes of the Byers  
406 Peninsula, concluding that the highest levels formed at 7.4 cal ka BP and confirming that  
407 the 6 m a.s.l. raised beach developed during the 15-17th centuries AD. The frontal ice-  
408 cored moraines in front of the Rotch Dome Glacier have been very stable over the last  
409 decades, as can be seen in photos and descriptions in old publications (John and Sugden,  
410 1971; López Martínez et al., 1996; Hall, 2010). The glacier has retreated from these  
411 moraines only in the vicinity of the northern coast and in the southern fringe, around Clark  
412 Nunatak (Martinez de Pisón et al., 1996). In the nearby peninsula of Elephant Point, only  
413 3 km SE of Clark Nunatak, a similar retreat occurred from 1956 to 2000 (Oliva and Ruiz-  
414 Fernández, 2015, 2017) (Fig. 2 and Table 3).

## 415 5. Methodology

### 416 5.1 Geomorphological research and sampling strategy

417 In the eastern fringe of the Byers Peninsula, next to Rotch Dome Glacier, an ice-cored  
418 moraine has been described to be in contact with the glacier front from 1966 to 1996  
419 (Araya and Hervé, 1966; John and Sugden, 1971; Martinez de Pisón et al., 1996) (Fig. 2).  
420 Over these thirty years, the limits, extent, and shape of the ice-cored moraine crests were  
421 identical to those described in earlier observations (Martinez de Pisón et al., 1996),  
422 showing evidence of the prevailing geomorphic stability at annual to decadal timescales  
423 (López Martínez et al., 1996; Hall, 2010). The ice-cored moraine system develops from  
424 a single polygenic ridge in the southern edge to a sequence of twelve ridges in its northern  
425 fringe next to Robbery beaches (Ruiz-Fernández et al., 2016). These ice-cored moraines

426 are similar to those described in other areas of the AP region (Hambrey et al., 2015). As  
427 for Hurd and Fildes peninsulas, Martínez de Pisón et al., (1996) proposed also a  
428 synchronicity between the timing of formation of raised beaches and moraines in the  
429 Byers Peninsula.

430 The objective of the geomorphological research was to explore the existence of moraines  
431 disconnected from the glacier front of the Roch Dome Glacier, which would suggest the  
432 occurrence of neoglacial advances. Roch Dome Glacier moraines include sediments  
433 transported by the glacier from the interior of the island, and, therefore, are mostly  
434 composed of basalts. We sampled some of these moraine boulders to apply CRE dating  
435 using *in situ*  $^{36}\text{Cl}$ . These moraines transgressed raised beaches whose age is already well  
436 constrained (Hall 2003 and 2010) and provide a minimum age for the development of the  
437 moraines that lay on them. In addition, researchers already identified the existence of ice-  
438 rafted granite boulders on these raised beaches (Hall and Perry, 2004). These boulders  
439 were sampled to be dated using the *in situ*-produced  $^{10}\text{Be}$  dating method to study their  
440 possible chronological relationship with the sampled moraine. Finally, we collected  
441 samples from glacially polished bedrock surfaces close to the present glacier front for  
442  $^{36}\text{Cl}$  dating in order to date the glacier retreated from this position.

### 443 3.2. CRE sampling and analytical procedures

444 During the fieldwork campaign, a total of 12 samples were taken from glacially polished  
445 outcrops and >1-m-diameter erratic/moraine boulders by means of hammer and chisel.  
446 We focused on flat gentle surfaces on the top of the boulders/outcrops and avoided steep  
447 surfaces and sharp crests in order to ensure the optimal cosmic-ray flux reception. We  
448 selected the most stable boulders, which were rooted in the moraines, with no signs of  
449 spalling or fracturing and that could not have been deposited through gravitational  
450 processes from rock walls. The thickness of the samples ranged from 1.8 to 4.5 cm (Table  
451 4). Following the sample collection, they were crushed and sieved to the 0.25-1 mm  
452 fraction at the “Physical Geography Laboratory” of the Complutense University of  
453 Madrid. Then the samples were physically and chemically processed at the “Laboratoire  
454 National des Nucléides Cosmogéniques” (LN2C) of the “Centre Européen de Recherche  
455 et d’Enseignement des Géosciences de l’Environnement” (CEREGE, Aix-en-Provence,  
456 France). As the sampled surfaces were constituted both by basaltic and granitic rocks  
457 (Table 4), samples were processed for measurement of the *in situ* cosmogenic nuclides  
458  $^{36}\text{Cl}$  (10 samples) and  $^{10}\text{Be}$  (2 samples) by accelerator mass spectrometry (AMS),



459 respectively.

460 In the case of the  $^{36}\text{Cl}$ , the sample preparation procedures were similar to those described  
461 in [Schimmelpfennig et al. \(2011\)](#). Magnetic separation was performed on one sample  
462 (BYC-10) to isolate the abundant feldspar minerals for  $^{36}\text{Cl}$  extraction by discarding the  
463 magnetic minerals with a magnetic separator “Frantz LB-1”.  $^{36}\text{Cl}$  extraction from whole  
464 rock was conducted for the other 9 samples, which had insufficient amounts of feldspar  
465 minerals. In both cases, aliquots of untreated bulk sample were taken to determine the  
466 sample composition (major and trace elements; Table 5). Samples with initial weights of  
467 120 g were rinsed and shaken with ultrapure water for 3 hours to remove dust and fines.  
468 After that, between 40 and 50% of the initial weight was dissolved with a mixture of  
469 diluted nitric acid (10%  $\text{HNO}_3$ ) and concentrated hydrofluoric acid (48% HF) in order to  
470 remove atmospheric  $^{36}\text{Cl}$  and potentially Cl-rich groundmass. After this partial  
471 dissolution, the remaining etched sample mass was rinsed and dried, and 2-g aliquots  
472 were taken to determine the major element concentrations (Table 6). Compositional  
473 analyses of all aliquots were performed at the “Service d’Analyse des Roches et des  
474 Minéraux” (SARM, CRPG, Nancy, France). Before total dissolution,  $\sim 260\ \mu\text{L}$  of a  $^{35}\text{Cl}$   
475 carrier (spike: 010813(4),  $6.92\ \text{mg Cl g}^{-1}$ ,  $^{35}\text{Cl}/^{37}\text{Cl}$  ratio 917.75) manufactured in-house  
476 were added to the samples for isotopic dilution ([Ivy-Ochs et al., 2004](#)), allowing for  
477 simultaneous determination of the  $^{36}\text{Cl}$  and Cl concentrations from the  $^{36}\text{Cl}/^{35}\text{Cl}$  and  
478  $^{35}\text{Cl}/^{37}\text{Cl}$  measurements. For the total dissolution of the rock samples, a mixture of 9 mL  
479 of 10%  $\text{HNO}_3$  per gram of sample and 4.5 mL of 48% HF per gram of sample was used.  
480 After the total dissolution, the samples were centrifuged to discard the undissolved  
481 residues and gel (fluoride complexes,  $\text{CaF}_2$ ). Then, the chlorine in the liquid solution was  
482 precipitated to silver chloride ( $\text{AgCl}$ ) by adding 2 ml of a silver nitrate ( $\text{AgNO}_3$ ) solution  
483 at 10%. To achieve this, samples were stored for 2 days in a dark place to allow the  $\text{AgCl}$   
484 to settle down on the bottom of the bottles. This enabled the extraction of the supernatant  
485 solution (excess HF and  $\text{HNO}_3$ ) by a peristaltic pump avoiding the disturbance of the  
486  $\text{AgCl}$  precipitate. In the next step, aiming to reduce the isobaric interferences of  $^{36}\text{S}$   
487 throughout the  $^{36}\text{Cl}$  measurements in the Accelerator Mass Spectrometer (AMS) sulphur  
488 was removed in the form of barium sulphate ( $\text{BaSO}_4$ ) obtained after the re-dissolution of  
489 this first  $\text{AgCl}$  precipitate and the addition of 1 mL of a saturated solution of barium  
490 nitrate ( $\text{Ba}(\text{NO}_3)_2$ ).  $\text{BaSO}_4$  was discarded by centrifuging and filtering the supernatant  
491 with a syringe and an acrodisc filter. Then,  $\text{AgCl}$  was precipitated again with 3-4 mL of

492 diluted HNO<sub>3</sub> (1:1 vol.). The precipitate was collected after centrifuging, and was rinsed  
493 and finally dried in the oven at 80 °C for 2 days. Once the AgCl precipitate was  
494 completely dried, it was loaded in cathodes. Subsequently, targets were stored in the oven  
495 in order to protect them from atmospheric humidity until they were measured by AMS.

496 For the <sup>10</sup>Be extraction, the processing started with the quartz isolation from the bulk rock.  
497 Magnetic minerals were discarded by using the magnetic separator “Frantz LB-1”. After  
498 that, the non-magnetic fraction was chemically attacked at successive rounds with a  
499 mixture of concentrated hydrochloric (1/3 HCl) and hexafluorosilicic (2/3 H<sub>2</sub>SiF<sub>6</sub>) acids  
500 aiming to dissolve non-quartz minerals. Then, the remaining minerals were  
501 decontaminated from meteoric <sup>10</sup>Be by means of three successive partial dissolutions with  
502 concentrated HF, which also dissolved the remaining impurities from the previous step.  
503 The samples yielded 60-80 g of purified quartz (Table 7). Before the total dissolution,  
504 150 µL of a <sup>9</sup>Be carrier solution (concentration: 3025 ± 9 µg g<sup>-1</sup>; [Merchel et al., 2008](#))  
505 manufactured in-house from a phenakite crystal were added to the samples. Quartz was  
506 totally dissolved in 48 % HF (3.6 mL per g of quartz + 30 mL in excess). The resulting  
507 solutions were evaporated until dryness and samples were recovered with hydrochloric  
508 acid. Subsequently samples were precipitated with ammonia before successive  
509 separations through an anion exchange column (Dowex 1X8) to remove iron and a cation  
510 exchange column (Dowex 50WX8) to discard boron (isobar) and recover Be (Merchel  
511 and Herpers, 1999). Finally, the eluted Be was precipitated to Be(OH)<sub>2</sub> with ammonia and  
512 oxidized to BeO at 700 °C. The targets were prepared by mixing Niobium powder with  
513 the BeO oxide for AMS measurements.

514 The final AgCl and BeO targets were analysed at the AMS facility ASTER “Accélérateur  
515 pour les Sciences de la Terre, Environnement et Risques” at CEREGE to measure the  
516 specific isotope ratios for <sup>36</sup>Cl (<sup>35</sup>Cl/<sup>37</sup>Cl and <sup>36</sup>Cl/<sup>35</sup>Cl) and <sup>10</sup>Be (<sup>10</sup>Be/<sup>9</sup>Be) dating. The  
517 <sup>36</sup>Cl measurements were normalized to the in-house standard SM-CL-12 with an assigned  
518 <sup>36</sup>Cl/<sup>35</sup>Cl ratio value of (1.428 ± 0.021) × 10<sup>-12</sup> ([Merchel et al., 2011](#)) and assuming a  
519 natural <sup>35</sup>Cl/<sup>37</sup>Cl ratio of 3.127. The <sup>10</sup>Be measurements were calibrated against the in-  
520 house standard STD-11, using an assigned <sup>10</sup>Be/<sup>9</sup>Be ratio of (1.191 ± 0.013) × 10<sup>-11</sup>  
521 ([Braucher et al., 2015](#)). Analytical 1σ uncertainties include uncertainties in AMS counting  
522 statistics, the standard <sup>10</sup>Be/<sup>9</sup>Be ratio, an external AMS error of 0.5% (Arnold et al., 2010)  
523 and a chemical blank measurement. A <sup>10</sup>Be half-life of (1.387 ± 0.0012) × 10<sup>6</sup> years was  
524 used ([Chmeleff et al., 2010](#); [Korschinek et al., 2010](#)).

525 We calculated  $^{36}\text{Cl}$  ages using two different procedures. On the one hand, the Excel™  
526 spreadsheet for *in situ*  $^{36}\text{Cl}$  exposure age calculations designed by Schimmelpfennig et al.  
527 (2009), as it allows using different  $^{36}\text{Cl}$  production rates from spallation. In this case, the  
528 elevation-latitude scaling factors were based on the time invariant “St” scheme (Stone,  
529 2000). The production rate of epithermal neutrons for fast neutrons in the atmosphere at  
530 the land/atmosphere interface was  $696\pm 185$  neutrons  $(\text{g air})^{-1} \text{ yr}^{-1}$  (Marrero et al., 2016).  
531 The high-energy neutron attenuation length value applied was  $160 \text{ g cm}^{-2}$ . We used the  
532 following  $^{36}\text{Cl}$  production rates –references to sea-level and high latitude (SLHL)– from  
533 spallation of different elements:  $42.2\pm 4.8$  atoms  $^{36}\text{Cl} (\text{g Ca})^{-1} \text{ yr}^{-1}$  for Ca spallation  
534 (Schimmelpfennig et al., 2011),  $148.1\pm 7.8$  atoms  $^{36}\text{Cl} (\text{g K})^{-1} \text{ yr}^{-1}$  for K spallation  
535 (Schimmelpfennig et al., 2014),  $13\pm 3$  atoms  $^{36}\text{Cl} (\text{g Ti})^{-1} \text{ yr}^{-1}$  for Ti spallation (Fink et al.,  
536 2000),  $1.9\pm 0.2$  atoms  $^{36}\text{Cl} (\text{g Fe})^{-1} \text{ yr}^{-1}$  for Fe spallation (Stone et al., 2005). On the other  
537 hand, we calculated the  $^{36}\text{Cl}$  exposure ages using the trial version of the online calculator  
538 CREp for  $^{36}\text{Cl}$  (Schimmelpfennig et al., 2019), where the “LSD” (Lifton-Sato-Dunai)  
539 elevation latitude scaling scheme was implemented, together with the LSD geomagnetic  
540 database framework (Lifton et al., 2014) and the same production rates from the spallation  
541 of the abovementioned elements. As Ca spallation is the most dominant  $^{36}\text{Cl}$  production  
542 reaction and the Schimmelpfennig et al. (2011) production rate was calibrated at the Etna  
543 volcano (i.e. an area with a different atmospheric setting from the Antarctica sampling  
544 sites), we corrected the atmospheric pressure of the sampling sites. South Shetland Islands  
545 are affected by permanent subpolar low-pressure systems, which affect the cosmic-ray  
546 particle flux so that it influences (i.e. increases) the local cosmogenic nuclide production  
547 rate. Consequently, this atmospheric pressure anomaly has to be taken into account when  
548 scaling the SLHL production rates. In fact, Dunai (2010) advises including any long-term  
549 atmospheric pressure anomaly at least for Holocene exposure periods. Thus, the  
550 atmospheric pressure value was corrected for the elevation of each sampling site by  
551 implementing the ERA40 (Uppala et al., 2005) atmosphere model using the MATLAB  
552 function “ERA40.mat” (Lifton et al., 2014). The specific Antarctica atmosphere model  
553 (Stone, 2000) was not used as the atmosphere in continental Antarctic is affected by the  
554 air flow over the ice-sheet, which impacts the elevation/air pressure relationship in the  
555 opposite way (thermal high pressure at surface level). The  $^{36}\text{Cl}$  ages that will be presented  
556 and discussed throughout this work are those obtained from the “LSD” scaling scheme  
557 so that they are comparable to the  $^{10}\text{Be}$  ages.

558 Finally,  $^{10}\text{Be}$  exposure ages were calculated by using the online calculator “CREp”  
559 (Martin et al., 2017; available online at: <http://crep.crpq.cnrs-nancy.fr/#/>). In this  
560 calculator, we applied again the “LSD” elevation latitude scaling scheme (Lifton et al.,  
561 2014), the ERA40 atmospheric model (Uppala et al., 2005) and the geomagnetic database  
562 based on the LSD framework (Lifton et al., 2014). These parameters yield a SLHL  $^{10}\text{Be}$   
563 production rate from Be spallation of  $3.98\pm 0.22$  atoms  $\text{g}^{-1} \text{yr}^{-1}$ .

564 We include the results, with total error and analytical errors in Table 7 and Fig. 3. In the  
565 text and in the figures we show the results with the total error. We do not have any  
566 quantitative information on the snow cover during the surface exposure duration.  
567 Therefore, samples were taken from surfaces that are exposed to strong winds, in order  
568 to limit the potential effects of prolonged snow cover on the cosmogenic nuclide  
569 production. We also avoided surfaces that showed signs of significant erosion or spalling.  
570 In addition, denudation rates in Antarctica are reported to be extremely low (0-1 m/Ma;  
571 e.g. Schäfer et al., 1999, Balco et al., 2014), thus having no significant effect on the  
572 Holocene exposure ages. Hence, no corrections for potential effects of snow cover or  
573 denudation were applied to the ages, in consistency with other studies from this region  
574 (e.g. Ciner et al., 2019).

575

## 576 **6. Results of the timing of neoglacial advance in the Byers Peninsula**

### 577 *6.1 Geomorphological setting of neoglacial landforms*

578 The ice-cored moraine system in the present front of the Roch Dome Glacier is formed  
579 by sharp-crested ridges standing 50 to 70 m above the adjacent bedrock surface, with  
580 blocks  $>1$  m in diameter (Fig. 4, 5 and 6). The extensive debris cover has a very high ice  
581 proportion, exceeding 60% of the total volume, according to field observations. The  
582 sediments are distributed in the direction of the glacier’s foliation and its lithology reflects  
583 that of the basalt bedrock, which indicates that the moraine results from basal and  
584 englacial debris. From the moraine crests, a steep ramp of ice ( $40^\circ$  slope) descends to the  
585 southern side of the peninsula. The unconsolidated sediments of the moraines are  
586 currently being intensely reworked by mass wasting processes, and are thus not  
587 appropriate for surface exposure dating methods (lichenometry or CRE).

588 This ice-cored moraine ridge overrides all raised beaches from the central plateau to the  
589 6 m a.s.l. raised beach in the N and S coastal fringes (Fig. 4). Our research focuses on the

590 southern sector of the moraine system, where it overlaps the raised beaches until the Clark  
591 Nunatak. Just SW of this nunatak, a small peninsula – called Rish Point – formed by a  
592 series of volcanic plugs stands only at 60 m from the coast line (Fig. 4, 5 and 6).

593 Next to the highest volcanic plug of the area (Ritli Hill, 45 m) (Fig. 4, 5, 6 and 7), we  
594 observed a glacial polished surface at an elevation of 28 m, and a distance of 600 m  
595 southwards of the present moraine ridge. Here, we collected the bedrock sample BYC-1.  
596 On another volcanic plug, only 350 m from the moraine ridge and at elevation of 47 m,  
597 another polished surface was observed with an erratic on it. Samples were taken from  
598 bedrock surface BYC-2 and from the erratic boulder BYC-3.

599 On the western side of the Clark Nunatak, the ice ramp descending from the external part  
600 of the ice-core moraine ridge does not connect with the bedrock surface but to thick layers  
601 of till, which rest on the 10-12 m a.s.l. raised beach. At the connection between the till  
602 deposits and the raised beach, there is a group of large, stable erratic glacial boulders,  
603 aligned parallel to the limit of the glacier. This line of erratic boulders is located about  
604 200 m to the S of the present glacier front and lies on the 10-12 m a.s.l. beach. These  
605 boulders are basalts and we assume that were deposited by Dome Rotch glacier during a  
606 small advance, when it trespassed the 10-12 m a.s.l. beach. The five largest and most  
607 stable basaltic boulders were selected from this line to take samples for <sup>36</sup>Cl dating (BYC-  
608 9, 10, 11, 13 and 14) (Fig. 5, 6, 8). In addition to the erratic basaltic boulders that rest on  
609 the 10-12 m a.s.l. raised beach, there are some granite boulders that were embedded in the  
610 sediments of this raised beach protruding around a meter above the beach sand level. We  
611 assume that these granitic boulders were transported by icebergs from the AP during the  
612 beach formation, as there are no granitic rocks in Byers bedrock (Hall and Perry, 2004).  
613 We sampled two of the ice rafted granitic boulders (BYB-10 and BYC-12) (Fig. 4, 5, 6,  
614 8 and 9). We assume that the ice-rafted boulders have been stable since they were  
615 deposited on the beach, and therefore CRE ages of these boulders must coincide with the  
616 age of formation of the beach where they are distributed.

617 On the other hand, there is a moraine ridge surrounding the W side of Clark Nunatak and  
618 with the eastern extreme of Rish Point, which trespassed the 4-6 m a.s.l. raised beach.  
619 This is one of the few sites in the Byers Peninsula where the current front of the glacier  
620 is separated from the ice-core moraine crest (distance of ca. 500 m). This moraine is  
621 formed by several crests and arcs that overlap one another. The youngest arcs constitute  
622 ice-cored moraine ridges and are very unstable and subject to mass movements and

623 intense remobilization. The outer most crests are stable. Two boulders from this stable  
624 older sector of the moraine were selected for CRE samples (BYC-4 and 5), located at  
625 elevation of 35 m (Fig. 4, 5, 6, and 10).

## 626 *6.2 CRE results*

627 CRE results show a complex spatio-temporal pattern with regards to the glacial evolution  
628 during the Mid-Late Holocene in the Byers Peninsula.

629 The oldest ages correspond to the deglaciation of the Rish Point. Samples BYC-1 and 2  
630 on the two polished surfaces located on the summit of volcanic plugs reported the same  
631  $^{36}\text{Cl}$  age of  $10.4 \pm 1.2$  and  $10.3 \pm 1.3$  ka. The erratic boulder BYC-3 deposited on the same  
632 polished surface as BYC-2 yielded a slightly younger  $^{36}\text{Cl}$  age of  $9.1 \pm 1.1$  ka. The  
633 arithmetic mean of these three samples is  $9.9 \pm 1.2$  ka ( $n=3$ ) (Fig. 3, 4, 5, 6 and Table 7).

634 The samples taken from the erratic boulders lying on the 10-12 m a.s.l. raised beach  
635 (BYC-9, 10, 11, 13 and 14) yielded the following  $^{36}\text{Cl}$  ages:  $3.0 \pm 0.7$ ,  $4.2 \pm 0.6$ ,  $3.6 \pm 0.6$ ,  
636  $4.7 \pm 0.6$  and  $3.6 \pm 0.7$  ka, respectively. The arithmetic mean is  $3.8 \pm 0.6$  ka ( $n=5$ ). The  
637 ages of the granitic boulders embedded in the 10-12 m a.s.l. raised beach (BYB-10) and  
638 on the littoral platform (BYC-12) give  $^{10}\text{Be}$  ages of  $3.5 \pm 0.4$  ka and  $5.5 \pm 0.4$  ka,  
639 respectively, with an arithmetic mean of  $4.4 \pm 0.4$  ka ( $n=2$ ). In fact all this ages are  
640 indistinguishable from each other with an average of  $4.1 \pm 0.5$  ka ( $n=7$ ) (Fig. 3, 4, 5, 6 and  
641 Table 7).

642 The two boulders distributed on the moraine from the eastern flank of the Clark Nunatak  
643 where the front of the glacier has significantly retreated over the last decades (BYC-4 and  
644 5) showed similar  $\text{Cl}^{36}$  ages of  $1.1 \pm 0.3$  and  $0.8 \pm 0.2$  ka, respectively. The mean is  $1.0 \pm$   
645  $0.2$  ka ( $n=2$ ) (Fig. 3, 4, 5, 6 and Table 7).

## 646 **7. Discussion**

### 647 *7.1 Analysis of the results in the context of the SSI and the AP*

648 The here presented first CRE dates from the Byers Peninsula indicate the existence of  
649 three different periods concerning glacier evolution in the area. The first group of  
650 landforms correspond to the polished surfaces and the erratic boulder located in Rish  
651 Point. These samples are indicative of the northwards retreat of Rotch Dome Glacier,  
652 which occurred at around 11-9 ka ( $9.9 \pm 1.2$  ka;  $n=3$ ). This ice-free corner was deglaciated  
653 prior to the oldest raised beaches distributed at 15-16 m a.s.l. that were dated at 7.4 cal ka



654 BP in the Byers Peninsula (Hall 2003; 2010). The age of these landforms fits also with  
655 the chronological framework of deglaciation inferred from lake records in this peninsula,  
656 suggesting that the initial deglaciation of the central plateau took place at 8.3 cal ka BP  
657 (Toro et al., 2013; Oliva et al., 2016). The Early Holocene deglaciation of coastal  
658 environments also occurred between 9 and 6 ka in the rest of the SSI (Barsch and  
659 Mäusbacher, 1986; Mäusbacher, 1991; Del Valle et al., 2002; Hall, 2003; Bentley et al.,  
660 2005; Hall, 2010; Watcham et al., 2011), or even before 9 ka (Milliken et al., 2009; Seong  
661 et al., 2009; Simms et al., 2011). This timing also coincides with data from other records  
662 from the AP, such as marine sediments, which show a clear warming trend beginning 12  
663 ka ago (Shevenell et al., 2011), as well as from CRE dating of glacial landforms in this  
664 peninsula (White et al., 2011; Glasser et al., 2014; Anderson et al., 2017) (Fig. 11).

665 A second group of landforms includes glacial basaltic boulders distributed on the beach  
666 and littoral platform at 10-12 m a.s.l (BYC 9, 10, 11, 13 and 14) and the two ice rafted  
667 granitic boulders embedded in the sediments of this raised beach (BYB 10) or located on  
668 the same littoral platform (BYC 12). The results obtained show very similar ages for all  
669 types of boulders, both basalts and granites, with an average of  $4.1 \pm 0.5$  ka ( $n=7$ ).  
670 Therefore, the ages of the stabilization of these boulders transported by the Rotch Dome  
671 Glacier should correspond to the age of this beach level, where ice rafted granitic boulders  
672 are embedded. Radiocarbon dating from whale bones of similar altitude raised beach in  
673 the South Beaches, suggested younger ages, between 2.6 and 2 cal ka BP (Hansom, 1979;  
674 Hall and Perry, 2004; Hall, 2003, 2010). These data coincide with OSL dates of this level  
675 of raised beaches from other islands in this archipelago, between 2.3 and 2.1 ka (Simms  
676 et al., 2011a and 2012). Our results from the ice-drafted granitic boulders indicated older  
677 ages for this raised beach,  $4.4 \pm 0.4$  ka ( $n=2$ ), which are synchronous with the glacial  
678 boulders that are distributed on it. There is a lack of correspondence between the older  
679 ages of the erratic and ice-rafted boulders and the former much younger radiocarbon dates  
680 attributed to this raised beach. To understand this apparent contradiction, it is important  
681 to highlight that there is no direct dating of the raised beach in the area. Landforms at  
682 similar altitudes within the same region do not necessarily have identical chronologies,  
683 as glacio-isostatic uplift rates enhanced also by neotectonic activity vary throughout the  
684 archipelago (Bentley et al., 2005; Fretwell et al., 2010; Simms et al., 2018). In fact, it  
685 seems reasonable that the raised beach at +10-12 m a.s.l where the erratic boulders are  
686 distributed may constitute an intermediate level between the raised beach dated at 2.6 and

687 2 cal ka BP in other sectors of the SSI and the highest raised beach of +15-17 m a.s.l.,  
688 which was dated at 7.4 cal ka BP in different areas of this archipelago (Fig. 11).

689 The ages of glacial boulders prove the existence of a neoglacial advance in the Byers  
690 Peninsula occurred ~4 ka. Until now, no such advance had been proposed, although [Hall  
691 and Perry \(2004\)](#) related the 10 m raised beach to a cold period with abundant rich ice-  
692 rafted debris, and [Everett \(1971\)](#) proposed the same for the 10-12 m a.s.l. raised beach  
693 existing in the Hurd Peninsula. Previous studies proposed that the glacier fronts in the  
694 Byers Peninsula, as well as in the rest of the SSI, were approximately at their present-day  
695 position by 5.5 ka ([Barsch and Mäusbacher, 1986; Mäusbacher et al., 1989; Björck et al.,  
696 1991, 1993, 1996b; Mäusbacher, 1991; Del Valle et al., 2002; Hall, 2003, 2010; Bentley  
697 et al., 2005; Watcham et al., 2011; Simms et al., 2011a and 2012; Toro et al., 2013; Oliva  
698 et al., 2016](#)). Our results highlight the occurrence of a limited neoglacial advance at ~4  
699 ka not exceeding 200 m from the present-day glacier front. Consequently, due to the small  
700 extent of this neoglacial expansion, it may have not been detected yet in other areas. There  
701 is evidence of a cold period in the SSI before 4 ka according to the analysis of lake ([Björck  
702 et al., 1991](#)) and marine sediments ([Milliken et al., 2009; Chu et al., 2017](#)). In the context  
703 of the entire AP area and the rest of the continent, as discussed above, there is robust  
704 paleoenvironmental evidence that colder conditions with neoglacial associated advances  
705 occurred around 5 ka and were interrupted by the thermal maximum around 4-3 ka ([Zale  
706 and Karlén, 1989; Mosley-Thompson, 1996; Ingólfsson et al., 1998, 2003; Khim et al.,  
707 2002; Strelin et al., 2006; Heroy et al., 2008; Bentley et al., 2009; Hall, 2009; Michalchuk  
708 et al., 2009; Davies et al., 2012; Shevenell et al., 2011; Carrivick et al., 2012; Cofaigh et  
709 al., 2014, \[Barnard et al., 2014; Davies et al., 2017; Kaplan et al., 2020\]\(#\)\) \(Fig. 11\).](#)

710 The last set of glacial landforms corresponds to the moraine ridges of the Rotch Dome  
711 Glacier on the southern flank of Clark Nunatak. This is the only area where the glacier is  
712 now spatially disconnected from the moraine and includes evidence of a Late Holocene  
713 advance of the glacier around the nunatak. Till and disperse erratic boulders are  
714 distributed on the 4-6 m a.s.l. raised beach. The BYC-4 and 5 samples were taken from  
715 the highest and most stable sector of the moraine showing an average age of ~1. ka.  
716 Although, to date, a similar advance has not been confirmed during this time in the SSI,  
717 there is some sedimentological evidence pointing to that fact. [Barsch and Mäusbacher  
718 \(1986\)](#) suggested two neoglacial advances at 3 and 1 cal ka BP in the SSI. [Björck et al.  
719 \(1991\)](#) proposed a cold period in the Byers Peninsula between 1.5 and 0.5 cal ka BP. [Hall](#)

720 and Perry (2004) delimited two cold periods at 0.25 and 1.7 cal ka BP. Hall (2009) used  
721 the CRE <sup>10</sup>Be methodology to date moraines in the Hurd Peninsula and Marion Cove to  
722 1.5–1.0 ka (Hall and Stone, personal communications). Simms et al. (2011a) indicated a  
723 neoglacial advance that ended at approximately 1.7 cal ka BP in Maxwell Bay (King  
724 George Island). Lake Domo, which is very close to the study area and located only 350  
725 m from the present-day glacier front, was deglaciated around 1.8 cal ka BP, probably after  
726 a neoglacial advance (Oliva et al., 2016). Chu et al. (2017) proposed the onset of  
727 neoglacial advances in the Fildes Peninsula at 2.7 cal ka BP. As discussed before, plentiful  
728 evidence from the AP confirm the occurrence of glacial advances between 2.8 and 1.4 ka  
729 (Mosley-Thompson, 1996; Björck et al., 1996; Khim et al., 2002; Heroy et al., 2008;  
730 Bentley et al., 2009; Yoon et al., 2010; Domack et al., 2001; Strelin et al., 2006;  
731 Michalchuk et al., 2009; Allen et al., 2010; Davies et al., 2012; Mulvaney et al., 2012;  
732 Shevenell et al., 2011; Mulvaney et al., 2012; Abram et al., 2013; Hodgson et al., 2013;  
733 Barnard et al., 2014; Davies et al., 2014; Čejka et al., 2019 and Kaplan et al., 2020) (Fig.  
734 11).

735 As in previous glacial landforms, the ages of the moraine boulder (~1.0 ka) contradict the  
736 age of the raised beach where they rest (LIA). In fact, this raised beach at about 6 m a.s.l.  
737 has been dated in the Byers Peninsula and other islands as belonging to the LIA, between  
738 approximately the 13 and 17th centuries AD (Everett, 1971; John and Sugden, 1971;  
739 John, 1972; Sugden and John, 1973; Curl, 1980; Sugden and Clapperton, 1986;  
740 Clapperton and Sugden, 1988; Hall, 2007; Hall, 2010; Simms et al., 2011a and 2012)  
741 (Fig. 11).

742 The only place where a moraine similar to the one studied in this work has been directly  
743 dated in the SSI was the Collins Glacier moraine in the Fildes Peninsula by Hall (2007),  
744 according to radiocarbon ages of mosses incorporated into the interior of the moraine. As  
745 in our study area, this sector of moraine was almost the only area where the moraine was  
746 separated from the present Collins Glacier front, and was also at a distance of about 500  
747 m. The first results of this work indicated that the most external advance was 2.8 to 1 cal  
748 ka BP, although Hall (2007) discards this possibility, precisely because the moraine rests  
749 on the 6 m a.s.l. beach.

750 The discordance between the ages of the moraines dated by CRE ages and the ages of  
751 raised beaches provided by radiocarbon dating of organic fragments present in their sands  
752 will remain a topic of debate until we directly date the studied raised beaches instead of

753 basing their age on a simple correlation of altitudes. This approach could lead to important  
754 errors related to the regional variability and local neo-tectonics (Bentley et al., 2005;  
755 Fretwell et al., 2010; Simms et al., 2018).

756 The results suggest that these younger moraines may be somewhat older than the LIA, as  
757 previously thought (Everett, 1971; John and Sugden, 1971; John, 1972; Sugden and John,  
758 1973; Curl, 1980; Sugden and Clapperton, 1986; Clapperton, and Sugden, 1988; Hall,  
759 2007; Hall, 2010). Our proposal is that they are polygenic moraines formed by several  
760 neoglacial advances driven by cold periods that may have expanded from 2 ka to the LIA,  
761 as has been proposed in many other areas of the AP (Zale and Karlén, 1989; Domack et  
762 al., 2001; Hall and Denton, 2002; Allen et al., 2010; Storey et al., 2010; Michalchuk et  
763 al., 2009; Balco et al., 2013; Davies et al., 2014; Davies et al., 2017). In fact, although the  
764 outermost crest of the moraine dates back to ~1.0 ka, based on our results (Fig. 4), the  
765 glacier must have retreated from the moraine limits very recently, probably after 1950, as  
766 occurred in the nearby peninsula of Elephant Point (Oliva and Ruiz-Fernández, 2015,  
767 2017) (Fig. 11).

768 The available proxy data for the Mid and Late Holocene does not yet allow to constrain  
769 which climate parameters are responsible for such glacial oscillations. Bentley et al.  
770 (2009) provided evidence of the occurrence of relative warmth from 4.5 to 2 cal. ka BP  
771 in the AP region, which is also confirmed by ice core records from the NE corner of the  
772 AP reporting relative stable temperature until 2.5 ka BP when climate cooled (Mulvaney  
773 et al., 2012). Past surface air temperature changes are similar to those inferred from  
774 several sites across the AP from moss banks (Charman et al., 2018).

## 775 *7.2 The Neoglaciation of the SSI and the AP in a global context*

776 Despite significant regional variations in the timing of Neoglaciation in the AP, there are  
777 some common patterns in all records: the end of maximum deglaciation occurred at  
778 around 7-6 ka and the first neoglacial started at 5 ka, with new and previously undated  
779 neoglacial advances between 2.7 and 1 ka, and even up to the LIA, before the RRW. Most  
780 records in the SSI are not concurrent with neoglacial timing in the AP. This can be related  
781 to the different nature of the records and dating methods used in each study. In fact, each  
782 of the proxies examined in this work (ice core, marine and lake sediments, raised beaches  
783 and glacial landforms) as well as the dating methods have been substantially refined over  
784 the last years and inter-comparisons between areas and methods are needed to  
785 homogenize and compare results (e.g. Simonsen et al., 2019; Singer et al., 2019; Sadatzki

786 [et al., 2019](#); [Čejka et al., 2019](#)). However, our data show that the chronology inferred  
787 directly from glacial landforms shows a similar timing for neoglacial advances in the SSI  
788 and the AP. Recently, [Kaplan et al. \(2020\)](#) highlighted synchronous millennial-scale  
789 neoglacial oscillations in the NE edge of the AP and in Patagonia. These authors proposed  
790 that these neoglacial advances coincided with negative phases of the Southern Annular  
791 Mode (SAM), when the westerly winds expanded towards the equator. In line with this,  
792 the current RRW coincides with a positive phase of the SAM that is favoring widespread  
793 glacial retreat in both regions ([Abram et al., 2014](#)).

794 The comparison of Neoglaciation in the AP with the Arctic records may reveal whether  
795 neoglacial advances follow interhemispheric connection between polar regions.  
796 However, neoglacial advances within the Arctic show a very different pattern, even more  
797 divergent than within the AP ([Solomina et al., 2015](#); [McKay, et al., 2018](#)). Throughout  
798 the Arctic, the end of deglaciation varied from 11 to 5 ka depending on the region  
799 ([Renssen et al., 2012](#)). The first phases of neoglacial advances were detected between 9  
800 to 7 ka in Scandinavia and 4 ka in Greenland ([Solomina et al., 2015](#); [McKay, et al., 2018](#)).  
801 In any case, there are also some common patterns for the entire Arctic, which are quite  
802 similar to those observed in the AP. According to the most recent synthesis, glaciers  
803 retreated throughout the Arctic from 8.6 to 5 ka ([Marcott et al., 2013](#); [Solomina et al.,](#)  
804 [2015](#); [Kaufman et al., 2016](#); [Sejrup et al., 2016](#); [Briner et al., 2016](#); [McKay, et al., 2018](#);  
805 [Geirsdóttir et al., 2019](#)), similarly to what happened in the SSI and the AP. After this  
806 widespread retreat, there are two main phases of generalized neoglacial expansion in  
807 (almost) all regions across the Arctic, one beginning at 4.5 ka and another from 2 ka to  
808 the LIA ([Solomina et al., 2015](#); [Miller et al., 2013](#); [Miller et al., 2017](#); [McKay, et al.,](#)  
809 [2018](#); [Geirsdóttir et al., 2019](#)). A similar timing for glacial advances was also identified  
810 in the SSI and the AP.

811 Therefore, there is a common global pattern at a millennia timescale with regards to the  
812 Neoglaciation dynamics in glaciers of the AP and in the Arctic. These patterns are similar  
813 to those found in the Byers Peninsula: intensive deglaciation around 8.6 to 5 ka, followed  
814 by the first neoglacial advances around 4.5 ka and new, intensive neoglacial advances  
815 around 2 ka. This Late Holocene glacier behavior in the high latitudes of both  
816 hemispheres is very different from the evolution of temperatures that occurred in the two  
817 regions during Termination I, when temperature changes were simultaneous but inverse  
818 in the two hemispheres, the pattern known as “bipolar seesaw” ([Broecker and Denton,](#)

1990; Barker et al., 2009, 2010). The opposite temperature trends recorded in Antarctica and Greenland during Termination I (seesaw pattern) have been confirmed by ice cores (Severinghaus and Brook, 1999; Brook and Buizert, 2018; Stolper et al., 2016) and are attributed to changes in the intensity of the Atlantic Meridional Overturning Circulation (AMOC, Baker et al., 2009, 2010). The cooling of the Northern Hemisphere reduces the strength of the AMOC (Deaney et al., 2017; Muschitiello et al., 2019), which, in turn, causes the ventilation of the Southern Hemisphere oceans and the emission of a large amount of CO<sub>2</sub> into the atmosphere, significantly warming Antarctica (Ahn et al., 2012; Beeman et al., 2019; Clementi and Sikes, 2019). Inverse temperatures between the two hemispheres during Termination I resulted in opposite behavior of the glaciers in each hemisphere (Jomelli et al., 2014; Darvill et al., 2016; Koffman et al., 2017; Shulmeister et al., 2019). However, this was not the case during the Holocene, mainly during Neoglaciation. The orbitally-forced changes in insolation are likely to be the main driver of Neoglaciation. In fact, negative Total Solar Irradiance anomalies are proposed as one of the main triggers of neoglacial advances into the large scale climatic transformations (Renssen 2006; Solomina et al., 2012), together with volcanic activity, which also played an important role in some of the neoglacial events (Miller et al., 2012, 2013). Both the HTM and the Neoglaciation are global-scale patterns, despite recording notable regional variability. This could be the critical difference with the current warm period (RRW), where the response of glaciers is almost global and synchronous (Renssen 2012; Solomina et al., 2012).

840

## 841 **7. Conclusions**

842 Establishing the chronology of deglaciation of ice-free areas in the AP region is of key  
843 importance in a changing climate scenario. To that purpose, we have reconstructed the  
844 calendar of the most recent glacial oscillations in the largest ice-free area in the SSI, the  
845 Byers Peninsula. Here, previous knowledge on the deglaciation was based on only a few  
846 radiocarbon dates from lake sediments that did not offer an accurate picture of the glacial  
847 evolution of the Mid-Late Holocene. We used CRE dating to examine the timing of  
848 neoglacial advances of Rotch Dome Glacier and compare it with other areas across the  
849 AP region.

850 Deglaciation of today's main ice-free areas in the SSI and the rest of the AP occurred  
851 between 9 and 6 ka, according to previous studies. After 6 ka, glaciers were similar or



852 smaller than their present-day size in most of the AP. The first neoglacial advance in this  
853 area took place from ~5.5 ka, followed by a warm period between 4 and 2.8 ka.  
854 Subsequently until 1.0 ka, there was another period of generalized neoglacial advance in  
855 the AP. In the SSI, there was evidence of cold periods from 5.8 to 5.6, and from 2.7 cal  
856 ka BP from some paleoclimatic proxies, but the glacial response to those climate shifts  
857 was still unknown. This study confirms that, as in other areas of the AP, glacial advances  
858 also occurred in the SSI during these Neoglaciation cold periods in ~4.1 and 1.0 ka.

859 The recent synthesis of glacial evolution in the Arctic since the Mid-Holocene shows that  
860 there was even larger regional diversity with regards to the chronology of neoglacial  
861 advances. In the Arctic, the regional climate forcings determine climate trends that can  
862 lead to glacial advance within a global tendency to warming. However, millennial-scale  
863 patterns between the Arctic and the AP region seem to follow common trends. This timing  
864 revealed by the neoglacial landforms should be taken into account when looking for the  
865 origin of climate changes that caused Neoglaciation, which was practically synchronous  
866 in both polar areas. Consequently, although the objective of this work was not to examine  
867 the origin and causes of Neoglaciation, we provide new evidence supporting a global  
868 background for neoglacial advances beyond hemispheric-scale factors, which would have  
869 favored neoglacial advances with different time ranges in both Polar Regions.

## 870 **Acknowledgements**

871 This paper was supported by the projects CTM2016-77878-P and CGL2015-65813-R  
872 (Spanish Ministry of Economy and Competitiveness), and NUNANTAR  
873 (02/SAICT/2017 – 32002; Fundação para a Ciência e a Tecnologia, Portugal). It also  
874 complements the research topics examined in the project PALEOGREEN (CTM2017-  
875 87976-P; Spanish Ministry of Economy and Competitiveness). We also thank the  
876 Portuguese Polar Program for their support in organizing field logistics. The <sup>10</sup>Be and  
877 <sup>36</sup>Cl measurements were performed at the ASTER AMS national facility (CEREGE, Aix  
878 en Provence), which is supported by the INSU/CNRS and the ANR through the “Projets  
879 thématiques d'excellence” program for the “Equipements d'excellence” ASTER-  
880 CEREGE action and IRD. David Palacios thanks to the Institute of Alpine and Arctic  
881 Research, at the University of Colorado, the facilities provided to coordinate this work  
882 during his Fulbright Grant stay there in 2019. Marc Oliva is supported by the Ramón y  
883 Cajal Program (RYC-2015-17597) and the Research Group ANTALP (Antarctic, Arctic,  
884 Alpine Environments; 2017-SGR-1102). We thank Dr. Vincent Jomelli, Dr. Jan-Hendrik

885 May one anonymous reviewers for their valuable suggestions that have greatly improved  
886 the paper.

887

888 **References**

- 889 Abram, N.J., Mulvaney, R., Wolff, E.W., Triest, J., Kipfstuhl, S., Trusel, L.D., ... & Arrowsmith, C. (2013).  
890 Acceleration of snow melt in an Antarctic Peninsula ice core during the twentieth century. *Nature*  
891 *Geoscience*, 6(5), 404. DOI: 10.1038/NGEO1787
- 892 Abram, N.J., Mulvaney, R., Vimeuz, F., Phipps, S.J., Turner, J., England, M.H., 2014. Evolution of the  
893 southern annular mode during the past millennium. *Nat. Cli-mate Change*4, 564–569.
- 894 Ahn, J., Brook, E.J.Schmittner, A., & Kreutz, K. (2012), Abrupt change in atmospheric CO<sub>2</sub> during the last  
895 ice age, *Geophys. Res. Lett.*, 39, L18711, DOI:10.1029/ 2012GL053018.
- 896 Alfaro, P., López-Martínez, J., Maestro, A., Galindo-Zaldívar, J., Durán-Valsero, J.J., & Cuchi, J.A. (2010).  
897 Recent tectonic and morphostructural evolution of Byers Peninsula (Antarctica): insight into the  
898 development of the South Shetland Islands and Bransfield Basin. *Journal of Iberian Geology* 36(1),  
899 21-38.
- 900 Allen, C.S., Oakes-Fretwell, L., Anderson, J.B., & Hodgson, D.A. (2010). A record of Holocene glacial  
901 and oceanographic variability in Neny Fjord, Antarctic Peninsula. *The Holocene*, 20(4), 551-564.  
902 DOI: 10.1177/0959683609356581
- 903 Almela, P., Velázquez, D., Rico, E., Justel, A., & Quesada, A. (2019). Carbon pathways through the food  
904 web of a microbial mat from Byers Peninsula, Antarctica. *Frontiers in microbiology*, 10, 628.  
905 <https://doi.org/10.3389/fmicb.2019.00628>
- 906 Anderson, J. T., Wilson, G. S., Fink, D., Lilly, K., Levy, R. H., & Townsend, D. (2017). Reconciling marine  
907 and terrestrial evidence for post LGM ice sheet retreat in southern McMurdo Sound, Antarctica.  
908 *Quaternary Science Reviews*, 157, 1-13. <https://doi.org/10.1016/j.quascirev.2016.12.007>
- 909 Araya, R., & Hervé, F. (1966). Estudio geomorfológico y geológico en las Islas Shetland del Sur Antártica.  
910 Instituto Antártico Chileno, N°8, Santiago, Chile. 76 pp.
- 911 Arche, A., López-Martínez, J., Serrano, J. & Martínez De Pisón, E. (1996). Marine landforms and deposits.  
912 In López-Martínez, J., Thomson, M.R.A. & Thomson, J.W., Eds. Geomorphological map of Byers  
913 Peninsula, Livingston Island. BAS GEOMAP series, sheet 5-a, 1:25 000, with supplementary text.  
914 Cambridge: British Antarctic Survey, 35-42.
- 915 Arnold, M., Merchel, S., Bourlès, D.L., Braucher, R., Benedetti, L., Finkel, R.C., Aumaître, G., Gott dang,  
916 A., Klein, M., 2010. The French accelerator mass spectrometry facility ASTER: Improved  
917 performance and developments. *Nuclear Instruments and Methods in Physics Research, Section*  
918 *B, Beam Interactions with Materials and Atoms*, 19th International Conference on Ion Beam  
919 Analysis 268, 1954–1959. <https://doi.org/10.1016/j.nimb.2010.02.107>
- 920 Balco, G., Schaefer, J. M., LARISSA group (2013). Exposure-age record of Holocene ice sheet and ice  
921 shelf change in the northeast Antarctic Peninsula. *Quaternary Science Reviews*, 59, 101-111. DOI:  
922 10.1016/j.quascirev.2012.10.022
- 923 Balco, G., Stone, J. O., Sliwinski, M. G., Todd, C. (2014). Features of the glacial history of the  
924 Transantarctic Mountains inferred from cosmogenic <sup>26</sup>Al, <sup>10</sup>Be and <sup>21</sup>Ne concentrations in  
925 bedrock surfaces. *Antarctic Science*, 26(6), 708-723. <https://doi.org/10.1017/S0954102014000261>
- 926 Bañón, M., Justel, A., Velázquez, D., & Quesada, A. (2013). Regional weather survey on Byers Peninsula,  
927 Livingston Island, South Shetland Islands, Antarctica. *Antarctic Science*, 25(2), 146-156.  
928 DOI:10.1017/S0954102012001046
- 929 Barker, S., Diz, P., Vautravers, M.J., Pike, J., Knorr, G., Hall, I.R., & Broecker, W.S. (2009).  
930 Interhemispheric Atlantic seesaw response during the last deglaciation. *Nature*, 457(7233), 1097.
- 931 Barker, S., Knorr, G., Vautravers, M.J., Diz, P., & Skinner, L.C. (2010). Extreme deepening of the Atlantic  
932 overturning circulation during deglaciation. *Nature Geoscience*, 3(8), 567.
- 933 Barnard, A., Wellner, J. S., & Anderson, J.B. (2014). Late Holocene climate change recorded in proxy

- 934 records from a Bransfield Basin sediment core, Antarctic Peninsula. *Polar Research*, 33(1), 17236.  
935 DOI: 10.3402/polar.v33.17236
- 936 Barsch, D., & Mäusbacher, R. (1986). New data on the relief development of the South Shetland Islands,  
937 Antarctica. *Interdisciplinary Science Reviews*, 11(2), 211-218. DOI: 10.1179/isr.1986.11.2.211
- 938 Beeman, C.J., Gest, L., Parrenin, F., Raynaud, D., Fudge, T.J., Buizert, C., & Brook, E.J. (2019). Antarctic  
939 temperature and CO<sub>2</sub>: Near-synchrony yet variable phasing during the last deglaciation. *Climate*  
940 *of the Past*, 15, 913-926, DOI: 10.5194/cp-15-913-2019.
- 941 Benayas, J., Pertierra, L., Tejado, P., Lara, F., Bermudez, O., Hughes, K. A., & Quesada, A. (2013). A  
942 review of scientific research trends within ASPA no. 126 Byers Peninsula, South Shetland Islands,  
943 Antarctica. *Antarctic Science*, 25(2), 128-145.
- 944 Bentley, M.J., Evans, D.J.A., Fogwill, C.J., Hansom, J.D., Sugden, D.E., & Kubik, P.W. (2007). Glacial  
945 geomorphology and chronology of deglaciation, South Georgia, sub-Antarctic. *Quaternary*  
946 *Science Reviews*, 26(5-6), 644-677. DOI:10.1016/j.quascirev.2006.11.019
- 947 Bentley, M.J., Hodgson, D.A., Smith, J.A., & Cox, N.J. (2005). Relative sea level curves for the South  
948 Shetland Islands and Marguerite Bay, Antarctic Peninsula. *Quaternary Science Reviews*, 24(10-  
949 11), 1203-1216. DOI:10.1016/j.quascirev.2004.10.004
- 950 Bentley, M.J., Hodgson, D.A., Smith, J.A., Cofaigh, C.O., Domack, E.W., Larter, R.D., ... & Hillenbrand,  
951 C.D. (2009). Mechanisms of Holocene palaeoenvironmental change in the Antarctic Peninsula  
952 region. *The Holocene*, 19(1), 51-69. DOI: 10.1177/0959683608096603
- 953 Bentley, M.J.; Hodgson, D.A. (2009). Antarctic Ice Sheet and climate history since the last Glacial  
954 Maximum. *Pages News*, 17(1), 28-29.
- 955 Bentley, M. J., Cofaigh, C. O., Anderson, J. B., Conway, H., Davies, B., Graham, A. G., ... & Mackintosh,  
956 A. (2014). A community-based geological reconstruction of Antarctic Ice Sheet deglaciation since  
957 the Last Glacial Maximum. *Quaternary Science Reviews*, 100, 1-9.  
958 <https://doi.org/10.1016/j.quascirev.2014.06.025>
- 959 Bertler, N.A.N., Mayewski, P.A., Carter, L. (2011). Cold conditions in Antarctica during the Little Ice Age  
960 e implications for abrupt climate change mechanisms. *Earth and Planetary Science Letters*, 308,  
961 41-51. DOI:10.1016/j.epsl.2011.05.021
- 962 Birkenmajer, K. (1995). Glacier retreat and raised marine beaches at Three Sisters Point, King George  
963 Island (South Shetland Islands, West Antarctica). *Bulletin of the Polish Academy of Sciences*, 43,  
964 135-41.
- 965 Birkenmajer, K. (1998). Quaternary geology at Potter Peninsula, King George Island (South Shetland  
966 Islands, West Antarctica). *Bulletin of the Polish Academy of Sciences*, 46, 9-20.
- 967 Birkenmajer, K. (2002). Retreat of Ecology Glacier, Admiralty Bay, King George Island (South Shetland  
968 Islands, West Antarctica), 1956–2001. *Bulletin of the Polish Academy of Sciences*, 50, 15-29.
- 969 Birkenmajer, K.. (1981). Raised marine features and glacial history in the vicinity of H. Arctowski Station,  
970 King George Island (South Shetland Islands, West Antarctica). *Bulletin of the Polish Academy of*  
971 *Sciences*, 29, 109-17.
- 972 Björck, S., Hakansson, H., Zale, R., Karlén, W. & Jónsson, B.L. (1991). A late Holocene lake sediment  
973 sequence from Livingston Island, South Shetland Islands, with palaeoclimatic implications.  
974 *Antarctic Science*, 3, 61-72.
- 975 Björck, S., Hakansson, H., Olsson, S., Barnekow, L. & Janssens, J. (1993). Palaeoclimatic studies in South  
976 Shetlands Islands, Antarctica, based on numerous stratigraphic variables in lake sediments. *Journal*  
977 *of Paleolimnology*, 8, 233-272.
- 978 Björck, S., Olsson, S., Ellis-Evans, C., Håkansson, H., Humlum, O., & de Lirio, J.M. (1996a). Late  
979 Holocene palaeoclimatic records from lake sediments on James Ross Island, Antarctica.  
980 *Palaeogeography, Palaeoclimatology, Palaeoecology*, 121(3-4), 195-220.
- 981 Björck, S., Hjort, C., Ingólfsson, Ó., Zale, R. & Ising, J. (1996b). Holocene glacial chronology from lake  
982 sediments. In López-Martínez, J., Thomson, M.R.A. & Thomson, J.W., Eds. *Geomorphological*  
983 *map of Byers Peninsula, Livingston Island. BAS GEOMAP series, sheet 5-a, 1:25 000, with*  
984 *supplementary text. Cambridge: British Antarctic Survey, 49-51.*

- 985 Braucher, R., Guillou, V., Bourlès, D.L., Arnold, M., Aumaître, G., Keddadouche, K., Nottoli, E., 2015.  
 986 Preparation of ASTER in-house  $^{10}\text{Be}/^9\text{Be}$  standard solutions. Nuclear Instruments and Methods in  
 987 Physics Research, Section B, Beam Interactions with Materials and Atoms, The Thirteenth  
 988 Accelerator Mass Spectrometry Conference 361, 335–340.  
 989 <https://doi.org/10.1016/j.nimb.2015.06.012>
- 990 Brightley, H. (2017). A Paleoclimate Reconstruction of the Little Ice Age to Modern Era Climate  
 991 Conditions in the Eastern Ross Sea, Antarctica as Captured in the RICE Ice Core. A thesis  
 992 submitted to Victoria University of Wellington in partial fulfilment of the requirements for the  
 993 degree of Master of Science in Geology, School of Geography, Environmental and Earth Sciences,  
 994 Victoria University of Wellington. <http://hdl.handle.net/10063/6394>
- 995 Briner, J.P., McKay, N.P., Axford, Y., Bennike, O., Bradley, R.S., de Vernal, A., ... & Jennings, A. (2016).  
 996 Holocene climate change in Arctic Canada and Greenland. *Quaternary Science Reviews*, 147, 340-  
 997 364.
- 998 Broecker, W.S. & Denton, G.H. (1990). The role of ocean-atmosphere reorganizations in glacial cycles.  
 999 *Quaternary Science Reviews*, 9, 305-341.
- 1000 Brook, E.J., & Buizert, C. (2018). Antarctic and global climate history viewed from ice cores. *Nature*,  
 1001 558(7709), 200.
- 1002 Carrivick, J.L., Davies, B.J., Glasser, N.F., Nývlt, D. (2012). Late Holocene changes in character and  
 1003 behaviour of land-terminating glaciers on James Ross Island, Antarctica. *Journal of Glaciology*,  
 1004 58, 1176-1190. DOI: 10.3189/2012JoG11J148
- 1005 Čejka, T., Nývlt, D., Kopalová, K., Bulínová, M., Kavan, J., Lirio, J. M., Coria, S.H. van de Vijver, B.  
 1006 2019. Timing of the Neoglacial onset on the north-eastern Antarctic Peninsula based on lacustrine  
 1007 archive from Lake Anónima, Vega Island. *Global and Planetary Change*, 184  
 1008 <https://doi.org/10.1016/j.gloplacha.2019.103050>.
- 1009 Charman, D.J., Amesbury, M.J., Roland, T.P., Royles, J., Hodgson, D.A., Convey, P., Griffiths, H., 2018.  
 1010 Spatially coherent late Holocene Antarctic Peninsula surface air temperature variability. *Geology*  
 1011 46, 1071–1074. <https://doi.org/10.1130/G45347.1>
- 1012 Chmeleff, J., von Blanckenburg, F., Kossert, K., Jakob, D., 2010. Determination of the  $^{10}\text{Be}$  half-life by  
 1013 multicollector ICP-MS and liquid scintillation counting *Nuclear Instruments and Methods in*  
 1014 *Physics Research, Section B, Beam Interactions with Materials and Atoms* 268, 192–199.  
 1015 <https://doi.org/10.1016/j.nimb.2009.09.012>
- 1016 Christ, A.J., Talaia-Murray, M., Elking, N., Domack, E.W., Leventer, A., Lavoie, C., ... & Petrushak, S.  
 1017 (2015). Late Holocene glacial advance and ice shelf growth in Barilari Bay, Graham Land, west  
 1018 Antarctic Peninsula. *GSA Bulletin*, 127(1-2), 297-315. DOI: 10.1130/B31035.1;
- 1019 Chu, Z., Sun, L., Wang, Y., Huang, T., & Zhou, X. (2017). Depositional environment and climate changes  
 1020 during the Holocene in Grande Valley, Fildes Peninsula, King George Island, Antarctica. *Antarctic*  
 1021 *Science*, 29(6), 545-554. <https://doi.org/10.1017/S095410201700030X>
- 1022 Çiner, A., Yildirim, C., Sarikaya, M. A., Seong, Y. B., Yu, B. Y. (2019). Cosmogenic  $^{10}\text{Be}$  exposure  
 1023 dating of glacial erratics on Horseshoe Island in western Antarctic Peninsula confirms rapid  
 1024 deglaciation in the Early Holocene. *Antarctic Science*, 31(6), 319-331.  
 1025 <https://doi.org/10.1017/S0954102019000439>
- 1026 Clapperton, C.M., & Sugden, D.E. (1988). Holocene glacier fluctuations in South America and Antarctica.  
 1027 *Quaternary Science Reviews*, 7(2), 185-198.
- 1028 Clementi, V.J., Sikes, E.L. 2019. Southwest Pacific vertical structure influences on oceanic carbon storage  
 1029 since the Last Glacial Maximum. *Paleoceanogr. Paleoclim.* 34, 734–754. 10.1029/2018PA003501
- 1030 Cofaigh, C.Ó., Davies, B.J., Livingstone, S.J., Smith, J.A., Johnson, J.S., Hocking, E.P., ... & Domack, E.  
 1031 (2014). Reconstruction of ice-sheet changes in the Antarctic Peninsula since the Last Glacial  
 1032 Maximum. *Quaternary Science Reviews*, 100, 87-110. DOI: 10.1016/j.quascirev.2014.06.023
- 1033 Cook, A. J., Fox, A.J., Vaughan, D.G., & Ferrigno, J.G. (2005). Retreating glacier fronts on the Antarctic  
 1034 Peninsula over the past half-century. *Science*, 308(5721), 541-544. DOI: 10.1126/science.1104235
- 1035 Correia, A., Oliva, M., & Ruiz-Fernández, J. (2017). Evaluation of frozen ground conditions along a coastal  
 1036 topographic gradient at Byers Peninsula (Livingston Island, Antarctica) by geophysical and

- 1037 geocological methods. *Catena*, 149, 529-537. DOI: 10.1016/j.catena.2016.08.006
- 1038 Curl, J.E. (1980). A glacial history of the South Shetland Islands, Antarctica. Institute of Polar Studies,  
1039 Intitute of Polar Studies, Report N° 63. The Ohio State University. 129 pp.
- 1040 Darvill, C.M., Bentley, M.J., Stokes C.R., Shulmeister, J. (2016). The timing and cause of glacial advances  
1041 in the southern mid-latitudes during the last glacial cycle based on a synthesis of exposure ages  
1042 from Patagonia and New Zealand. *Quaternary Science Reviews*, 149, 200-214.
- 1043 Davies, B.J., Glasser, N.F., Carrivick, J.L., Hambrey, M.J., Smellie, J.L., & Nývlt, D. (2013). Landscape  
1044 evolution and ice-sheet behaviour in a semi-arid polar environment: James Ross Island, NE  
1045 Antarctic Peninsula. *Geological Society, London, Special Publications*, 381(1), 353-395.  
1046 DOI:10.1144/SP381.1
- 1047 Davies, B.J., Golledge, N.R., Glasser, N.F., Carrivick, J.L., Ligtenberg, S.R., Barrand, N.E., ... & Smellie,  
1048 J.L. (2014). Modelled glacier response to centennial temperature and precipitation trends on the  
1049 Antarctic Peninsula. *Nature Climate Change*, 4(11), 993. DOI: 10.1038/NCLIMATE2369
- 1050 Davies, B.J., Hambrey, M.J., Glasser, N.F., Holt, T., Rodés, A., Smellie, J.L., ... & Blockley, S.P. (2017).  
1051 Ice-dammed lateral lake and epishelf lake insights into Holocene dynamics of Marguerite Trough  
1052 Ice Stream and George VI Ice Shelf, Alexander Island, Antarctic Peninsula. *Quaternary Science  
1053 Reviews*, 177, 189-219. DOI: 10.1016/j.quascirev.2017.10.016
- 1054 Davies, B.J., Hambrey, M.J., Smellie, J.L., Carrivick, J.L., & Glasser, N.F. (2012). Antarctic Peninsula ice  
1055 sheet evolution during the Cenozoic Era. *Quaternary Science Reviews*, 31, 30-66.  
1056 DOI:10.1016/j.quascirev.2011.10.012
- 1057 De Pablo, M. A., Ramos, M., & Molina, A. (2014). Thermal characterization of the active layer at the  
1058 Linnopolar Lake CALM-S site on Byers Peninsula (Livingston Island), Antarctica. *Solid Earth*,  
1059 5(2), 721-739. DOI:10.5194/se-5-721-2014
- 1060 Deaney, E.L., Barker, S., & Van De Flierdt, T. (2017). Timing and nature of AMOC recovery across  
1061 Termination 2 and magnitude of deglacial CO<sub>2</sub> change. *Nature communications*, 8, 14595.
- 1062 Del Valle, R.A., Montalti, D., & Inbar, M. (2002). Mid-Holocene macrofossil-bearing raised marine  
1063 beaches at Potter Peninsula, King George Island, South Shetland Islands. *Antarctic Science*, 14(3),  
1064 263-269. DOI: 10.1017/S0954102002000081
- 1065 Domack, E., Ishman, S., Stein, A.B., McClennen, C.E., Jull, A.J.T. (1995). Late Holocene advance of  
1066 Müller Ice Shelf, Antarctic Peninsula: sedimentological, geochemical, and palaeontological  
1067 evidence. *Antarctic Science* 7, 159-170.
- 1068 Domack, E.W., Leventer, A., Dunbar, G.B., Taylor, F., Brachfeld, S., Sjunneskog, C., Party, O.L.S., (2001).  
1069 Chronology of the Palmer Deep site, Antarctic Peninsula: A Holocene palaeoenvironmental  
1070 reference for the circum-Antarctic. *The Holocene* 11, 1-9.
- 1071 Dunai, T.J., 2010. *Cosmogenic Nuclides*. Cambridge University Press, Cambridge.  
1072 doi:10.1017/CBO9780511804519
- 1073 Engel, Z., Láská, K., Nývlt, D., Stachoň, Z. (2018). Surface Mass Balance of Small Glaciers on James Ross  
1074 Island, North-Eastern Antarctic Peninsula, during 2009-2015. *Journal of Glaciology*, 64 (245),  
1075 349-361.
- 1076 Everett, K.R. (1971). Observations on the glacial history of Livingston Island. *Arctic*, 41-50.
- 1077 Fretwell, P. T., Hodgson, D. A., Watcham, E. P., Bentley, M. J., & Roberts, S. J. (2010). Holocene isostatic  
1078 uplift of the South Shetland Islands, Antarctic Peninsula, modelled from raised beaches.  
1079 *Quaternary Science Reviews*, 29(15-16), 1880-1893. DOI:10.1016/j.quascirev.2010.04.006
- 1080 Fink, D., Vogt, S., Hotchkis, M., 2000. Cross-sections for <sup>36</sup>Cl from Ti at Ep=35–150 MeV: Applications  
1081 to in-situ exposure dating. *Nucl. Instruments Methods Phys. Res. Sect. B Beam Interact. with  
1082 Mater. Atoms* 172, 861–866. doi:10.1016/S0168-583X(00)00200-7
- 1083 Geirsdóttir, Á., Miller, G.H., Andrews, J.T., Harning, D.J., Anderson, L.S., Florian, C., ... & Thordarson,  
1084 T. (2019). The onset of neoglaciation in Iceland and the 4.2 ka event. *Climate of the Past*, 15(1),  
1085 25-40. DOI: 10.5194/cp-15-25-2019
- 1086 Glasser, N.F., Davies, B.J., Carrivick, J.L., Rodés, A., Hambrey, M.J., Smellie, J.L., & Domack, E. (2014).  
1087 Ice-stream initiation, duration and thinning on James Ross Island, northern Antarctic Peninsula.

- 1088 Quaternary Science Reviews, 86, 78-88. DOI: 10.1016/j.quascirev.2013.11.012
- 1089 Guglielmin, M., Convey, P., Malfasi, F., Cannone, N. (2016). Glacial fluctuations since the ‘Medieval  
1090 warm period’ at Rothera Point (western Antarctic Peninsula). *The Holocene*, 26(1), 154-158. DOI:  
1091 10.1177/0959683615596827
- 1092 Hall, B.L. (2003). An overview of late Pleistocene glaciation in the South Shetland Islands. *Antarctic  
1093 Research Series*, 79, 103-113. DOI: 10.1029/079ARS09
- 1094 Hall, B.L. (2007). Late-Holocene advance of the Collins Ice Cap, King George Island, South Shetland  
1095 Islands. *The Holocene*, 17(8), 1253-1258. DOI: 10.1177/0959683607085132
- 1096 Hall, B.L. (2009). Holocene glacial history of Antarctica and the sub-Antarctic islands. *Quaternary Science  
1097 Reviews*, 28(21-22), 2213-2230. DOI:10.1016/j.quascirev.2009.06.011
- 1098 Hall, B.L., & Denton, G.H. (1999). New relative sea-level curves for the southern Scott Coast, Antarctica:  
1099 evidence for Holocene deglaciation of the western Ross Sea. *Journal of Quaternary Science*, 14(7),  
1100 641-650.
- 1101 Hall, B.L., Denton, G. (2002). Holocene history of the Wilson Piedmont Glacier along the southern Scott  
1102 Coast. *The Holocene* 12, 619-627. DOI: 10.1191/0959683602hl572rp
- 1103 Hall, B.L., & Perry, E.R. (2004). Variations in ice rafted detritus on beaches in the South Shetland Islands:  
1104 a possible climate proxy. *Antarctic Science*, 16(3), 339-344. DOI: 10.1017/S0954102004002147
- 1105 Hall, B.L., Koffman, T., Denton, G. H. (2010). Reduced ice extent on the western Antarctic Peninsula at  
1106 700–970 cal. yr BP. *Geology*, 38(7), 635-638. DOI: 10.1130/G30932.1
- 1107 Hall, B.L. (2010). Holocene relative sea-level changes and ice fluctuations in the South Shetland Islands.  
1108 *Global and Planetary Change* 74, 15-26.
- 1109 Hambrey, M.J., Davies, B.J., Glasser, N.F., Holt, T.O., Smellie, J.L., & Carrivick, J.L. (2015). Structure  
1110 and sedimentology of George VI Ice Shelf, Antarctic Peninsula: implications for ice-sheet  
1111 dynamics and landform development. *Journal of the Geological Society*, 172(5), 599-613. DOI:  
1112 10.1144/jgs2014-134
- 1113 Hansom, J. D. (1979). Radiocarbon dating of a raised beach at 10 m in the South Shetland Islands. *British  
1114 Antarctic Survey Bulletin*, 49, 287-288.
- 1115 Hathway, B. & Lomas, S.A. (1998). The Upper Jurassic-Lower cretaceous Byers Group, South Shetland  
1116 Islands, Antarctica: revised stratigraphy and regional correlations. *Cretaceous Research*, 19, 43-  
1117 67.
- 1118 Heroy, D.C., Sjunneskog, C., & Anderson, J.B. (2008). Holocene climate change in the Bransfield Basin,  
1119 Antarctic Peninsula: evidence from sediment and diatom analysis. *Antarctic Science*, 20(1), 69-  
1120 87. DOI: 10.1017/S0954102007000788
- 1121 Hodgson, D.A., Roberts, S.J., Smith, J.A., Verleyen, E., Sterken, M., Labarque, M., ... & Bryant, C. (2013).  
1122 Late Quaternary environmental changes in Marguerite Bay, Antarctic Peninsula, inferred from  
1123 lake sediments and raised beaches. *Quaternary Science Reviews*, 68, 216-236.  
1124 DOI:10.1016/j.quascirev.2011.10.011
- 1125 Hrbáček, F., Oliva, M., Láska, K., Ruiz-Fernandez, J., de Pablo, M.A., Vieira, G., Ramos, M. & Nývlt, D.  
1126 (2016). Active layer thermal regime in two climatically contrasted sites of the Antarctic Peninsula  
1127 region. *Cuadernos de Investigación Geográfica*, 42(2), 457-474.
- 1128 Ingólfsson, Ó., Hjort, C., & Humlum, O. (2003). Glacial and climate history of the Antarctic Peninsula  
1129 since the Last Glacial Maximum. *Arctic, Antarctic, and Alpine Research*, 35(2), 175-186. DOI:  
1130 10.1657/1523-0430(2003)035[0175:GACHOT]2.0.CO;2
- 1131 Ingólfsson, Ó., Hjort, C., Berkman, P.A., Björck, S., Colhoun, E., Goodwin, I.D., ... & Prentice, M.L.  
1132 (1998). Antarctic glacial history since the Last Glacial Maximum: an overview of the record on  
1133 land. *Antarctic science*, 10(3), 326-344.
- 1134 Ivy-Ochs, S., Synal, H.-A., Roth, C., Schaller, M., 2004. Initial results from isotope dilution for Cl and  
1135 <sup>36</sup>Cl measurements at the PSI/ETH Zurich AMS facility. *Nucl. Instruments Methods Phys. Res.  
1136 Sect. B Beam Interact. with Mater. Atoms* 223–224, 623–627. doi:10.1016/j.nimb.2004.04.115
- 1137 John, B.S. (1972). Evidence from the South Shetland Islands towards a glacial history of West Antarctica.



- 1138 Institute of British Geographers, Special Publication, 4, 75-89.
- 1139 John, B.S., & Sugden, D.E. (1971). Raised marine features and phases of glaciation in the South Shetland  
1140 Islands. *British Antarctic Survey Bulletin*, 24, 45-111.
- 1141 Jomelli, V., Favier, V., Vuille, M., Braucher, R., Martin, L., Blard, P.H., Colose, C., Brunstein, D., He, F.,  
1142 Khodri, M., Bourles, D.L., Leanni, L., Rinterknecht, V., Grancher, D., Francou, B., Ceballos, J.L.,  
1143 Fonseca, H., Liu, Z., Otto-Bliesner, B.L. (2014). A major advance of tropical Andean glaciers  
1144 during the Antarctic cold reversal. *Nature*, 513, 224-228.
- 1145 Kaplan, M. R., Strelin, J. A., Schaefer, J. M., Peltier, C., Martini, M. A., Flores, E. Winckler, G. Schwartz,  
1146 R. (2020). Holocene glacier behavior around the northern Antarctic Peninsula and possible causes.  
1147 *Earth and Planetary Science Letters*, 534, 116077. <https://doi.org/10.1016/j.epsl.2020.116077>
- 1148 Kaufman, D.S., Ager, T.A., Anderson, N.J., Anderson, P.M., Andrews, J.T., Bartlein, P.J., ... & Dyke, A.S.  
1149 (2004). Holocene thermal maximum in the western Arctic (0–180 W). *Quaternary Science*  
1150 *Reviews*, 23(5-6), 529-560. DOI:10.1016/j.quascirev.2003.09.007
- 1151 Kaufman, D.S., Axford, Y.L., Henderson, A.C., McKay, N.P., Oswald, W.W., Saenger, C., ... & Hu, F.S.  
1152 (2016). Holocene climate changes in eastern Beringia (NW North America)—A systematic review  
1153 of multi-proxy evidence. *Quaternary Science Reviews*, 147, 312-339.
- 1154 Khim, B.K., Yoon, H.I., Kang, C.Y., Bahk, J.J. (2002). Unstable climate oscillations during the late  
1155 Holocene in the eastern Bransfield Basin, Antarctic Peninsula. *Quaternary Research*, 58, 234-245.  
1156 DOI:10.1006/qres.2002.2371
- 1157 Koffman, T.N., Schaefer, J.M., Putnam, A.E., Denton, G.H., Barrell, D.J., Rowan, A.V., ... & Brocklehurst,  
1158 S.H. (2017). A beryllium-10 chronology of late-glacial moraines in the upper Rakaia valley,  
1159 Southern Alps, New Zealand supports Southern-Hemisphere warming during the Younger Dryas.  
1160 *Quaternary Science Reviews*, 170, 14-25.
- 1161 Korschinek, G., Bergmaier, A., Faestermann, T., Gerstmann, U.C., Knie, K., Rugel, G., Wallner, A.,  
1162 Dillmann, I., Dollinger, G., von Gostomski, C.L., Kossert, K., Maiti, M., Poutivtsev, M., Remmert,  
1163 A., 2010. A new value for the half-life of <sup>10</sup>Be by Heavy-Ion Elastic Recoil Detection and liquid  
1164 scintillation counting. *Nuclear Instruments and Methods in Physics Research, Section B, Beam*  
1165 *Interactions with Materials and Atoms* 268, 187–191. <https://doi.org/10.1016/j.nimb.2009.09.020>
- 1166 Kunz, M., King, M.A., Mills, J.P., Miller, P.E., Fox, A.J., Vaughan, D.G., Marsh, S.H. (2012). Multi-  
1167 Decadal Glacier Surface Lowering in the Antarctic Peninsula. *Geophysical Research Letters*, 39  
1168 (19), 1-5.
- 1169 Larter, R.D., Anderson, J.B., Graham, A.G., Gohl, K., Hillenbrand, C.D., Jakobsson, M., ... & Witus, A.E.  
1170 (2014). Reconstruction of changes in the Amundsen Sea and Bellingshausen sea sector of the West  
1171 Antarctic ice sheet since the last glacial maximum. *Quaternary Science Reviews*, 100, 55-86. DOI:  
1172 10.1016/j.quascirev.2013.10.016
- 1173 Li, Y., Cole-Dai, J., & Zhou, L. (2009). Glaciochemical evidence in an East Antarctica ice core of a recent  
1174 (AD 1450–1850) neoglacial episode. *Journal of Geophysical Research: Atmospheres*, 114(D8) 1-  
1175 11. DOI:10.1029/2008JD011091,
- 1176 Lifton, N., Sato, T., Dunai, T.J., 2014. Scaling in situ cosmogenic nuclide production rates using analytical  
1177 approximations to atmospheric cosmic-ray fluxes. *Earth Planet. Sci. Lett.* 386, 149-160.  
1178 <http://dx.doi.org/10.1016/j.epsl.2013.10.052>
- 1179 Lindsay, D.C. (1971). Vegetation of the South Shetland Islands. *British Antarctic Survey Bulletin*, 25, 59-  
1180 83.
- 1181 Lorius, C., Jouzel, J., Raynaud, D., Hansen, J., & Le Treut, H. (1990). The ice-core record: climate  
1182 sensitivity and future greenhouse warming. *Nature*, 347(6289), 139-145.
- 1183 López-Martínez, J., Martínez de Pisón, E., Arche, A. (1992). Geomorphology of Hurd Peninsula,  
1184 Livingston Island, South Shetland Islands. In: Yoshida, Y., Kaminuma, K., Shiraishi, K. (Eds.),  
1185 *Recent Progress in Antarctic Earth Science*. Terra Scientific Publishing Company, Tokyo, pp. 751-  
1186 756.
- 1187 López-Martínez, J., Serrano, E., Schmid, T., Mink, S. & Linés, C. (2012). Periglacial processes and  
1188 landforms in the South Shetland Islands (northern Antarctic Peninsula region). *Geomorphology*,  
1189 155/156, 62-79.

- 1190 Mackintosh, A.N., Verleyen, E., O'Brien, P.E., White, D.A., Jones, R.S., McKay, R., ... & Miura, H. (2014).  
 1191 Retreat history of the East Antarctic Ice Sheet since the last glacial maximum. *Quaternary Science*  
 1192 *Reviews*, 100, 10-30. DOI: 10.1016/j.quascirev.2013.07.024
- 1193 Mackintosh, A., Golledge, N., Domack, E., Dunbar, R., Leventer, A., White, D., ... & Gore, D. (2011).  
 1194 Retreat of the East Antarctic ice sheet during the last glacial termination. *Nature Geoscience*, 4(3),  
 1195 195. DOI: 10.1038/NGEO1061
- 1196 Marcott, S. A., Shakun, J. D., Clark, P. U., & Mix, A. C. (2013). A reconstruction of regional and global  
 1197 temperature for the past 11,300 years. *Science*, 339(6124), 1198-1201. DOI:  
 1198 10.1126/science.1228026
- 1199 Martin, L.C.P., Blard, P.-H., Balco, G., Lavé, J., Delunel, R., Lifton, N., Laurent, V., 2017. The CREp  
 1200 program and the ICE-D production rate calibration database: A fully parameterizable and updated  
 1201 online tool to compute cosmic-ray exposure ages. *Quat. Geochronol.* 38, 25–49.  
 1202 <https://doi.org/10.1016/J.QUAGEO.2016.11.006>
- 1203 Martínez De Pisón, E., Serrano, E., Arche, A. & López-Martínez, J. (1996). Glacial geomorphology. In  
 1204 López-Martínez, J., Thomson, M.R.A. & Thomson, J.W., Eds. *Geomorphological map of Byers*  
 1205 *Peninsula, Livingston Island. BAS GEOMAP series, sheet 5-a, 1:25000, with supplementary text.*  
 1206 Cambridge: British Antarctic Survey, 23-27.
- 1207 Mäusbacher, R. (1991). Die jungquartäre Relief- und Klimageschichte im Bereich der Fildeshalbinsel Sü-d-  
 1208 Shetland-Inseln, Antarktis. Ph.D. dissertation, Geographisches Institut der Universität Heidelberg,  
 1209 382 pp.
- 1210 Mäusbacher, R., Müller, J., Schmidt, R. (1989). Evolution of postglacial sedimentation in Antarctic lakes  
 1211 (King George Island), *Zeitschrift Fur Geomorphologie*, 33(2), 219-234.
- 1212 Marrero, S.M., Phillips, F.M., Caffee, M.W., Gosse, J.C. 2016. CRONUS – Earth cosmogenic <sup>36</sup>Cl  
 1213 calibration. *Quat. Geochronol.* 31, 199–219. 10.1016/j.quageo.2015.10.002
- 1214 McKay, N.P., Kaufman, D.S., Routson, C.C., Erb, M.P., & Zander, P.D. (2018). The onset and rate of  
 1215 Holocene Neoglacial cooling in the Arctic. *Geophysical Research Letters*, 45(22), 12-487.  
 1216 10.1029/2018GL079773
- 1217 Merchel, S., Herpers, U. 1999. An update on radiochemical separation techniques for the determination of  
 1218 long-lived radionuclides via accelerator mass spectrometry. *Radiochimica Acta*, 84(4), 215-220.
- 1219 Merchel, S., Arnold, M., Aumaître, G., Benedetti, L., Bourlès, D.L., Braucher, R., Alfimov, V., Freeman,  
 1220 S.P.H.T., Steier, P., Wallner, A., 2008. Towards more precise <sup>10</sup>Be and <sup>36</sup>Cl data from  
 1221 measurements at the 10–14 level: Influence of sample preparation. *Nuclear Instruments and*  
 1222 *Methods in Physics Research, Section B, Beam Interactions with Materials and Atoms* 266, 4921–  
 1223 4926. <https://doi.org/10.1016/j.nimb.2008.07.031>
- 1224 Merchel, S., Bremsler, W., Alfimov, V., Arnold, M., Aumaître, G., Benedetti, L., Bourlès, D.L., Caffee, M.,  
 1225 Fifield, L.K., Finkel, R.C., Freeman, S.P.H.T., Martschini, M., Matsushi, Y., Rood, D.H., Sasa,  
 1226 K., Steier, P., Takahashi, T., Tamari, M., Tims, S.G., Tosaki, Y., Wilcken, K.M., Xu, S., 2011.  
 1227 Ultra-trace analysis of <sup>36</sup>Cl by accelerator mass spectrometry: an interlaboratory study. *Anal. Bio-*  
 1228 *anal. Chem.* doi:10.1007/s00216-011-4979-2.
- 1229 Michalchuk, B.R., Anderson, J.B., Wellner, J.S., Manley, P.L., Majewski, W., & Bohaty, S. (2009).  
 1230 Holocene climate and glacial history of the northeastern Antarctic Peninsula: the marine  
 1231 sedimentary record from a long SHALDRIL core. *Quaternary Science Reviews*, 28(27-28), 3049-  
 1232 3065. DOI:10.1016/j.quascirev.2009.08.012
- 1233 Miller, G.H., Geirsdóttir, Á., Zhong, Y., Larsen, D.J., Otto-Bliesner, B.L., Holland, M.M., Bailey, D.A.,  
 1234 Refsnider, K.A., Lehman, S.J., Southon, J.R., Anderson, C., Björnsson, H., Thordarson, T. (2012).  
 1235 Abrupt onset of the Little Ice Age triggered by volcanism and sustained by sea-ice/ocean  
 1236 feedbacks. *Geophysical Research Letters*, 39, L02708. DOI: 10.1029/2011GL050168
- 1237 Miller, G.H., Landvik, J.Y., Lehman, S.J., & Southon, J.R. (2017). Episodic Neoglacial snowline descent  
 1238 and glacier expansion on Svalbard reconstructed from the <sup>14</sup>C ages of ice-entombed plants.  
 1239 *Quaternary Science Reviews*, 155, 67-78.
- 1240 Miller, G.H., Lehman, S.J., Refsnider, K.A., Southon, J.R., & Zhong, Y. (2013). Unprecedented recent  
 1241 summer warmth in Arctic Canada. *Geophysical Research Letters*, 40, 5745–5751. DOI:  
 1242 10.1002/2013GL057188

- 1243 Milliken, K.T., Anderson, J.B., Wellner, J.S., Bohaty, S.M., & Manley, P.L. (2009). High-resolution  
1244 Holocene climate record from Maxwell Bay, South Shetland Islands, Antarctica. *Holocene climate*  
1245 *record from Maxwell Bay. GSA Bulletin*, 121(11-12), 1711-1725.
- 1246 Mosley-Thompson, E. (1996). Holocene climate changes recorded in an East Antarctica ice core. Climatic  
1247 variations and forcing mechanisms of the last 2,000. In Jones, P.D., Bradley, R. and Jouzel, J.,  
1248 editors, *NATO advanced research series I 41*, 263-79.
- 1249 Mosley-Thompson, E., Thompson, L.G., Grootes, P.M., & Gundestrup, N. (1990). Little ice age  
1250 (neoglacial) paleoenvironmental conditions atiple station, Antarctica. *Annals of Glaciology*, 14,  
1251 199-204.
- 1252 Mulvaney, R., Abram, N.J., Hindmarsh, R.C., Arrowsmith, C., Fleet, L., Triest, J., ... & Foord, S. (2012).  
1253 Recent Antarctic Peninsula warming relative to Holocene climate and ice-shelf history. *Nature*,  
1254 489(7414), 141. DOI:10.1038/nature11391
- 1255 Muschitiello, F., D'Andrea, W.J., Schmittner, A., Heaton, T.J., Balascio, N.L., Caffee, M.W., ... & Dokken,  
1256 T.M. (2019). Deep-water circulation changes lead North Atlantic climate during deglaciation.  
1257 *Nature communications*, 10(1), 1272.
- 1258 Navarro, F., Jonsell, U., Corcuera, M.I., Martín Español, A.- (2013). Decelerated mass loss of Hurd and  
1259 Johnsons Glaciers, Livingston Island, Antarctic Peninsula. *Journal of Glaciology*, 59 (213), 115-  
1260 128.
- 1261 Oliva, M., & Ruiz-Fernández, J. (2015). Coupling patterns between para-glacial and permafrost degradation  
1262 responses in Antarctica. *Earth Surface Processes and Landforms*, 40(9), 1227-1238. DOI:  
1263 10.1002/esp.3716
- 1264 Oliva, M., Navarro, F., Hrbáček, F., Hernández, A., Nývlt, D., Pereira, P., ... & Trigo, R. (2017a). Recent  
1265 regional climate cooling on the Antarctic Peninsula and associated impacts on the cryosphere.  
1266 *Science of the Total Environment*, 580, 210-223. DOI: 10.1016/j.scitotenv.2016.12.030
- 1267 Oliva, M., & Ruiz-Fernández, J. (2017). Geomorphological processes and frozen ground conditions in  
1268 Elephant Point (Livingston Island, South Shetland Islands, Antarctica). *Geomorphology*, 293, 368-  
1269 379. DOI: 10.1016/j.geomorph.2016.01.020
- 1270 Oliva, M., Antoniades, D., Giralt, S., Granados, I.,  
1271 Pla-Rabes, S., Toro, M., ... & Vieira, G. (2016). The Holocene deglaciation of the Byers Peninsula  
1272 (Livingston Island, Antarctica) based on the dating of lake sedimentary records. *Geomorphology*,  
261, 89-102. DOI: 10.1016/j.geomorph.2016.02.029
- 1273 Oliva, M., Hrbacek, F., Ruiz-Fernández, J., de Pablo, M. Á., Vieira, G., Ramos, M., & Antoniades, D.  
1274 (2017b). Active layer dynamics in three topographically distinct lake catchments in Byers  
1275 Peninsula (Livingston Island, Antarctica). *Catena*, 149, 548-559. DOI:  
1276 10.1016/j.catena.2016.07.011
- 1277 Oliva, M., Antoniades, D., Giralt, S., Granados, I., Pla-Rabes, S., Toro, M., Liu, E.J., Sanjurjo, J., Vieira,  
1278 G. 2016. The Holocene deglaciation of the Byers Peninsula (Livingston Island, Antarctica) based  
1279 on the dating of lake sedimentary records. *Geomorphology* 261, 89–102.  
1280 <https://doi.org/10.1016/j.geomorph.2016.02.029>.
- 1281 Parica, C.A., Salani, F.M., Vera, E., Remesal, M. & Césari, S.N. (2007). Geología de la formación Cerro  
1282 Negro (Cretácico) en la isla Livingston: aportes a su geocronología y contenido paleontológico.  
1283 *Revista de la Asociación Geológica Argentina*, 62, 553-567.
- 1284 Porter S.C.; Denton, G.H. (1967). Chronology of the neoglaciation in the North American cordillera,  
1285 *American Journal of Science*, 265(3), 177-210.
- 1286 Porter, S.C. (2000). Onset of neoglaciation in the Southern Hemisphere. *Journal of Quaternary Science:*  
1287 *Published for the Quaternary Research Association*, 15(4), 395-408.
- 1288 Pritchard, H.D., Ligtenberg, S.R.M., Fricker, H.A., Vaughan, D.G., van den Broeke, M.R., Padman, L.  
1289 (2012). Antarctic ice-sheet loss driven by basal melting of ice shelves. *Nature*, 484, 502-505. DOI  
1290 DOI:10.1038/nature10968
- 1291 Reilly, B. T., Natter, C. J., & Brachfeld, S. A. (2016). Holocene glacial activity in Barilari Bay, west  
1292 Antarctic Peninsula, tracked by magnetic mineral assemblages: Linking ice, ocean, and  
1293 atmosphere. *Geochemistry, Geophysics, Geosystems*, 17(11), 4553-4565. DOI:  
1294 10.1002/2016GC006627

- 1295 Renssen, H., Seppä, H., Crosta, X., Goosse, H., & Rotche, D. M. (2012). Global characterization of the  
1296 Holocene thermal maximum. *Quaternary Science Reviews*, 48, 7-19. DOI:  
1297 10.1016/j.quascirev.2012.05.022
- 1298 Renssen, H., Seppä, H., Heiri, O., Rotche, D. M., Goosse, H., & Fichetef, T. (2009). The spatial and  
1299 temporal complexity of the Holocene thermal maximum. *Nature Geoscience*, 2(6), 411. DOI:  
1300 10.1038/NGEO513
- 1301 Roberts, S.J., Hodgson, D.A., Sterken, M., Whitehouse, P.L., Verleyen, E., Vyverman, W., ... & Moreton,  
1302 S.G. (2011). Geological constraints on glacio-isostatic adjustment models of relative sea-level  
1303 change during deglaciation of Prince Gustav Channel, Antarctic Peninsula. *Quaternary Science*
- 1304 Rothwell, R. G., Rack, F. R. (2006). New techniques in sediment core analysis: an introduction. *Geological*  
1305 *Society, London, Special Publications*, 267(1), 1-29. *Reviews*, 30(25-26), 3603-3617.  
1306 DOI:10.1016/j.quascirev.2011.09.009
- 1307 Ruiz-Fernández, J. & Oliva, M. (2016). Relative paleoenvironmental adjustments following deglaciation  
1308 of the Byers Peninsula (Livingston Island, Antarctica). *Arctic, Antarctic, and Alpine Research*,  
1309 48(2), 345-359. DOI: 10.1657/AAAR0015-014
- 1310 Ruiz-Fernández, J., Oliva, M. & García-Hernández, C. (2016). Procesos geomorfológicos y formas del  
1311 relieve en dos cuencas lacustres de la Península Byers (Isla Livingston, Antártida Marítima):  
1312 implicaciones paleoambientales. *Polígonos, Revista de Geografía*, 28, 211-237.
- 1313 Sadatzki, H., Dokken, T. M., Berben, S. M., Muschitiello, F., Stein, R., Fahl, K., ... & Jansen, E. (2019).  
1314 Sea ice variability in the southern Norwegian Sea during glacial Dansgaard-Oeschger climate  
1315 cycles. *Science advances*, 5(3), eaau6174. DOI: 10.1126/sciadv.aau6174
- 1316 Sancho, L.G., Pintado, A., Navarro, F., Ramos, M., De Pablo, M.A., Blanquer, J.M., ... & Green, T.G.A.  
1317 (2017). Recent warming and cooling in the Antarctic Peninsula region has rapid and large effects  
1318 on lichen vegetation. *Scientific reports*, 7(1), 5689. DOI:10.1038/s41598-017-05989-4
- 1319 Schäfer, J. M., Ivy-Ochs, S., Wieler, R., Leya, I., Baur, H., Denton, G. H., & Schlüchter, C. (1999).  
1320 Cosmogenic noble gas studies in the oldest landscape on earth: surface exposure ages of the Dry  
1321 Valleys, Antarctica. *Earth and Planetary Science Letters*, 167(3-4), 215-226.  
1322 [https://doi.org/10.1016/S0012-821X\(99\)00029-1](https://doi.org/10.1016/S0012-821X(99)00029-1)
- 1323 Schimmelpfennig, I., Benedetti, L., Finkel, R., Pik, R., Blard, P.H., Bourlès, D., Burnard, P., Williams, A.,  
1324 2009. Sources of in-situ <sup>36</sup>Cl in basaltic rocks. Implications for calibration of production rates.  
1325 *Quat. Geochronol.* 4, 441–461. doi:10.1016/j.quageo.2009.06.003
- 1326 Schimmelpfennig, I., Benedetti, L., Garreta, V., Pik, R., Blard, P.H., Burnard, P., Bourlès, D., Finkel, R.,  
1327 Ammon, K., Dunai, T., 2011. Calibration of cosmogenic <sup>36</sup>Cl production rates from Ca and K  
1328 spallation in lava flows from Mt. Etna (38°N, Italy) and Payun Matru (36°S, Argentina). *Geochim.*  
1329 *Cosmochim. Acta* 75, 2611–2632. doi:10.1016/j.gca.2011.02.013
- 1330 Schimmelpfennig, I., Schaefer, J.M., Putnam, A.E., Koffman, T., Benedetti, L., Ivy-Ochs, S., Team, A.,  
1331 Schlüchter, C., 2014. <sup>36</sup>Cl production rate from K-spallation in the European Alps (Chironico  
1332 landslide, Switzerland). *J. Quat. Sci.* 29, 407–413. doi:10.1002/jqs.2720
- 1333 Schimmelpfennig, I., Tesson, J., Blard, P.H., Benedetti, L., Zakari, M., Balco, G., 2019. The CREP  
1334 Chlorine-36 exposure age and depth profile calculator. Goldschmidt. Barcelona, Spain.  
1335 <https://goldschmidtabstracts.info/2019/2996.pdf>
- 1336 Sejrup, H.P., Seppä, H., McKay, N.P., Kaufman, D.S., Geirsdóttir, Á., de Vernal, A., ... & Andrews, J.T.  
1337 (2016). North Atlantic-Fennoscandian Holocene climate trends and mechanisms. *Quaternary*  
1338 *Science Reviews*, 147, 365-378.
- 1339 Seong, Y. B., Owen, L. A., Lim, H. S., Yoon, H. I., Kim, Y., Lee, Y. I., & Caffee, M. W. (2009). Rate of  
1340 late Quaternary ice-cap thinning on King George Island, South Shetland Islands, West Antarctica  
1341 defined by cosmogenic <sup>36</sup>Cl surface exposure dating. *Boreas*, 38(2), 207-213.  
1342 <https://doi.org/10.1111/j.1502-3885.2008.00069.x>
- 1343 Serrano, E., Martínez De Pisón, E. & López-Martínez, J. (1996). Periglacial and nival landforms and  
1344 deposits. In López-Martínez, J., Thomson, M.R.A. & Thomson, J.W., eds. *Geomorphological map*  
1345 *of Byers Peninsula, Livingston Island. BAS GEOMAP Series, Sheet 5-A, Scale 1:25 000.*  
1346 Cambridge: British Antarctic Survey, 28-34.

- 1347 Severinghaus, J.P.; Brook, E.. (1999). Abrupt climate change at the end of the last glacial period inferred  
1348 from trapped air in polar ice. *Science*, 286, 930-934.
- 1349 Shevenell, A.E., Ingalls, A.E., Domack, E.W., & Kelly, C. (2011). Holocene Southern Ocean surface  
1350 temperature variability west of the Antarctic Peninsula. *Nature*, 470(7333), 250.  
1351 DOI:10.1038/nature09751
- 1352 Shulmeister, J., Thackray, G.D., Rittenour, T.M., Fink, D., & Patton, N.R. (2019). The timing and nature  
1353 of the last glacial cycle in New Zealand. *Quaternary Science Reviews*, 206, 1-20.
- 1354 Simkins, L.M., Simms, A.R., & DeWitt, R. (2013). Relative sea-level history of Marguerite Bay, Antarctic  
1355 Peninsula derived from optically stimulated luminescence-dated beach cobbles. *Quaternary  
1356 Science Reviews*, 77, 141-155. DOI:10.1016/j.quascirev.2013.07.027
- 1357 Simms, A.R., De Witt, R., Kouremenos, P., & Drewry, A.M. (2011b). A new approach to reconstructing  
1358 sea levels in Antarctica using optically stimulated luminescence of cobble surfaces. *Quaternary  
1359 Geochronology*, 6(1), 50-60.
- 1360 Simms, A.R., Ivins, E.R., DeWitt, R., Kouremenos, P., & Simkins, L.M. (2012). Timing of the most recent  
1361 Neoglacial advance and retreat in the South Shetland Islands, Antarctic Peninsula: insights from  
1362 raised beaches and Holocene uplift rates. *Quaternary Science Reviews*, 47, 41-55.  
1363 DOI:10.1016/j.quascirev.2012.05.013
- 1364 Simms, A.R., Milliken, K.T., Anderson, J.B., & Wellner, J.S. (2011a). The marine record of deglaciation  
1365 of the South Shetland Islands, Antarctica since the Last Glacial Maximum. *Quaternary Science  
1366 Reviews*, 30(13-14), 1583-1601. DOI:10.1016/j.quascirev.2011.03.018
- 1367 Simms, A. R., Whitehouse, P. L., Simkins, L. M., Nield, G., DeWitt, R., Bentley, M. J. 2018. Late Holocene  
1368 relative sea levels near Palmer Station, northern Antarctic Peninsula, strongly controlled by late  
1369 Holocene ice-mass changes. *Quaternary Science Reviews*, 199, 49-59.  
1370 <https://doi.org/10.1016/j.quascirev.2018.09.017>
- 1371 Simonsen, M.F., Baccolo, G., Blunier, T. et al. East Greenland ice core dust record reveals timing of  
1372 Greenland ice sheet advance and retreat. *Nat Commun* 10, 4494 (2019).  
1373 <https://doi.org/10.1038/s41467-019-12546-2>
- 1374 Singer, B. S., Jicha, B. R., Mochizuki, N., & Coe, R. S. (2019). Synchronizing volcanic, sedimentary, and  
1375 ice core records of Earth's last magnetic polarity reversal. *Science advances*, 5(8), eaaw4621. DOI:  
1376 10.1126/sciadv.aaw4621
- 1377 Smellie, J.L., Davies, R.E.S., & Thomson, M.R.A. (1980). Geology of a Mesozoic intra-arc sequence on  
1378 Byers Peninsula, Livingston Island, South Shetland Islands. *British Antarctic Survey Bulletin*, 50,  
1379 55-76.
- 1380 Solomina, O.N., Bradley, R.S., Hodgson, D.A., Ivy-Ochs, S., Jomelli, V., Mackintosh, A.N., ... & Young,  
1381 N.E. (2015). Holocene glacier fluctuations. *Quaternary Science Reviews*, 111, 9-34. DOI:  
1382 10.1016/j.quascirev.2014.11.018
- 1383 Stolper, D., Bender, M., Dreyfus, G., Yan, Y. & Higgins, J.A. (2016). Pleistocene ice core record of  
1384 atmospheric O<sub>2</sub> concentrations. *Science* 353, 1427–1430.
- 1385 Stone, J.O., 2000. Air pressure and cosmogenic isotope production. *J. Geophys. Res. Solid Earth* 105,  
1386 23753–23759. doi:10.1029/2000JB900181
- 1387 Storey, B.C., Fink, D., Hood, D., Joy, K., Shulmeister, J., Riger-Kusk, M., & Stevens, M.I. (2010).  
1388 Cosmogenic nuclide exposure age constraints on the glacial history of the Lake Wellman area,  
1389 Darwin Mountains, Antarctica. *Antarctic Science*, 22(6), 603-618.  
1390 DOI:10.1017/S0954102010000799
- 1391 Strelin, J., Sone, T., Mori, J., Torielli, C., Nakamura, T. (2006). New data related to Holocene landform  
1392 development and climatic change from James Ross Island, Antarctic Peninsula. In: Fu" tterer, D.,  
1393 Damaske, D., Kleinschmidt, G., Miller, H., Tessensohn, F. (Eds.), *Antarctica: Contributions to  
1394 Global Earth Sciences*. Springer-Verlag, New York, pp. 455–460.
- 1395 Sugden, D.E., & Clapperton, C.M. (1986). Glacial history of the Antarctic Peninsula and South Georgia.  
1396 *South African Journal of Science*, 82(9), 508-509.
- 1397 Sugden, D.E. & John, B.S. (1973). The ages of glacier fluctuations in the South Shetland Islands,  
1398 Antarctica. In: van Zinderen Bakker, E.M. (ed.), *Palaeoecology of Africa, the Surrounding Islands*

- 1399 and Antarctica, 8, 141-159. Balkema, Cape Town.
- 1400 Toro, M., Granados, I., Pla, S., Giralt, S., Antoniades, D., Galán, L., ... & Appleby, P.G. (2013).  
1401 Chronostratigraphy of the sedimentary record of Limnopolar Lake, Byers Peninsula, Livingston  
1402 Island, Antarctica. *Antarctic Science*, 25(2), 198-212. DOI:10.1017/S0954102012000788
- 1403 Turner, J., Colwell, S.R., Marshall, G.J., Lachlan-Cope, T.A., Carleton, A.M., Jones, P.D., ... & Iagovkina,  
1404 S. (2005). Antarctic climate change during the last 50 years. *International journal of Climatology*,  
1405 25(3), 279-294. DOI: 10.1002/joc.1130
- 1406 Turner, J., Lu, H., White, I., King, J.C., Phillips, T., Hosking, J.S., ... & Deb, P. (2016). Absence of 21st  
1407 century warming on Antarctic Peninsula consistent with natural variability. *Nature*, 535(7612),  
1408 411. DOI:10.1038/nature18645
- 1409 Uppala, S.M., Kållberg, P.W., Simmons, A.J., Andrae, U., da Costa Bechtold, V., Fiorino, M., Gibson,  
1410 J.K., Haseler, J., Hernandez, A., Kelly, G.A., Li, X., Onogi, K., Saarinen, S., Sokka, N., Allan,  
1411 R.P., Andersson, E., Arpe, K., Balmaseda, M.A., Beljaars, A.C.M., van de Berg, L., Bidlot, J.,  
1412 Bormann, N., Caires, S., Chevallier, F., Dethof, A., Dragosavac, M., Fisher, M., Fuentes, M.,  
1413 Hagemann, S., Hólm, E., Hoskins, B.J., Isaksen, I., Janssen, P.A.E.M., Jenne, R., McNally, A.P.,  
1414 Mahfouf, J.F., Morcrette, J.J., Rayner, N.A., Saunders, R.W., Simon, P., Sterl, A., Trenberth, K.E.,  
1415 Untch, A., Vasiljevic, D., Viterbo, P., Woollen, J., 2005. The ERA-40 re-analysis. *Q. J. R. Meteorol. Soc.* 131, 2961–3012. <https://doi.org/10.1256/qj.04.176>
- 1417 Vaughan, D.G. & Doake, C.S.M. 1996: Recent atmospheric warming and retreat of ice shelves on the  
1418 Antarctic Peninsula. *Nature* 379, 328–31.
- 1419 Vaughan, D.G., Marshall, G., Connolley, W.M., Parkinson, C., Mulvaney, R., Hodgson, D.A., King, J.C.,  
1420 Pudsey, C.J., Turner, J. & Wolff, E. (2003). Recent rapid regional climate warming on the  
1421 Antarctic Peninsula. *Climatic Change* 60, 243-74.
- 1422 Vera, M. (2013). Distribution and reproductive capacity of *Deschampsia antarctica* and *Colobanthus*  
1423 *quitensis* on Byers Peninsula, Livingston Island, South Shetland Islands, Antarctica. *Antarctic*  
1424 *Science*, 25, DOI: 10.1017/S0954102012000995.
- 1425 Watcham, E.P., Bentley, M.J., Hodgson, D.A., Roberts, S.J., Fretwell, P.T., Lloyd, J.M., ... & Moreton,  
1426 S.G. (2011). A new Holocene relative sea level curve for the South Shetland Islands, Antarctica.  
1427 *Quaternary Science Reviews*, 30(21-22), 3152-3170. DOI:10.1016/j.quascirev.2011.07.021
- 1428 White, D. A., Fink, D., & Gore, D. B. (2011). Cosmogenic nuclide evidence for enhanced sensitivity of an  
1429 East Antarctic ice stream to change during the last deglaciation. *Geology*, 39(1), 23-26  
1430 <https://doi.org/10.1130/G31591.1>
- 1431 Yoo, K.C., Yoon, H.I., Kim, J.K., & Khim, B.K. (2009). Sedimentological, geochemical and  
1432 palaeontological evidence for a neoglacial cold event during the late Holocene in the continental  
1433 shelf of the northern South Shetland Islands, West Antarctica. *Polar Research*, 28(2), 177-192.  
1434 DOI:10.1111/j.1751-8369.2009.00109.x
- 1435 Yoon, H.I., Yoo, K.C., Bak, Y.S., Lim, H.S., Kim, Y., & Lee, J.I. (2010). Late Holocene cyclic  
1436 glaciomarine sedimentation in a subpolar fjord of the South Shetland Islands, Antarctica, and its  
1437 paleoceanographic significance: sedimentological, geochemical, and paleontological evidence.  
1438 *Bulletin*, 122(7-8), 1298-1307.
- 1439 Zale, R., & Karlén, W. (1989). Lake sediment cores from the Antarctic Peninsula and surrounding islands.  
1440 *Geografiska Annaler: Series A, Physical Geography*, 71(3-4), 211-220.
- 1441



1442 **Figure captions**

1443 Figure 1. Location of areas cited in the text related to Antarctica. A) Antarctic Ice Sheet;  
1444 B) Ross Ice Shelf; C) Antarctic Peninsula; D) Graham Land. This figure is available in  
1445 colour in the online version.

1446 Figure 2. Location of the areas cited in the text. A) South Shetland Islands; B) Hurd  
1447 Peninsula; C) Fildes and Barton peninsulas; D) Byers Peninsula. This figure is available  
1448 in colour in the online version.

1449 Figure 3. Probability density plots of CRE ages for differentiated chronostratigraphical  
1450 units: A) Deglaciation, b) First Neoglacial advance and c) Second Neoglacial advance.  
1451 This figure is available in colour in the online version.

1452 Figure 4. Location of the study area, with the main geomorphological features, CRE  
1453 samples and their ages plotted in a Google Earth satellite image. This figure is available  
1454 in colour in the online version.

1455 Figure 5. Geomorphological sketch with CRE arithmetic mean ages for each  
1456 geomorphological unit. This figure is available in colour in the online version.

1457 Figure 6. Geomorphological transect of the main features with arithmetic mean of the  
1458 CRE ages in each unit. This figure is available in colour in the online version.

1459 Figure 7. BYC-1 and -2 samples and CRE ages in Rish Point, Byers Peninsula. This  
1460 figure is available in colour in the online version.

1461 Figure 8. BYC-11 and -12 and BYB-10 samples and CRE ages on South Beaches area,  
1462 Byers Peninsula. This figure is available in colour in the online version.

1463 Figure 9. BYC-12 and -13 samples and CRE ages in front of Rish Point, Byers Peninsula.  
1464 This figure is available in colour in the online version.

1465 Figure 10. BYC-4 and -5 samples and CRE ages in the moraine between Rish Point and  
1466 Clark Nunatak, Byers Peninsula. This figure is available in colour in the online version.

1467 Figure 11. Summary table comparing the timing of neoglacial expansion in the AP region  
1468 and the results of this work. This figure is available in colour in the online version.

1469 **Table captions**

1470 Table 1. Timing of Neoglacial advances in the AP region.

1471 Table 2. Timing of the end of deglaciation and geomorphic evidence of Neoglacial  
1472 advances in the SSI.

1473 Table 3. End of deglaciation, Neoglacial evidence and related features in the Byers  
1474 Peninsula.

1475 Table 4. Geographic location of samples, topographic shielding factor, sample thickness  
1476 and distance from terminus.

1477 Table 5. Chemical composition of the bulk rock samples before chemical treatment. The  
1478 data in italics correspond to the average values of the element concentrations of the  
1479 samples BYC-2, BYC-4, BYC-11 (included in this studio) and others of similar lithology  
1480 collected in nearby areas, but not included in this study. These average values have been  
1481 used for the age-exposure calculations of those samples without bulk chemical  
1482 composition analysis.

1483 Table 6. Concentrations of the major elements determined in splits taken after the

1484 chemical pre-treatment (acid etching).  $P_2O_5$  (%) concentrations are below detection limit  
1485 ( $0.10 \pm 0.015$ ).

1486 Table 7. AMS analytical data and calculated exposure ages.  $^{36}Cl/^{35}Cl$ ,  $^{35}Cl/^{37}Cl$  and  
1487  $^{10}Be/^9Be$  ratios were inferred from measurements at the ASTER AMS facility. The  
1488 numbers in italics correspond to the internal (analytical) uncertainty at one standard level.

AUTHOR'S FINAL VERSION

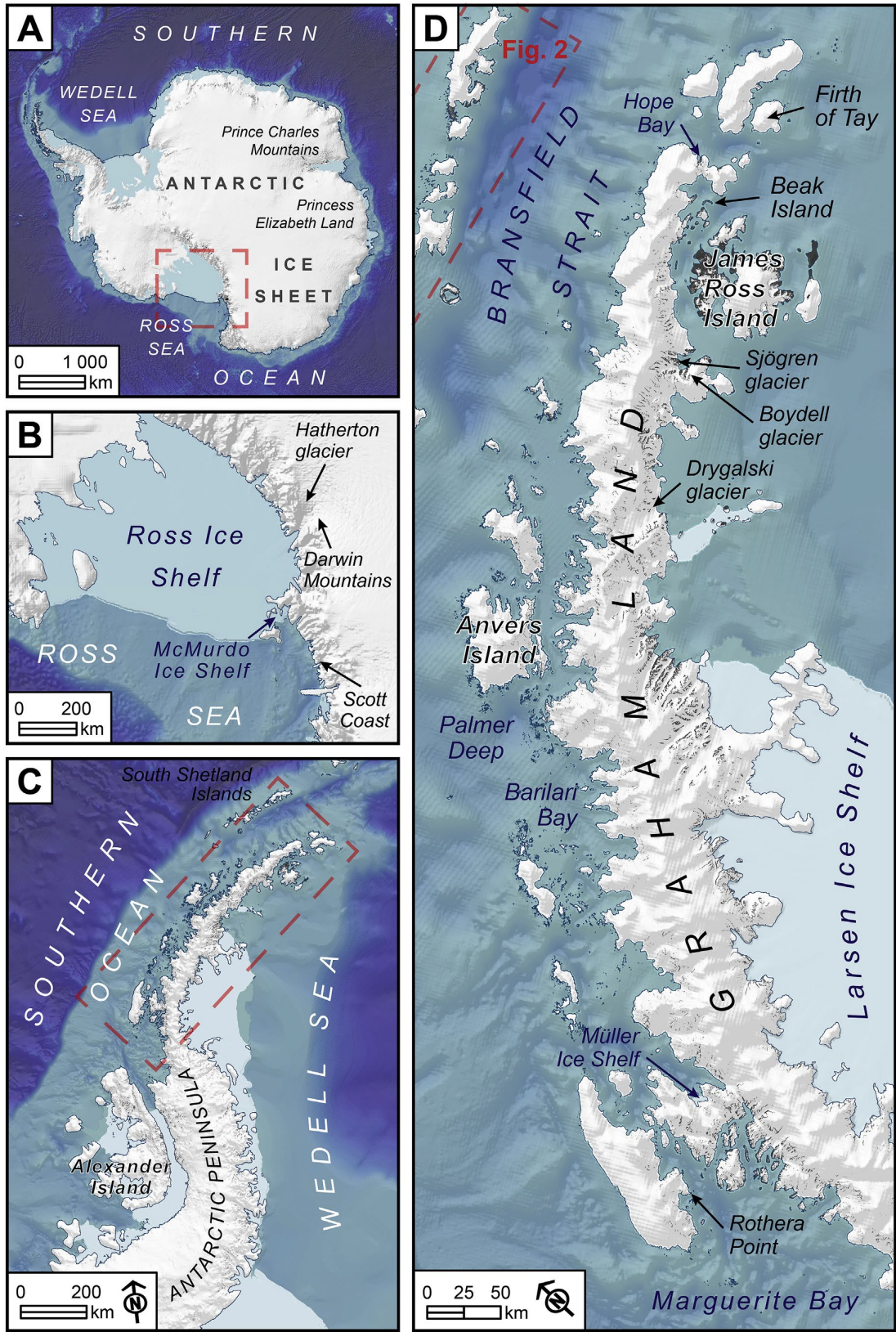


Fig. 1. Location of areas cited in the text related to Antarctica. A) Antarctic Ice Sheet; B) Ross Ice Shelf; C) Antarctic Peninsula; D) Graham Land.



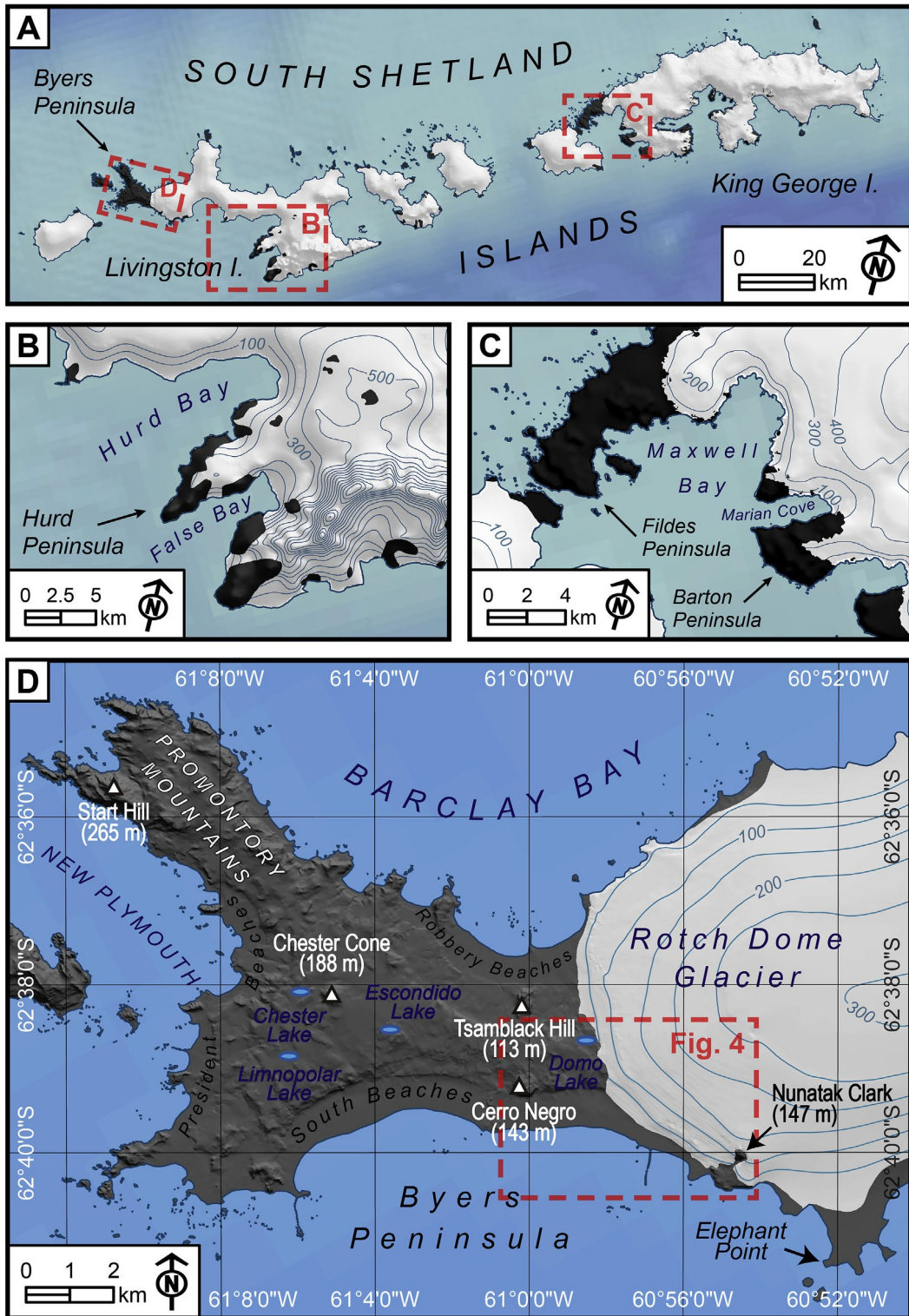


Fig. 2. Location of the areas cited in the text. A) South Shetland Islands; B) Hurd Peninsula; C) Fildes and Barton peninsulas; D) Byers Peninsula.

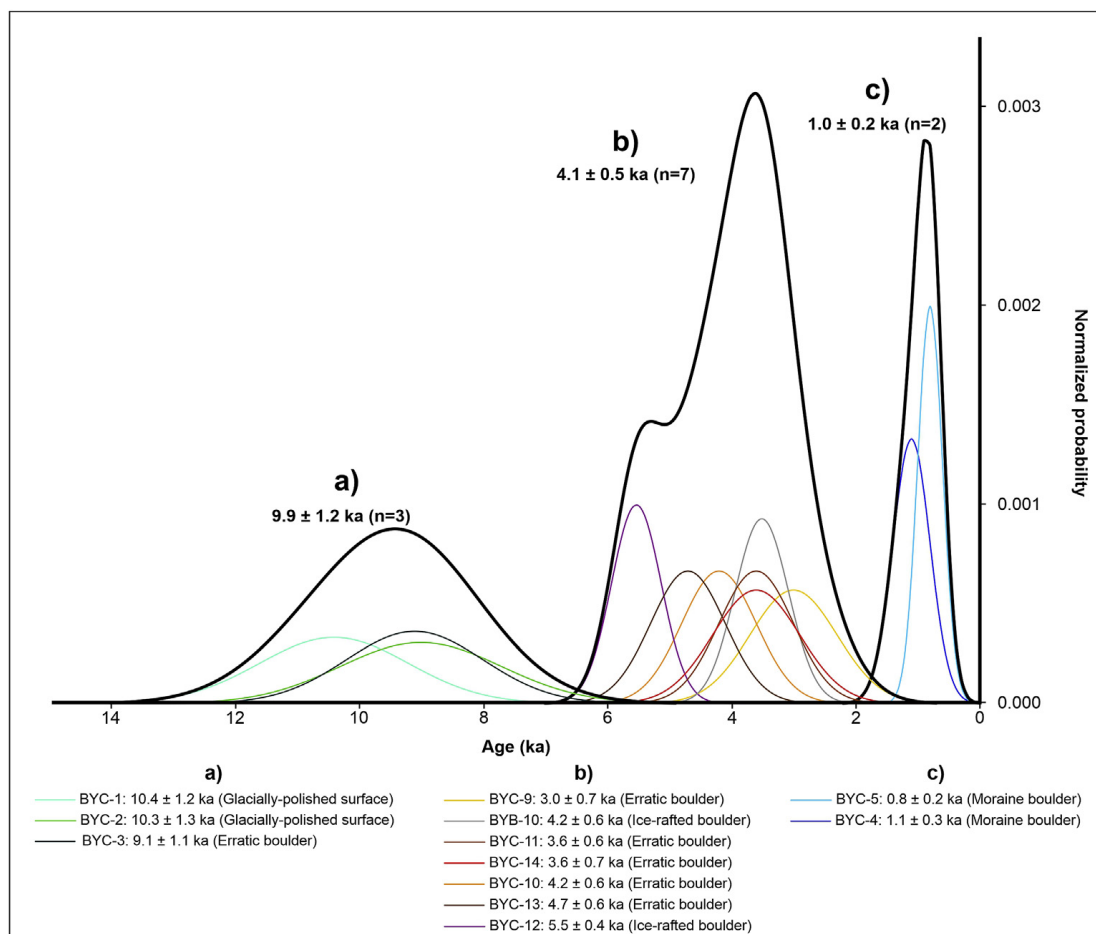


Fig. 3. Probability density plots of CRE ages for differentiated chronostratigraphical units: A) Deglaciation, b) First Neoglacial advance and c) Second Neoglacial advance.

AUTHOR'S

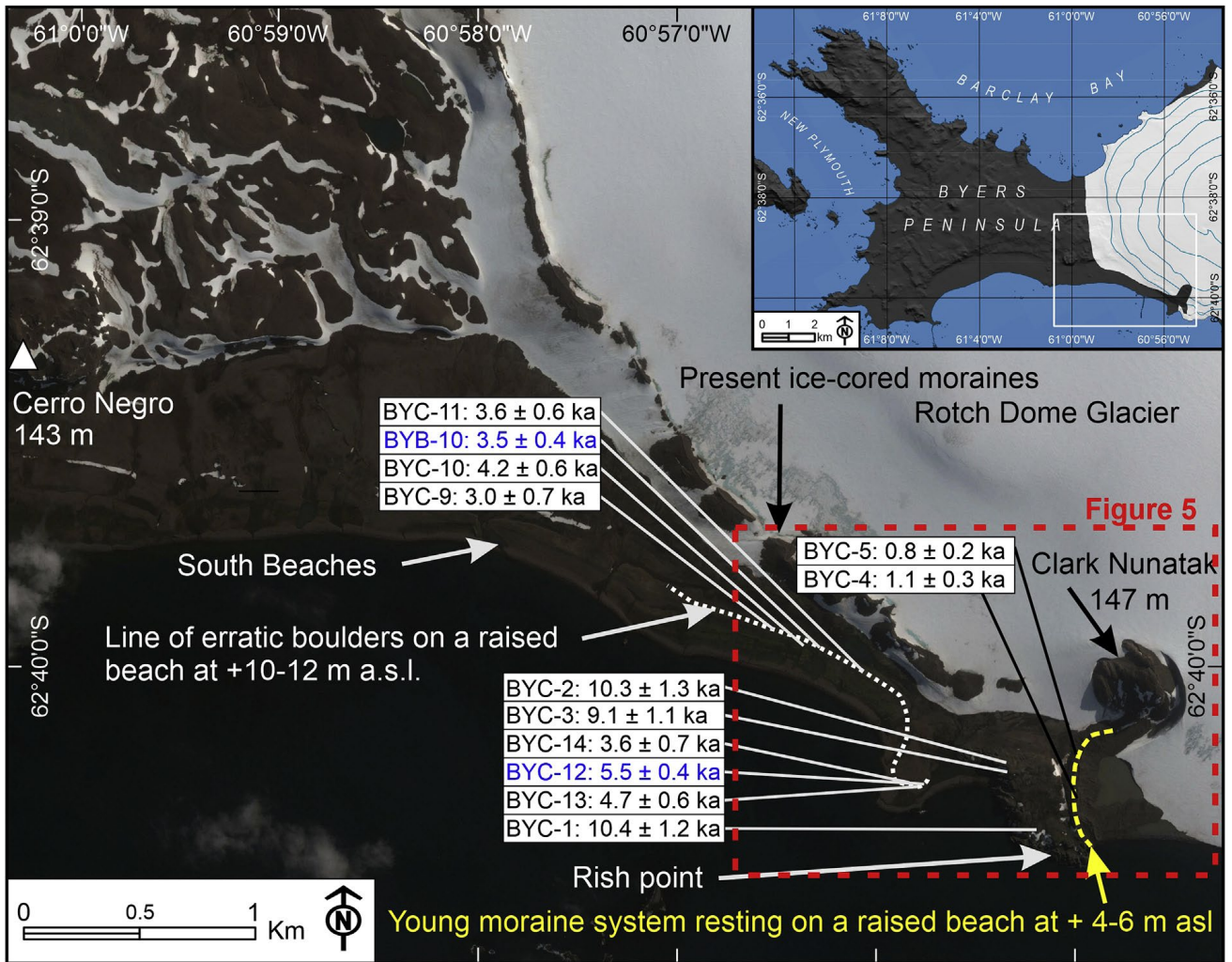


Fig. 4. Location of the study area, with the main geomorphological features, CRE samples and their ages plotted in a Google Earth satellite image.

AUTHOR



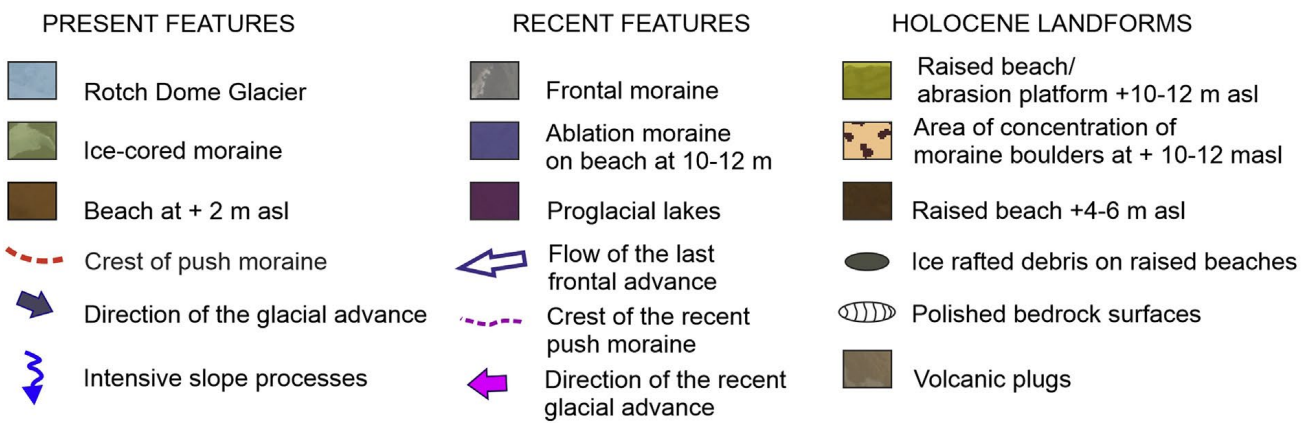
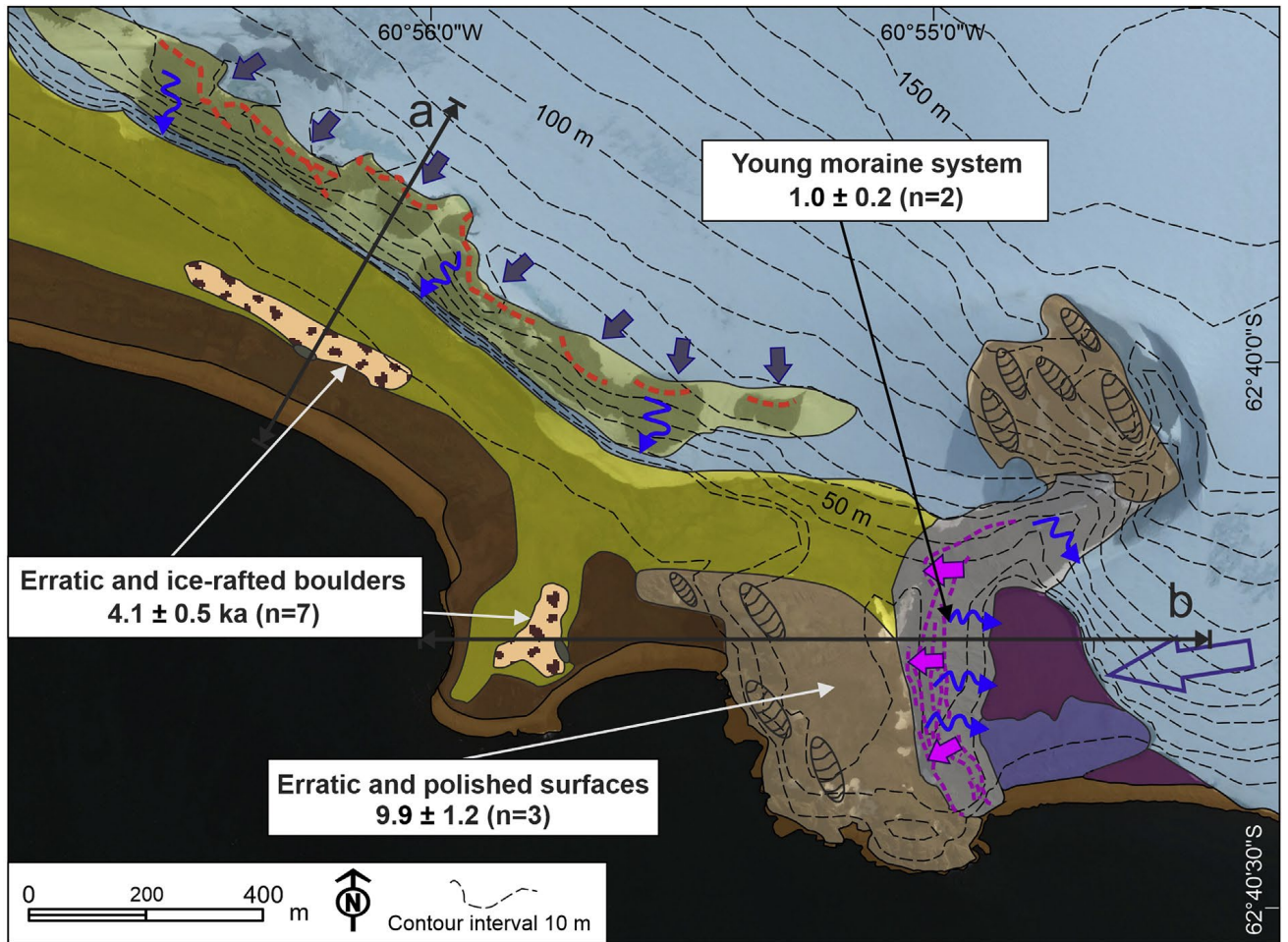


Fig. 5. Geomorphological sketch with CRE arithmetic mean ages for each geomorphological unit.

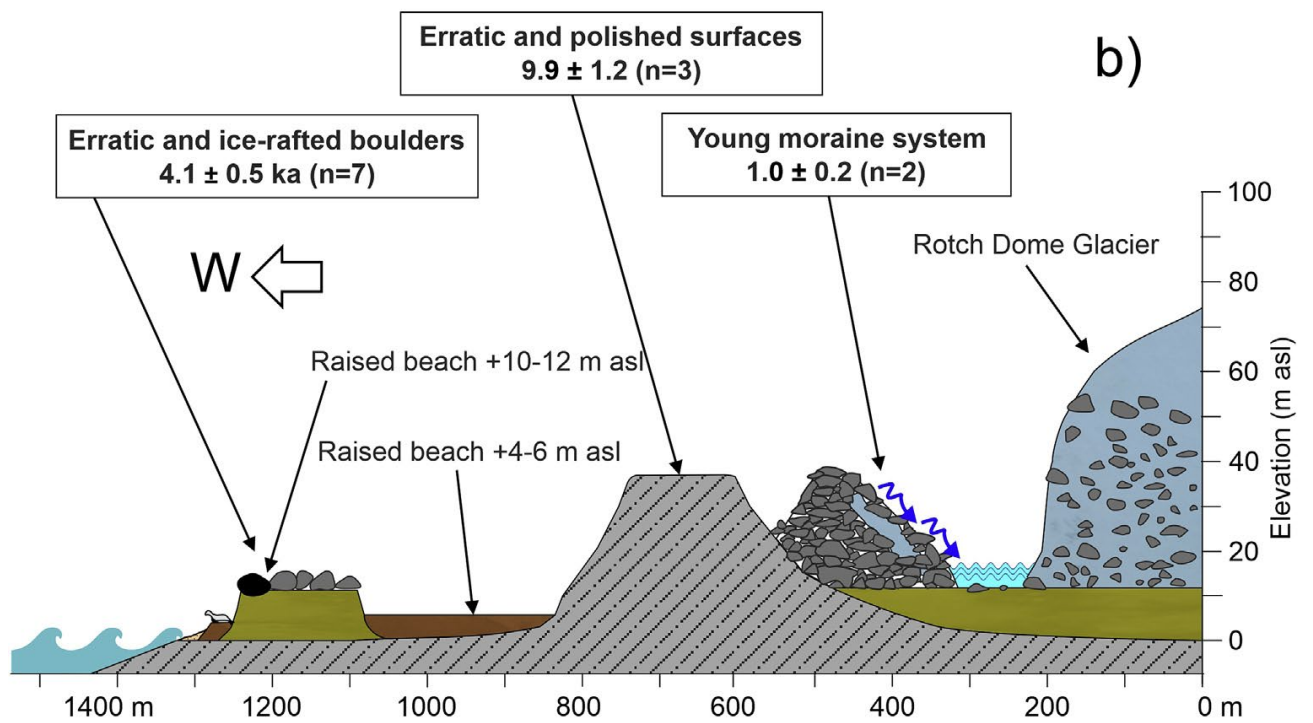
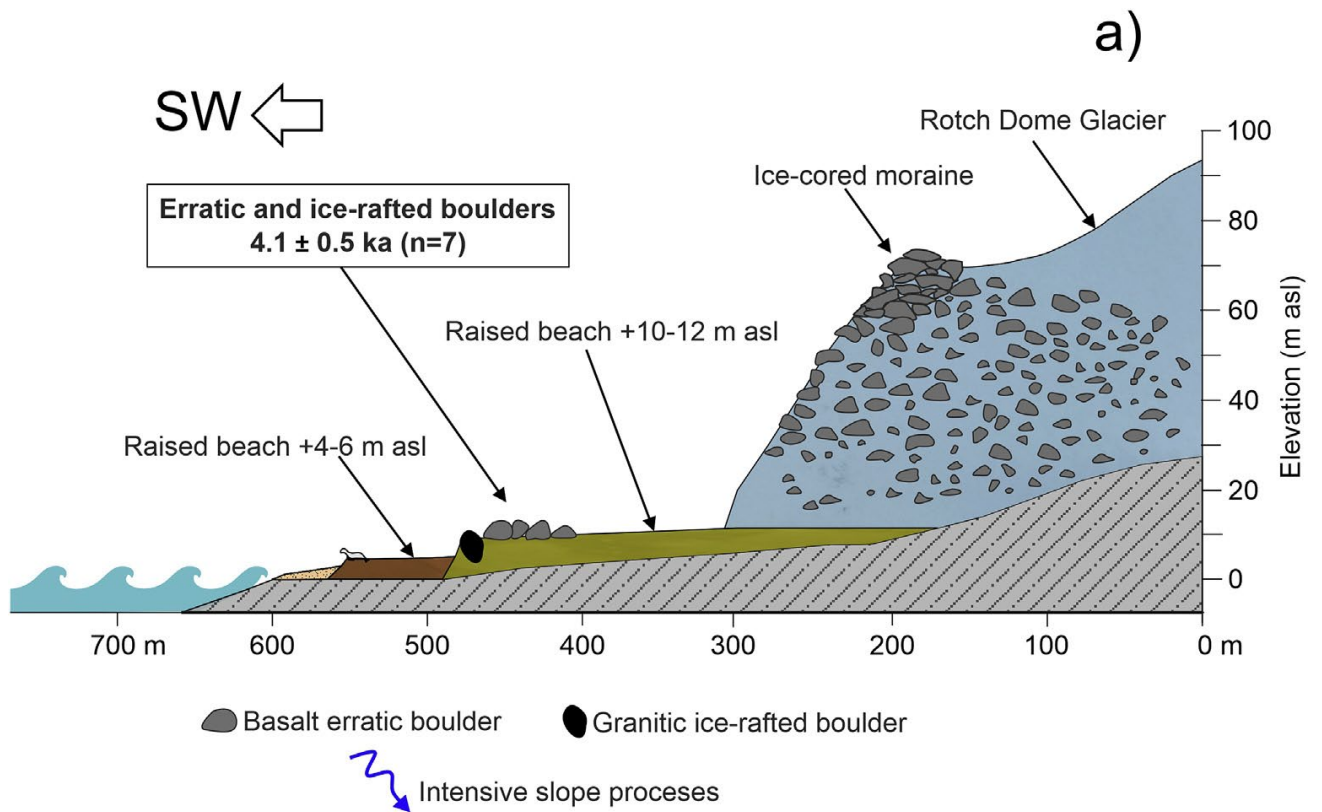


Fig. 6. Geomorphological transect of the main features with arithmetic mean of the CRE ages in each unit.



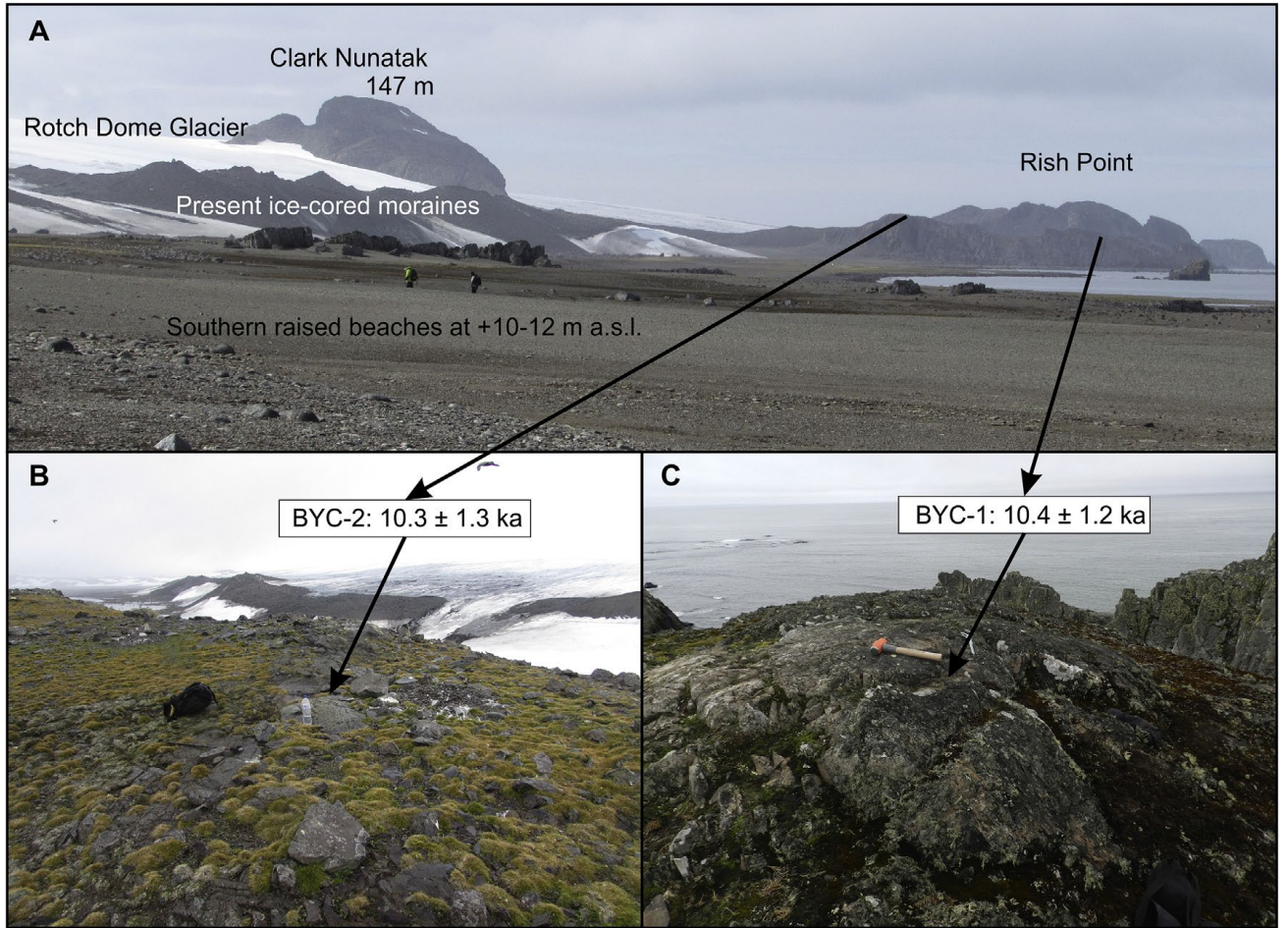


Fig. 7. BYC-1 and -2 samples and CRE ages in Rish Point, Byers Peninsula.

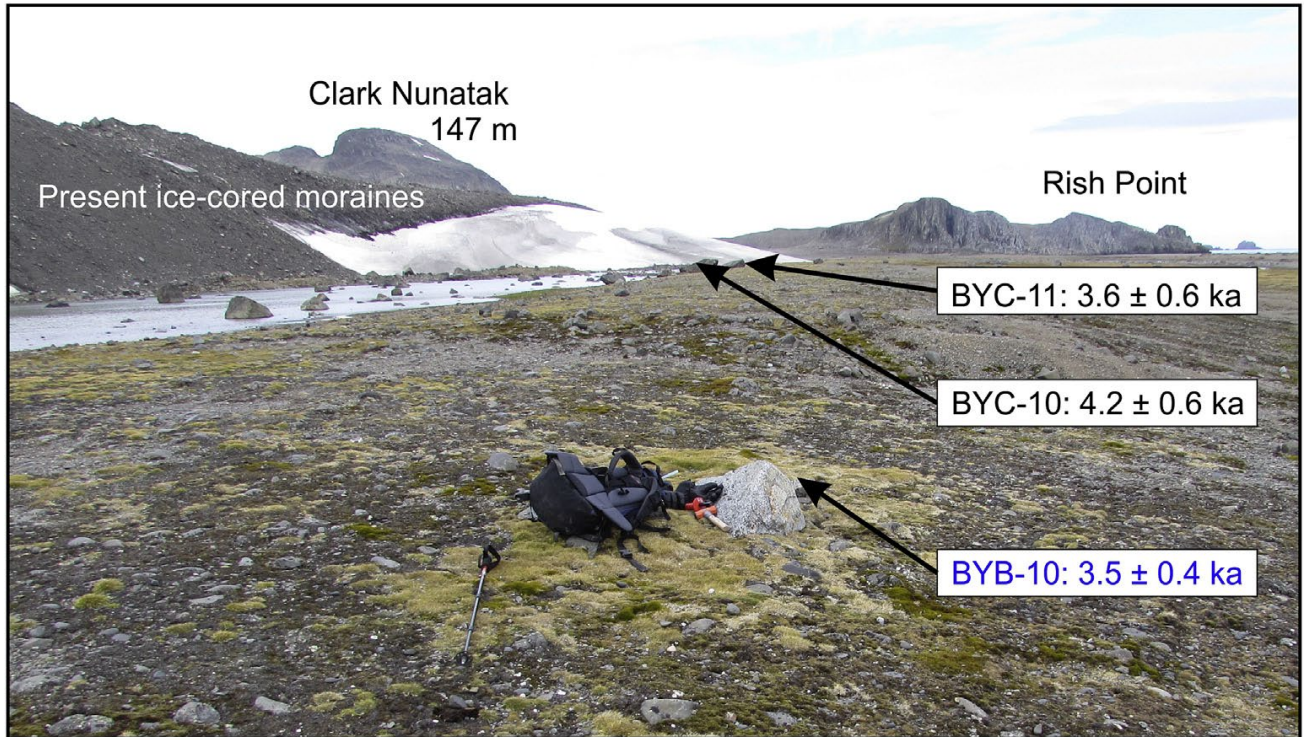


Fig. 8. BYC-11 and -12 and BYB-10 samples and CRE ages on South Beaches area, Byers Peninsula.

AUTHOR'S FINAL



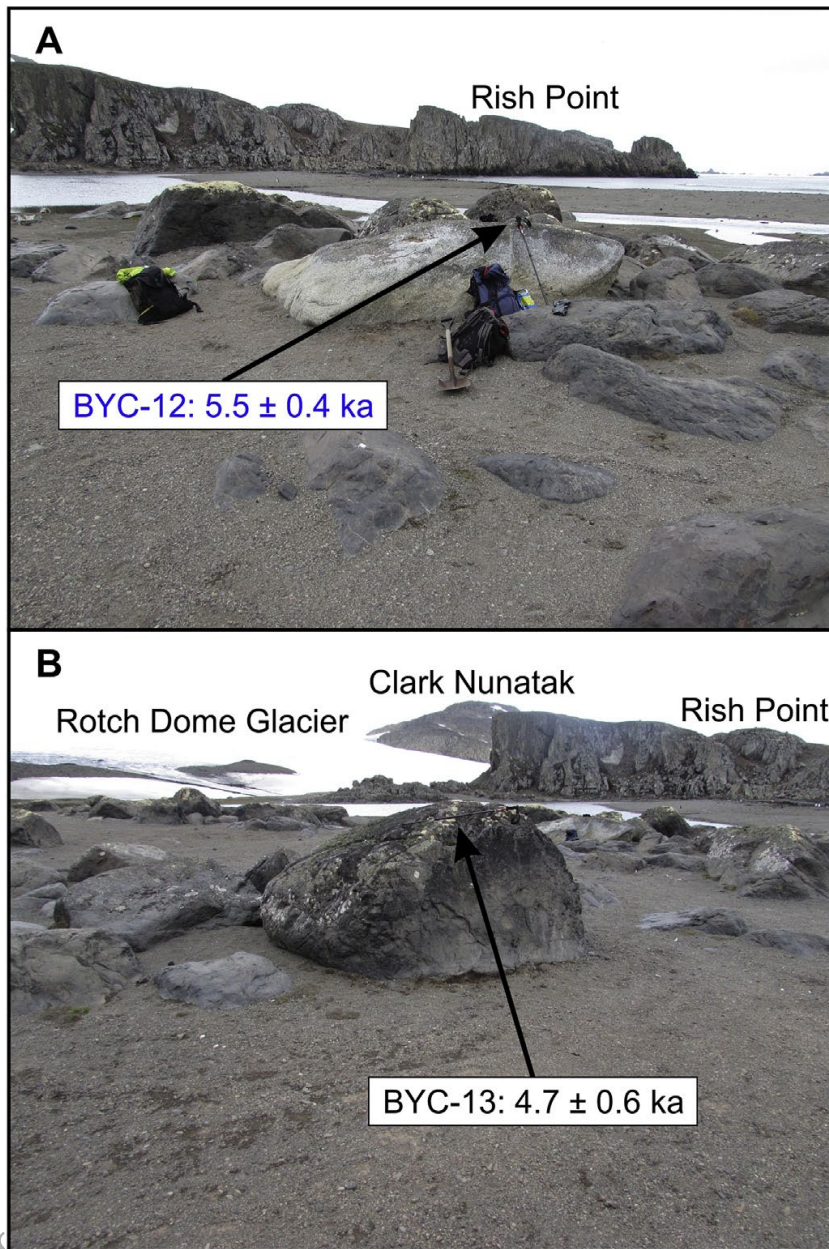


Fig. 9. BYC-12 and -13 samples and CRE ages in front of Rish Point, Byers Peninsula.

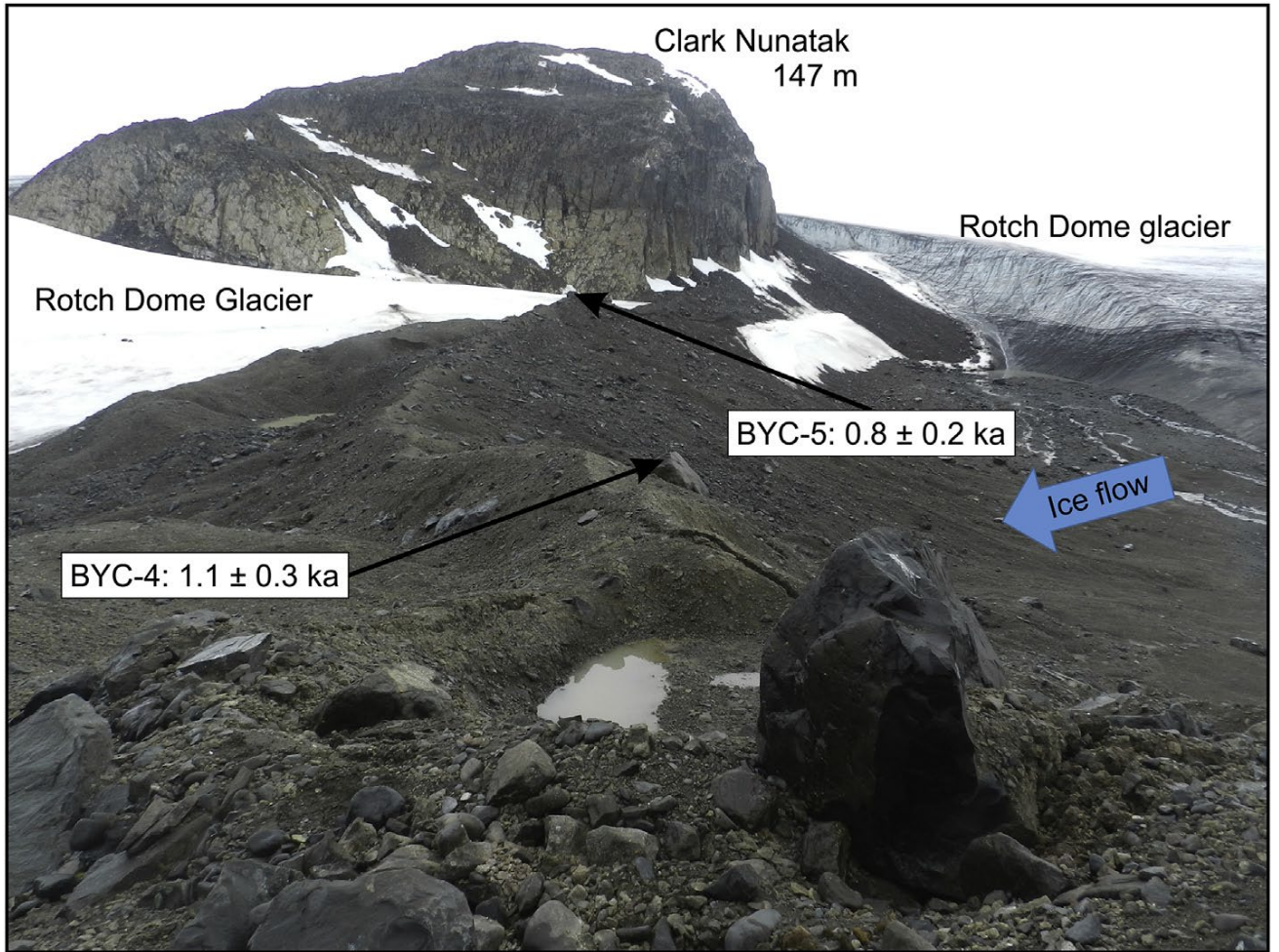


Fig. 10. BYC-4 and -5 samples and CRE ages in the moraine between Rish Point and Clark Nunatak, Byers Peninsula.



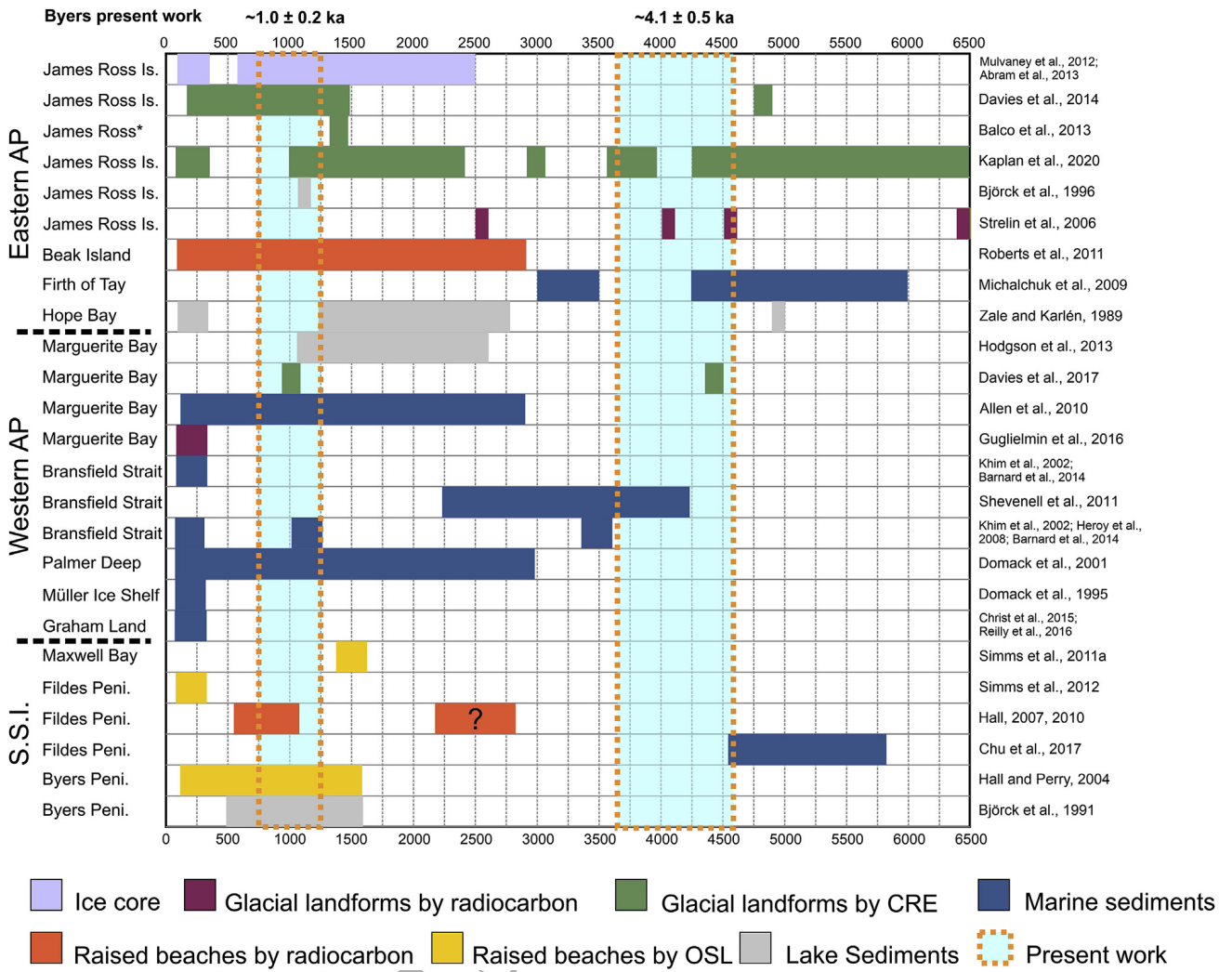


Fig. 11. Summary table comparing the timing of neoglacial expansion in the AP region and the results of this work.

*AUTHOR'S FINAL VERSION*

Table 1 Timing of neoglacial advances in the Antarctic Peninsula.

Location	Evidence	Chronology of related events	Neoglacial environments and landforms	References
James Ross Island	Ice cores	From 2.5 to 0.6 cal ka BP, especially around 1.4 cal ka BP	Cold period	Mulvaney et al., 2012; Abram et al., 2013
James Ross Island	Lake sediments	At 1.2 cal ka BP	Glacial advance	Björck et al., 1996
James Ross Island	Glacial landforms	At 6.5, 4.6, 3.9, 2.6 cal ka BP	Glacial advances	Strelin et al., 2006
James Ross Island	Glacial landforms	At 4.8 ka Be <sup>10</sup>	Glacial advance	Davies et al., 2014
James Ross Island	Glacial landforms	From 1.5 to 0.3 ka Be <sup>10</sup>	Glacial advances	Davies et al., 2014
Bransfield Strait	Marine sediments	At 4.5 and 2.5 cal ka BP	Cold periods	Shevenell et al., 2011
Bransfield Strait	Marine sediments	At 3.5 and 1.2 cal ka BP	Cold periods	Khim et al., 2002; Heroy et al., 2008; Barnard et al., 2014
Marguerite Bay	Marine sediments	From 2.8 to 0.2 cal ka BP	Cold period	Allen et al., 2010
Marguerite Bay	Lake sediments	From 2.6 / 2.0 to 1.1 cal ka BP	Cold periods	Hodgson et al., 2013
Marguerite Bay	Glacial landforms	At 4.4 ± 0.7 ka Be <sup>10</sup>	Glacial advance	Davies et al., 2017
Marguerite Bay	Glacial landforms	At 1 ka Be <sup>10</sup>	Formation of ice-cored moraines	Davies et al., 2017
Palmer Deep	Marine sediments	From 3.3 to 0.1 cal ka BP	Cold period	Domack et al., 2001
Firth of Tay	Marine sediments	Between 6.0 and 4.5 cal ka BP	Minor glacial advance	Michalchuk et al., 2009
Firth of Tay	Marine sediments	From 3.5 cal ka BP	General neoglaciation	Michalchuk et al., 2009
Hope Bay	Lake sediments	Around 5 ka	Glacial advance	Zale and Karlén, 1989

Beak Island	Raised beaches	From 2.9 cal ka BP	Decreased rates of sea level rise associated with neoglacial events	Roberts et al., 2011
Scott Coast	Glacial landforms	From 3.5 ka to the LIA	Glacial advances	Hall and Denton, 2002
Anvers Island	Glacial landforms	Until 0.7-0.9 cal ka BP	Glacial advances followed by retreat	Hall et al., 2010
Sjögren, Boydell and Drygalski glaciers	Glacial landforms	After 1.4 ka	Glacial advances	Balco et al., 2013
Hatherton Glacier, Darwin Mountains	Glacial landforms	Between 3 and 0.5 ka Be <sup>10</sup>	Formation of moraines	White et al., 2011
Bransfield Strait	Marine sediments	LIA	Glacial advance	Khim et al., 2002; Barnard et al., 2014
Müller Ice Shelf	Marine sediments	LIA	Glacial advance	Domack et al., 1995
Palmer Deep One	Marine sediments	LIA	Glacial advance	Domack et al., 2001
Barilari Bay, Graham Land	Marine sediments	LIA	Glacial advance	Christ et al., 2015; Reilly et al., 2016
Hope Bay	Lake sediments	LIA	Glacial advance	Zale and Karlén, 1989
James Ross Island	Glacial landforms	LIA	Glacial advance	Strelin et al., 2006
Marguerite Bay	Glacial landforms	LIA	Glacial advance	Guglielmin et al., 2016

Table 2 Timing of the end of deglaciation and geomorphic evidence of neoglacial advances in the South Shetland Islands

Location	Chronology of related events	Neoglacial environments and landforms	References
Several raised beaches in Livingston and King George islands	At 5.5 cal ka BP	Raised beaches distributed at about 16-20 m a.s.l. indicate that the glaciers were close to their current position at that time	Barsch and Mäusbacher, 1986; Mäusbacher, 1991; Del Valle et al., 2002; Hall, 2003; Bentley et al., 2005; Hall, 2010; Watcham et al., 2011
Several lakes in Livingston and King George islands	At 4-5 cal ka BP	Total deglaciation and glaciers close to their current position	Mäusbacher et al., 1989; Björck et al., 1991, 1993, 1996b
Maxwell Bay (King George Island)	Around 5.9 cal ka BP	Deglaciation was completed	Simms et al., 2011a
Maxwell Bay (King George Island)	From 5.9 cal ka BP	Gradual cooling and more extensive sea-ice cover in the bay	Milliken et al., 2009
Maxwell Bay (King George Island)	Until 1.7 ka	Neoglacial advance	Simms et al., 2011a
Several areas in King George Island	13-17th centuries	Occurrence of two glacial advances: (i) a 2-3 km long advance was dated at the 13th to early 15th CE related to the raised beach 6 m a.s.l., (ii) and another smaller glacial expansion of 0.25-1 km at the 16-17th CE related to raised beach 2-3 m a.s.l.	Curl, 1980; Sugden and Clapperton, 1986; Clapperton, and Sugden, 1988; Birkenmajer, 1981, 1995; 1998
Fildes Peninsula (King George Island)	16-18th centuries AD, OSL ages	Moraine associated with the development of the raised beach 4-6 m a.s.l.	Simms et al., 2011a, 2012
Fildes Peninsula (King George Island)	At 0.65 cal ka BP, but possible older advances occurred from 2.8 cal ka BP onwards	Moraine associated with the development of the raised beach 4-6 m a.s.l.	Hall, 2007; Hall, 2010
Fildes Peninsula (King George Island)	From 5.8 to 4.8 cal ka BP	Cold period	Chu et al., 2017
Fildes Peninsula (King George Island)	From 2.7 cal ka BP	Beginning of neoglacial advances	Chu et al., 2017
Byers and Fildes peninsulas	From 3 to 1.5 ka cal ka BP	Two glacial advances	Barsch and Mäusbacher, 1986

Byers and Fildes peninsulas	At 0.4-0.7 cal ka BP	Glacial advances associated with the development of the raised beach 4-6 m a.s.l.	<a href="#">John and Sugden, 1971</a> ; <a href="#">John, 1972</a> ; <a href="#">Sugden and John, 1973</a>
Hurd Peninsula (Livingston Island)	Middle and Late Holocene	Two glacial advances related to raised beach 10-12 m a.s.l. and 4-6 m a.s.l.	<a href="#">Everett, 1971</a>
Byers Peninsula (Livingston Island)	At 5.9 cal ka BP	Deglaciation of the central plateau	<a href="#">Toro et al., 2013</a> ; <a href="#">Oliva et al., 2016</a>
Byers Peninsula (Livingston Island)	From 1.7 to 0.25 cal ka BP	Cold periods of increased glacial extent and greater iceberg delivery	<a href="#">Hall and Perry, 2004</a>
Byers Peninsula (Livingston Island)	Between 1.5 and 0.5 cal ka BP	Cold period	<a href="#">Björck et al., 1991</a>
Byers Peninsula (Livingston Island)	Around 1.8 cal ka BP	Deglaciation of the area close to the present glacial front of Dome Roch glacier	<a href="#">Oliva et al., 2016</a>

AUTHOR'S FINAL VERSION



Table 3 End of deglaciation, Neoglacial evidence and related features in the Byers Peninsula.

Location	Evidence	Chronology of related events	Neoglacial environments and landforms	References
From West to East	Lake sediments	From 8.3 to 1.8 cal ka BP	Deglaciation of the entire peninsula	<a href="#">Toro et al., 2013; Oliva et al., 2016</a>
Front of the Rotch Dome glacier	Geomorphic evidence	LIA?	Ice-cored moraines distributed on the raised beach 4-5 m a.s.l.	<a href="#">John and Sugden, 1971; López Martínez et al., 1996.</a>
Domo Lake	Lake sediments	Slightly younger than 1.8 cal ka BP	Deglaciation of the lake	<a href="#">Oliva et al., 2016</a>
Midge Lake	Lake sediments	Between 1.5 and 0.5 cal ka BP	Cold periods	<a href="#">Björck et al., 1991</a>
Southern Beaches	Raised beaches	1.8 cal ka BP	Raised beach 10 m a.s.l.	<a href="#">Hansom, 1979</a>
Southern Beaches	Raised beaches	15-17th centuries CE	Raised beach 6 m a.s.l.	<a href="#">Curl, 1980</a>
Southern Beaches	Raised beaches	1.7 cal ka BP	Raised beach 6 and 10 m a.s.l. with ice rafted debris	<a href="#">Hall and Perry, 2004</a>
Southern Beaches	Raised beaches	From 7.4 cal ka BP to 15-17th centuries CE	Raised beaches from 15 to 6 m a.s.l.	<a href="#">Hall, 2003, 2010</a>
West front of the Rotch Dome glacier	Aerial imagery	From 1971	Stable ice-cored moraines	<a href="#">John and Sugden, 1971; López Martínez et al., 1996; Hall, 2010</a>
South front of the Rotch Dome glacier	Aerial imagery	From 1956 to 2000	Retreat of ice-cored moraines	<a href="#">Oliva and Ruiz-Fernández, 2015, 2017</a>

Table 4. Geographic location of samples, topographic shielding factor, sample thickness and distance from terminus.

Sample name	Geomorphological unit	Landform	Latitude (DD)	Longitude (DD)	Elevation (m a.s.l.)	Topographic shielding factor	Thickness (cm)	Dist. from present moraine ridge	Isotope
BYC-1	Deglaciated bedrock	Glacially-polished surface	-62.6731	-60.9199	28	0.9961	1.8	600	<sup>36</sup> Cl
BYC-2	Deglaciated bedrock	Glacially-polished surface	-62.6705	-60.9223	47	0.9995	4.8	350	<sup>36</sup> Cl
BYC-3	Deglaciated bedrock	Erratic boulder	-62.6707	-60.9223	47	0.9912	4.0	350	<sup>36</sup> Cl
BYC-4	Moraine (nunatak Clark, W)	Moraine boulder	-62.6716	-60.9163	36	0.9963	4.5	-	<sup>36</sup> Cl
BYC-5	Moraine (nunatak Clark, W)	Moraine boulder	-62.6704	-60.9166	35	0.9956	3.5	-	<sup>36</sup> Cl
BYC-9	Raised beach (+10/12 m)	Erratic boulder	-62.6654	-60.9409	11	0.9992	3.0	200	<sup>36</sup> Cl
BYC-10	Raised beach (+10/12 m)	Erratic boulder	-62.6660	-60.9386	10	0.9992	2.0	200	<sup>36</sup> Cl
BYC-11	Raised beach (+10/12 m)	Erratic boulder	-62.6668	-60.9349	10	0.9992	3.1	200	<sup>36</sup> Cl
BYC-12	Raised beach (+10/12 m)	Ice-rafted boulder	-62.6714	-60.9293	4	0.9900	3.5	-	<sup>10</sup> Be
BYC-13	Raised beach (+10 m)	Erratic boulder	-62.6714	-60.9295	5	0.9900	3.2	-	<sup>36</sup> Cl
BYC-14	Raised beach (+10 m)	Erratic boulder	-62.6713	-60.9298	5	0.9900	1.8	-	<sup>36</sup> Cl
BYB-10	Raised beach (+10/12 m)	Ice-rafted boulder	-62.6663	-60.9380	8	0.9988	3.5	-	<sup>10</sup> Be

Table 5. Chemical composition of the bulk rock samples before chemical treatment. The data in italics correspond to the average values of the element concentrations of the samples BYC-2, BYC-4, BYC-11 (included in this study) and others of similar lithology collected in nearby areas, but not included in this study. These average values have been used for the age-exposure calculations of those samples without bulk chemical composition analysis.

<b>Sample name</b>	<b>CaO (%)</b>	<b>K<sub>2</sub>O (%)</b>	<b>TiO<sub>2</sub> (%)</b>	<b>Fe<sub>2</sub>O<sub>3</sub> (%)</b>	<b>Cl (ppm)</b>	<b>SiO<sub>2</sub> (%)</b>	<b>Na<sub>2</sub>O (%)</b>	<b>MgO (%)</b>	<b>Al<sub>2</sub>O<sub>3</sub> (%)</b>	<b>MnO (%)</b>	<b>P<sub>2</sub>O<sub>5</sub> (%)</b>	<b>Li (ppm)</b>	<b>B (ppm)</b>	<b>Sm (ppm)</b>	<b>Gd (ppm)</b>	<b>Th (ppm)</b>	<b>U (ppm)</b>
BYC-2	8.989	0.432	1.411	12.575	145	51.580	3.053	4.749	14.928	0.203	0.230	9.800	5.200	3.484	3.877	0.620	0.174
BYC-4	8.920	0.498	1.419	12.515	74	50.670	3.244	4.867	15.233	0.184	0.210	5.550	4.400	3.410	3.773	0.632	0.192
BYC-11	9.565	0.482	1.305	12.175	58	50.580	2.625	5.388	15.008	0.192	0.190	3.830	2.900	3.096	3.392	0.600	0.194
<i>Average</i>	<i>9.651</i>	<i>0.524</i>	<i>1.094</i>	<i>10.741</i>	<i>74</i>	<i>48.099</i>	<i>3.082</i>	<i>4.746</i>	<i>15.906</i>	<i>0.211</i>	<i>0.194</i>	<i>48.099</i>	<i>3.082</i>	<i>4.746</i>	<i>15.906</i>	<i>0.211</i>	<i>0.194</i>

AUTHOR'S FINAL VERSION

Table 6. Concentrations of the major elements determined in splits taken after the chemical pre-treatment (acid etching). P<sub>2</sub>O<sub>5</sub> concentrations are below detection limit (0.015%).

Sample name	CaO (%)	K <sub>2</sub> O (%)	TiO <sub>2</sub> (%)	Fe <sub>2</sub> O <sub>3</sub> (%)	SiO <sub>2</sub> (%)	Al <sub>2</sub> O <sub>3</sub> (%)	MnO (%)	MgO (%)	Na <sub>2</sub> O (%)
BYC-1	8.99 ± 0.45	0.40 ± 0.10	0.78 ± 0.16	10.21 ± 0.20	55.49 ± 1.11	14.37 ± 0.29	0.19 ± 0.04	4.38 ± 0.44	8.99 ± 0.29
BYC-2	8.06 ± 0.40	0.39 ± 0.10	1.07 ± 0.11	10.71 ± 0.21	58.03 ± 1.16	13.45 ± 0.27	0.19 ± 0.04	3.86 ± 0.39	8.06 ± 0.30
BYC-3	8.15 ± 0.41	0.43 ± 0.11	1.40 ± 0.14	10.54 ± 0.21	57.13 ± 1.14	13.24 ± 0.26	0.18 ± 0.04	4.67 ± 0.47	8.15 ± 0.27
BYC-4	8.21 ± 0.41	0.49 ± 0.12	0.74 ± 0.15	9.30 ± 0.93	56.98 ± 1.14	14.41 ± 0.29	0.17 ± 0.03	4.01 ± 0.40	8.21 ± 0.33
BYC-5	8.20 ± 0.41	0.41 ± 0.04	0.87 ± 0.17	10.70 ± 0.21	57.04 ± 1.14	13.35 ± 0.27	0.20 ± 0.04	4.53 ± 0.45	8.20 ± 0.30
BYC-9	8.71 ± 0.44	0.29 ± 0.07	1.22 ± 0.12	11.03 ± 0.22	57.09 ± 1.14	11.31 ± 0.23	0.20 ± 0.04	5.75 ± 0.12	2.27 ± 0.23
BYC-10	7.51 ± 0.38	0.49 ± 0.12	1.19 ± 0.12	8.77 ± 0.88	61.48 ± 1.23	10.86 ± 0.22	0.16 ± 0.03	4.51 ± 0.45	2.00 ± 0.20
BYC-11	8.35 ± 0.42	0.35 ± 0.09	1.22 ± 0.12	10.00 ± 1.00	57.42 ± 1.15	11.45 ± 0.23	0.18 ± 0.04	5.46 ± 0.11	2.07 ± 0.21
BYC-13	8.22 ± 0.41	0.49 ± 0.12	1.04 ± 0.10	9.67 ± 0.97	57.94 ± 1.16	12.55 ± 0.25	0.18 ± 0.04	4.84 ± 0.48	2.39 ± 0.24
BYC-14	8.75 ± 0.44	0.32 ± 0.08	1.27 ± 0.13	10.70 ± 0.21	57.05 ± 1.14	11.84 ± 0.24	0.19 ± 0.04	5.58 ± 0.11	2.23 ± 0.22

AUTHOR'S FINAL VERSION

Table 7. AMS analytical data and calculated exposure ages.  $^{36}\text{Cl}/^{35}\text{Cl}$ ,  $^{35}\text{Cl}/^{37}\text{Cl}$  and  $^{10}\text{Be}/^9\text{Be}$  ratios were inferred from measurements at the ASTER AMS facility. The numbers in italics correspond to the internal (analytical) uncertainty at one standard deviation. Note that the  $^{36}\text{Cl}$  ages reported for “St” scaling were calculated through the Excel™ spreadsheet by Schimmelpfennig et al. (2009) and those for “LSD” scaling were calculated through the trial version of the CREp online calculator (Schimmelpfennig et al., 2019).

<b><math>^{36}\text{Cl}</math> samples</b>								
Sample name	Sample weight (g)	mass of Cl in spike (mg)	$^{35}\text{Cl}/^{37}\text{Cl}$	$^{36}\text{Cl}/^{35}\text{Cl}$ ( $10^{-14}$ )	[Cl] in sample (ppm)	$[^{36}\text{Cl}]$ ( $10^4$ atoms $\text{g}^{-1}$ )	Age (ka) “St” scaling	Age (ka) “LSD” scaling
BYC-1	78.58	1.821	$13.808 \pm 0.231$	$11.015 \pm 0.702$	8.8	$5.54 \pm 0.37$	$11.0 \pm 1.4$ ( <i>1.0</i> )	$10.4 \pm 1.2$ ( <i>0.7</i> )
BYC-2	76.22	1.777	$7.833 \pm 0.138$	$8.731 \pm 0.681$	20.4	$5.70 \pm 0.47$	$11.0 \pm 1.5$ ( <i>1.2</i> )	$10.3 \pm 1.3$ ( <i>1.0</i> )
BYC-3	66.44	1.809	$13.201 \pm 0.220$	$8.028 \pm 0.575$	10.9	$4.79 \pm 0.36$	$9.7 \pm 1.2$ ( <i>1.0</i> )	$9.1 \pm 1.1$ ( <i>0.8</i> )
BYC-4	75.32	1.807	$8.490 \pm 0.142$	$1.207 \pm 0.197$	18.3	$0.68 \pm 0.13$	$1.2 \pm 0.3$ ( <i>0.3</i> )	$1.1 \pm 0.3$ ( <i>0.2</i> )
BYC-5	75.46	1.811	$10.409 \pm 0.171$	$1.093 \pm 0.176$	13.4	$0.53 \pm 0.11$	$1.0 \pm 0.2$ ( <i>0.2</i> )	$0.8 \pm 0.2$ ( <i>0.2</i> )
BYC-9	74.98	1.819	$3.962 \pm 0.066$	$1.927 \pm 0.263$	120.8	$3.69 \pm 0.59$	$3.4 \pm 0.8$ ( <i>0.7</i> )	$3.0 \pm 0.7$ ( <i>0.6</i> )
BYC-10	68.10	1.814	$25.547 \pm 0.495$	$3.983 \pm 0.390$	4.6	$1.95 \pm 0.21$	$4.4 \pm 0.7$ ( <i>0.6</i> )	$4.2 \pm 0.6$ ( <i>0.4</i> )
BYC-11	67.49	1.821	$6.966 \pm 0.121$	$2.753 \pm 0.330$	29.0	$2.19 \pm 0.29$	$3.9 \pm 0.7$ ( <i>0.6</i> )	$3.6 \pm 0.6$ ( <i>0.5</i> )
BYC-13	70.44	1.819	$19.341 \pm 0.347$	$4.606 \pm 0.422$	6.3	$2.32 \pm 0.23$	$5.0 \pm 0.7$ ( <i>0.6</i> )	$4.7 \pm 0.6$ ( <i>0.5</i> )
BYC-14	69.89	1.799	$5.217 \pm 0.088$	$2.623 \pm 0.335$	51.0	$2.77 \pm 0.39$	$4.0 \pm 0.8$ ( <i>0.7</i> )	$3.6 \pm 0.7$ ( <i>0.6</i> )
<i><math>^{36}\text{Cl}</math> Blanks</i>					<i>Total atoms Cl</i>	<i>Total atoms <math>^{36}\text{Cl}</math></i>		
					( $10^{17}$ )	( $10^4$ )		
BL-1	-	1.805	$353.174 \pm 11.131$	$0.265 \pm 0.073$	$2.252 \pm 0.160$	$8.264 \pm 2.264$	-	-
BL-5	-	1.822	$362.525 \pm 8.014$	$0.290 \pm 0.075$	$2.177 \pm 0.133$	$9.133 \pm 2.377$	-	-
<b><math>^{10}\text{Be}</math> samples</b>								
Sample name	Quartz weight (g)	mass of carrier ( $^9\text{Be}$ mg)		$^{10}\text{Be}/^9\text{Be}$ ( $10^{-14}$ )		$[^{10}\text{Be}]$ ( $10^4$ atoms $\text{g}^{-1}$ )		Age (ka)
BYC-12	64.5799	152.29		$5.644 \pm 0.286$		$2.701 \pm 0.137$		$5.5 \pm 0.4$ ( <i>0.3</i> )
BYB-10	82.2924	151.98		$4.719 \pm 0.496$		$1.762 \pm 0.185$		$3.5 \pm 0.4$ ( <i>0.4</i> )
<i><math>^{10}\text{Be}</math> Blank</i>								
BYB-BK	-	151.29			-	-	-	-